Universidade de Aveiro
Departamento de
Eletrónica, Telecomunicações e Informática
2018

Ricardo José Coelho de Figueiredo

Caracterização Não-Linear de Agregados de Antenas para Aplicações 5G

Nonlinear Characterization of Antenna Arrays for 5G Applications

Ricardo José Coelho de Figueiredo

Caracterização Não-Linear de Agregados de Antenas para Aplicações 5G

Nonlinear Characterization of Antenna Arrays for 5G Applications

Dissertação apresentada à Universidade de Aveiro para cumprimento dos requisitos necessários à obtenção do grau de Mestre em Engenharia Eletrónica e Telecomunicações, realizada sob a orientação científica do Doutor Nuno Miguel Gonçalves Borges de Carvalho, Professor Catedrático do Departamento de Eletrónica, Telecomunicações e Informática da Universidade de Aveiro e a co-orientação do Professor Doutor Pedro Pinho, do Instituto Superior de Engenharia de Lisboa.

o júri / the jury

presidente / president

Pedro Miguel Ribeiro Lavrador
Professor Auxiliar da Universidade de Aveiro

vogais / examiners committee

Sérgio Carlos da Conceição Pires
Group Leader da Ampleon Netherlands Bv (arguente principal)

Nuno Miguel Gonçalves Borges de Carvalho
Professor Catedrático da Universidade de Aveiro (orientador)

agradecimentos / acknowledgements

There are several people to whom I must thank for aiding me in the completion of this MSc dissertation journey.

Firstly, I would like to thank Andreia who has accompanied me in this journey of life for the last seven years. Thank you for all your love, support and criticism.

Secondly, I would like to thank my parents for their endless support in all stages of my life and, in this case, for their investment in my education.

Thank you to Jorge and Lúcia Alves for treating me like a son.

A special thanks to my closest group of friends who have joined me in this journey. Thank you to Samuel, who has been my best work partner during this course. Thank you for your patience, work ethic, effort and all the help you gave me. Thank you Louro for your honest opinions and your way in life. Thank you to Jomi for being Jomi and doing things like Jomi. Thank you to Rui for your willingness to see things from a different perspective and change your unfounded opinions. Thank you to Patrícia for all the productive discussions we had about antennas during this dissertation and for you calm approach to life.

Thank you to Daniel Belo for your experienced active antenna array design advice.

A special thank you to Paulo Gonçalves for producing my board designs. Without him my work would have been greatly difficulted.

Thank you to Hugo Mostardinha for helping me with the anecoic chamber measurements.

Finally, a much deserved thank you to my supervisor, professor Nuno Borges Carvalho. Thank your for all the opportunities you have given me, for the freedom you allowed me to have during this work and for your brilliant advice.

Palavras-Chave

5G, ADS, Agregados de Antenas, Antena, Comunicações Sem Fios, CST, Diagrama de Radiação, Distorção, Massive MIMO, Microstrip, Multiplexagem Espacial, Não-Linear, Rádio Frequência, Redes Móveis.

Resumo

As crescentes exigências das redes móveis estão a levar a infraestrutura de telecomunicações ao seu limite. Novas tecnologias centradas em agregados de antenas e multiplexagem espacial têm sido propostas para ultrapassar os desafios impostos por tais exigências. Este trabalho apresenta uma visão abrangente das redes móveis atuais, escrutinando as suas exigências, as soluções apresentadas, os desafios adjacentes, bem como a opinião da indústria.

Os problemas mais críticos do hardware de radio frequência para a quinta geração de redes móveis são apurados a partir de uma análise detalhada do cenário das redes sem fios, sendo apresentado um plano a longo prazo para abordar estas problemáticas. A curto prazo o trabalho foca-se em caracterização de antenas, visto que as antenas são um ponto central nas comunicações sem fios do futuro.

Inicialmente são apresentados conceitos básicos sobre antenas, dando-se de seguida ênfase às antenas microstrip, sendo apresentado todo o processo de síntese, otimização e caracterização de uma antena microstrip retangular e de um agregado de antenas linear de oito elementos com frequência de operação $5.67GHz$. Neste âmbito, algumas propriedades dos agregados, como o varrimento angular do feixe eletromagnético e técnicas de síntese de fonte eletromagnética, são também exploradas.

Finalmente, apresenta-se um estudo sobre o impacto que a distorção não linear de sinal pode ter no diagrama de radiação do agregado de antenas. O objetivo é expandir os conhecimentos do estado-da-arte acerca das limitações que a distorção não linear pode impor na multiplexagem espacial. Neste sentido, um modelo teórico descritivo deste fenómeno é proposto e validado por simulação eletromagnética e por medições experimentais.

Keywords

5G, ADS, Antenna, Antenna Arrays, CST, Distortion, Massive MIMO, Microstrip, Mobile Networks, Nonlinear, Radiation Pattern, Radio Frequency, Spatial Multiplexing, Wireless Communications.

Abstract

The present mobile scenario demands are stretching the existing telecom infrastructure to the limit. New technologies centred around antenna arrays and spatial multiplexing have been proposed to overcome the challenges imposed by these demands. This work overviews the mobile scenario, scrutinizing demands, presented solutions, challenges and the industry's perspective of the Fifth Generation of mobile communications.

From a careful analysis, the 5G's most critical radio frequency hardware issues are detailed, and a long-term approach to address them is presented. On the short-term the work focuses on antenna characterization, because antennas are a central part of future wireless communications.

Initially, basic antenna concepts are presented, then emphasis is given to microstrip antennas, going through all the steps of designing, optimizing and measuring a rectangular microstrip antenna and an eight element linear antenna array for $5.67GHz$. Array features such as scanning and source synthesis are also explored.

Finally, the impact of signal nonlinear distortion on the antenna array pattern is studied, aiming to expand state-of-the-art knowledge on how signal nonlinear distortion can limit spatial multiplexing. A theoretical model of the phenomenon is proposed and validated both by electromagnetic simulation and measurements.

Table of Contents

Preface

The present wireless communication scenario is demanding radical architectural changes in all communication layers. This work is mostly motivated by the hardware changes required to achieve the mobile communication vision portrayed by researchers, being a continuous search to understand what hardware is needed in next-generation Radio Frequency (RF) transceivers.

This dissertation, beyond the presentation of the developed work, aims to give: a good overview of the present wireless communication scenario; a basic reference guide to beginner microstrip antenna designers, presented from the familiar point-of-view of someone who is still very much a beginner, giving basic notes on theory, design and simulation procedures to help jump-start someone that is stuck; and a bold attempt to address state-of-the-art issues.

Chapter 1 presents an overview of the present wireless telecommunication scenario and of the Fifth Generation (5G) proposal, giving contextualization for the whole document. This chapter details the most relevant aspects of the 5G proposal, from the demands, solutions and challenges to the industry's perspective on 5G. The focus is on hardware problems. At the end of chapter 1 the author's interpretation of 5G is presented. From this interpretation, a set of important long-term goals is defined and compiled into a vision to address the major RF problems in the 5G scenario. Due to time constraints, this long-term plan was broken down into a short-term approach that defines the pathway for the work developed during this MSc dissertation.

Chapter 2 addresses antenna theory and design in an academic\educational approach. First important antenna concepts are explained, and then the document moves toward microstrip antenna design, proceeding with array theory, focusing not only on array design, but also on source synthesis problems.

Chapter 3 describes the author's attempt to address state-of-the-art issues. The issue at hand is the impact of signal distortion on the antenna array pattern. First a brief state-of-the-art is presented, then a model for this phenomenon is presented theoretically and validated both by simulation and measurement.

Chapter 4 evaluates the developed work, pointing out victories and shortcomings, alerting for possible improvements. A final note is given toward the possibilities of future work.

The author wishes the reader to pleasurably flow through this document, enjoying not only the presented work, but also the reading experience. The very best hopes are that the reader finds something new in this work, and even if that is not the case, a critical mindset and advice for improvement are expected.

Chapter 1

Next-Gen Wireless Communications: An Overview

1.1 Introduction

Before diving into technical work it is important to understand the present conjecture of telecom services. Why are disruptive reforms required in next generation wireless communication services? Understanding this was the major propeller toward the definition of a pathway for this MSc dissertation, giving purpose to the developed technical work. This chapter is dedicated to the portrayal of such conjecture, emphasizing its cornerstone role in the developed work, presenting the reader with some contextualization.

This dissertation is, in its broadest scope, about the comprehension of the requirements and the implementation hazards of analogue RF transceivers for beyond 5G wireless communications. So, in order to perceive the required RF solutions, the following discussion is mostly shifted toward the scrutinization of the presented proposals in terms of hardware implications.

Some important questions must be raised... What requirements are demanding for such radical changes in the telecom infrastructure? What plausible technological solutions have been proposed? What are the major implementation challenges to be faced? What shortcomings can be foreseen? Is this merely a research topic or are manufacturers on the edge of the developments being carried out toward a new generation of mobile telecommunications? Answers, supported by research and technical documents, are presented in the following sections.

1.2 5G: Demands for Next-Gen Wireless Communications

The evolution of wireless telecommunications can be viewed as a continuous attempt to grasp aspects of the real world experience, embed them in the cellphone and provide them as a service to every interested user. In the beginning, telecom services merely included phone calls and messages, which, at the time, was a major breakthrough that improved mail response time from weeks to instants, and enabled distant users to speak as if they were in the same room, independently of their location. Meanwhile, more services, such as MMSs and video calls, have been added to wireless communications. The Internet alone opened the door for a new world of service opportunities, and in present day there is a real world counterpart for every institution

or service available at the app store. One can access and be identified by governmental, legal, financial and banking institutions through the mobile network. Mainstream media had to reinvent itself because people are now using phones to get informed. With a smartphone one can do groceries, holiday planning, housekeeping... People are replacing personal computers by a smartphones. Everything can be done using a smartphone! In a way, it can be said that on the contrary to the early days, where providers tried to convince users about the value of their telecom services, in present day it seams that the users are the ones who are demanding ever more challenging services to suit their needs, and providers are the ones who are struggling to comply.

Due to the utility provided by mobile networks, the number of traditional wireless devices is growing exponentially [1], being common for a single user to have multiple phones. This is exponentially intensifying the demand for data rate heavy traffic like 4K video streaming. Such trend is expected to prevail and raises concerns about the congestion of existing mobile networks.

Besides the growth in traditional devices, mobile networks are expanding toward new kinds of terminals and applications. Among these are virtual reality applications, which require high throughput and low latency, and safety and medical applications, which traditionally relied on high fidelity wired connections and are now embracing wireless [2], looking to profit from their almost ubiquitous features. This stresses the mobile infrastructure to provide high reliability links, something it was not initially designed to do.

Smart technologies are yet another newcomer to mobile, i.e. smart-cities, smart-grid, smart-roads, smart-vehicles and so on... These technologies act based on real world events, so they require real time operation to optimize user experiences like household maintenance, power consumption or reduction of traffic fatality. Smart tech, like smart-roads and vehicle-to-x communication, pressure the network for links with very low latency and high reliability, requesting access to high throughput cloud computing to guarantee user safety [2], once again pushing the limits of the existing infrastructure.

Large amounts of data are required to support smart tech; sensors are required to collect data; to make sensors smarter they must be connected to the web. With this emerged the Internet of Things (IoT) concept. IoT, in its core, consists in placing low cost and low power sensors in everything, allowing the network to access any real world data it might require. IoT will skyrocket the number of wireless terminals. Considering that even pieces of clothing will have at least one IoT sensor, one will easily find over a thousand devices connected to the web in a single household. Even though a well defined number cannot be determined, it is certain that IoT will be massive. Some predictions point to twenty five billion IoT devices connected worldwide [3]. This raises the question: how to provide service to so many terminals? A single Base Station (BS) will have to service about ten thousand devices [1], something that clearly surpasses present capabilities. Additionally, IoT sensors are typically low rate devices. This raises the question: how to avoid network congestion? For few byte transmissions, the protocol burden of traditional wireless communications generates overhead and congestion while almost no service is being provided [1]. These technical challenges must be overcome before a sustainable IoT implementation is possible, which is a cornerstone of next-gen wireless communications. IoT is one of the major forces pressing for architectural reforms in wireless networks.

As was evidenced in previous paragraphs, the concept of what is a mobile device has broadened far beyond the cellphone; the distinction between mobile cellphone users and wireless Internet users is rendered futile in the view of next-gen telecommunications, where both

are viewed as terminals serviced by a given BS in a heterogeneous network. This heterogeneity raises new problems because each type of terminal will have different optimal performance criteria. The nodes must be capable of dynamically adapting features, such as transmitted power, data rate and protocol, to the terminal in order to enhance link quality and improve overall network capacity [2]. In present architectures nodes can't have such flexibility.

As the reader might already have realized, to comply with the massive demands described in the previous paragraphs modern wireless networks require massive improvements. The total rate provided by the network, the aggregate rate, must increase a thousandfold while the worst rate serviced to a given terminal, the edge rate, must improve a hundred times [1]. Link latency must drop to a millisecond, this corresponds to a order of magnitude decrease [1]. High fidelity links must be supported. BSs must evolve to provide service to large number of devices while being flexible enough to best service the heterogeneity of existing terminals. To achieve all of these requirements, the incremental approach used in LTE doesn't seam to cut it; especially when considering that spectral efficiency must improve fiftyfold when compared to 4G and that mobile bands have scarce available spectrum [1, 4]. This is probably the major weakness of current architectures, because, as is stated in [4], the demand for wireless data will always increase, but the available RF spectrum is limited.

In summary, the current wireless infrastructure was stretched to its limits and it can no longer comply with emerging demands. So, as has been stress in this text, new technological solutions are required to suppress the evolving wireless telecommunication needs. The following section is dedicated the scrutinization of the most relevant solution proposed so far.

1.3 5G: Technological Solutions

A large spectre of technical challenges must be overcome to implement the architectural revolution that will make next-gen wireless telecommunications a reality. Reforms are required all the way from the hardware until the higher abstraction layers of the network. Therefore, this is an optimal time for technological innovation and the rise of out-the-box ideas. This telecom renaissance is what this section is about.

Among the innovative solutions is local-caching, which has been proposed to deal with the growing number of traditional mobile devices and their demand for heavy throughputs [2]. Local-caching consists on storing the most trending web content on the BS side, and then, when it is requested by the user, transferring them as fast as possible to the terminal device, where it is to be stored while under use. This takes into consideration the increasing storage capacity available at the terminal side, and hopes to circumvent the typical transitions between abundance and deprivation of service in wireless communications.

However, additional technological solutions are required to enhance throughput to the extent described in the previous section. Among the possibilities is spectrum re-farming [4]. This consists on reorganizing legacy communication channels to free usable spectrum in the mobile bands. Spectrum re-farming has been pursued with small success, since the available spectrum is much smaller than required. Innovative solutions, like market-based spectrum allocation and spectrum sharing [1], have been presented to relax and optimize spectrum usage. The idea is that instead of having spectrum statically allocated, spectrum should be used by whomever is requiring it in a given moment. This virtually increases the available spectrum. The major shortcomings of such solution are bureaucratic barriers and some of the used techniques, like cognitive radio, that require large processing power and processing

times. So, the ultimate solution for the spectrum crunch in wireless telecom is to go up in frequency, specifically to millimetre wave bands [1]. In millimetre wave large bandwidths are available, allowing for channels with 500MHz bandwidth, which enlarges the 20MHz bandwidth channels existing in LTE in more than a order of magnitude.

Nevertheless, millimetre wave is just a part of the technological solution for enormous throughput. Three potential technologies in this regard are cooperative BSs, small-cell densification and multiple antenna access points [1, 4]. Cooperative BSs increase network capacity because they reduce inter-cell interference and enhance the handoff procedure. Small-cell densification, as the name suggests, consists in increasing the amount of BSs per area and reducing their area of coverage, this creates the so-called small-cells. Through densification capacity gains are obtained. The emerging multiple antenna technology is Massive Multiple Input Multiple Output (MIMO), which consists on using large antenna arrays in the BS and performing multiple adaptive beamforming. Each beam creates an independent link between the BS and the user terminal. Besides having orthogonal links for each user, Massive MIMO increases selectivity and reduces interference. All together, these factors make Massive MIMO the most promising technology for 5G and beyond applications, with the potential to provide massive throughputs to multiple users, giving a structure for the implementation of several other crucial technologies. So, its successful implementation is key.

The latency issue demands for the definition of more efficient protocols and for improvements in existing ones [1]. The best way to do this is yet undiscovered and no general consensual solution has been presented. However, specific solutions have emerged for technologies demanding high fidelity and throughput links[1]. Machine to Machine (M2M) communications is the most prolific of such solutions [2], being of special interest for industrial applications. M2M allows fast exchange of large amounts of data between machines without BS control. Besides reducing latency and providing the required redundancy to assure link reliability, M2M communications can be optimized using Artificial Intelligence (AI). This might improve factory production to an extent presently unpredictable, being a step toward the so-called device centric paradigm [2], where control is taken away from the BS and given to terminals.

Device to Device (D2D) communications is a technological solutions on the same line of M2M communications, but for low data rate devices [2]. D2D allows direct communication between devices, reducing several hops to a single hop. This way, low coding efficiencies associated with this kind of communication are overcome. As a consequence, path loss and interference are reduced. This results in lower power requirements for communication, which in an IoT scenario reduces battery drain and allows Wireless Power Transfer (WPT) solutions to be incorporated. All these benefits enabled by the D2D are essential for a sustainable IoT, but the question of how to incorporate uplink and downlink procedures in this solution is still unanswered. Besides this, a bigger question must be addressed when talking about IoT: how can such a massive number of devices be supported? Internet of Space (IoS) solutions have been proposed to answer this [3]. IoS uses satellites to provide worldwide Internet coverage, aiming mostly to provide web services to less developed countries and remote locations. IoS is considered a key enabler technology for IoT, because of its ubiquity and the inherent flexibility. IoS can be specifically tailored to support large numbers of low data rate terminals.

Another matter that deserved special attention from techies was how to improve the flexibility and adaptability of nodes in such a heterogeneous network environment. Centralized Radio Access Network (C-RAN) technology uses the optical fibre infrastructure to decouple

[1] Applications like control, safety, medical and smart-vehicle applications.

service distribution from the end user. Data is carried indiscriminately and C-RAN operates in the same manner if signals are to be distributed through copper or wirelessly. Such features make C-RAN the skeleton to address the flexibility and adaptability issue. C-RAN allied with virtualization technologies, such as Software Defined Network (SDN) and Virtual Network Function (VNF), decouples nodes from hardware [1, 2], allowing hardware allocation to be optimized for each terminal using selection metrics which can be controlled by AI.

So far, an overview of the most promising technological solutions for next-gen wireless communication has been presented. However, as stated previously, this work mainly concerns with analogue RF transceivers for beyond 5G wireless communications. As such, more focus will be given to the technologies that will demand the most radical changes in the hardware infrastructure. Special attention will be given to small-cell densification, millimetre wave, Massive MIMO and IoS, which are not only the most revolutionizing technologies in terms of hardware, but are also considered 5G key enabler technologies in several reference articles [1, 2, 3].

1.3.1 Small-Cell Densification

Making cells smaller and increasing the number of nodes per area and per Hertz is a classical approach to increase communication capacity[2]. Innovative ways of producing densification, such as D2D and Massive MIMO, have been theorized in the perspective of 5G. Small-cell densification, however, remains true to the classical approach to solve the capacity issue.

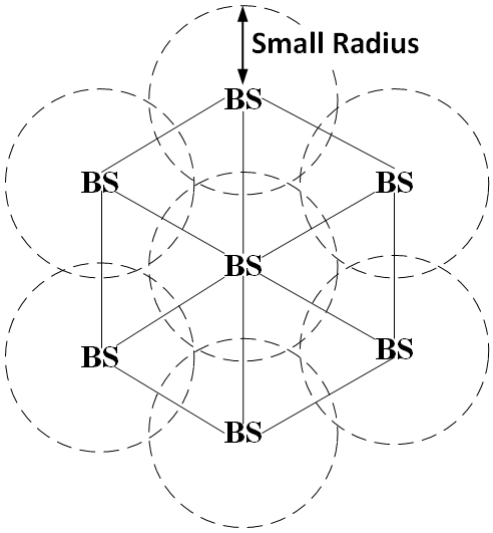

Figure 1.1: Conceptual representation of Small-Cell Densification.

More explicitly, small-cell densification proposes a large increase of BS density while reducing area of coverage. This practice bring some obvious benefits, especially in very crowded metropolitan environments. Firstly, because densification increases spatial re-usage. This optimizes usage of available sprectrum [1]. Secondly, because the BS covers a smaller area, it will, in principle, serve less terminals. Therefore, each cell provides its backhaul connec-

[2]This is what is usually meant by densification.

tion to less devices, allowing each terminal to request higher data rates [1]. With proper dimensioning, small-cells increase service while maintaining interference levels controlled.

The problem lies precisely in the aforementioned point, the dimensioning. Densification must be planned with care in order to guarantee capacity gains. This implies balancing service providing, interference levels and cost-effectiveness. The move to millimetre wave is the best choice in terms of gains, boosting small-cell densification capacity gains far beyond unity [1]. However, millimetre wave demands short cell radius, optimally radius can't pass 200 metres [5]. This raises hardware problems.

Although millimetre wave bands have enormous potential, millimetre wave technology has non-trivial handicaps both in terms of reliability and cost, especially for mass production applications. Both aspects must improve, otherwise implementing densification becomes infeasible at such bands. This urges for improvement and further developments in silicon, Integrated Circuit (IC) and System on Chip (SoC) solutions for millimetre wave [6], as well as improvements in measurement equipment and techniques for millimetre wave applications [7].

1.3.2 Massive MIMO

Massive MIMO is one of those out-of-the-box ideas where a radically novel wireless infrastructure is proposed. It emerged from the innovative environment of the mobile reform. It is so well thought out that it has been in the 5G discussion since the beginning [1]. Massive MIMO ranges all communication layers. The amount of changes proposed is so very large that the discussion must be narrowed down. The focus here is on the technological essence of Massive MIMO as well as its major benefits and challenges. Emphasis is given to hardware implications.

Massive MIMO proposes a BS with a very large antenna array with low power Power Amplifiers (PAs) integrated in each element. The BS serves a constant number of terminals in an M to K configuration, where M is the number of BS antennas, which tend to infinity, and K is the number of single antenna terminals. The array is capable of performing multiple adaptative beamforming, i.e. the array can direct the radiation pattern maximum of each beam toward the desired terminal while placing nulls in the location of the remaining ones [1, 8, 9]. In summary, the array performs spatial multiplexing. This allow the BS to feed different signals to different terminals using the same time-frequency resources. No prior knowledge or assumption is made about the channel. Channel State Information (CSI) is obtained though uplink and downlink protocols using orthogonal pilot signals [9]. Contrarily to Long Term Evolution (LTE), reciprocity is assumed and only the BS acquires CSI. This modification enables Massive MIMO to be scalable. As the number of elements of the BS array increase, the channels supported by the BS become statistically independent, i.e. cross-products between propagation vectors increase slower than self-products [1, 4, 9]. In other words, propagation vectors become uncorrelated as the number of elements in the array increase, and, as a consequence, interference is attenuated and signal power is improved, enhancing Signal-to-Interference Ratio (SIR). This allows the use of linear precoding and linear decoding techniques, lowering the cost and complexity of the implementation.

This new architecture is packed with benefits. The use of spatial multiplexing increases spectral efficiency, data rates and overall network capacity without densification [4]. The use of highly directive arrays reduces interference and circumvents the effects of uncorrelated noise and fast-fading present in the communication channel [9]. The excess of degrees of freedom available allow lower quality hardware to de used, increase robustness against jammers and

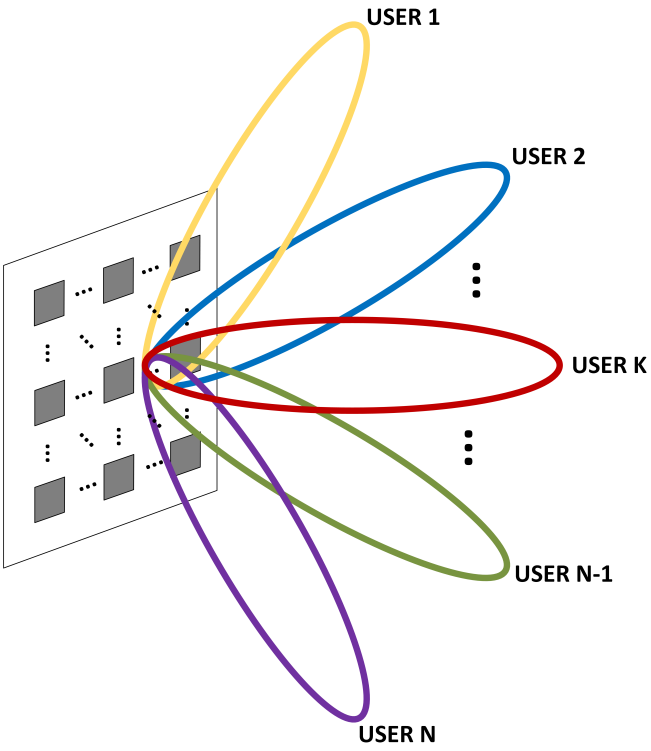

Figure 1.2: Conceptual representation of Massive MIMO theory.

can simplify the MAC layer [2, 8]. This enables the implementation of simpler transceiver architectures that transmit power more efficiently and have lower sensitivity. Therefore, transmitted RF power can be reduced [8]. Additionally, Massive MIMO performance can be enhanced by moving to millimetre wave. By doing this, interference is further reduced and miniaturization helps with the portability of the solution [1]. However, along with the impressive benefits of Massive MIMO come challenging problems that must be solved, some related with the theory it self, and others related with the hardware solutions required.

A foundational shortcoming of Massive MIMO is its need for a large null space to produce the desired spatial multiplexing. However, small-cell densification appears to provide the required null space, making it a Massive MIMO key enabler technology [1]. Another troubling issue of the Massive MIMO theory is pilot contamination. As explained before, pilots are signals used to acquire CSI during the uplink and downlink protocols. In a given cell, pilots are orthogonal, this means they retrieve uncorrelated information to the BS. However, pilots must be reused along cells, causing links from different BS to be correlated. This produces intercell interference, which critically harms the potential gains of Massive MIMO [1, 2]. Some unconvincing solutions, such as less aggressive pilot reuse and cooperative BSs [9], have been presented to solve this, but new solutions are desperately needed. CSI acquisition procedures also raise issues related with pilots, threatening to reduce the number of users that can be served. The problem is: what portion of the uplink and downlink protocols should be allocated to CSI acquisition so that communications are efficient? The goal is to eliminate overhead. Warm debates about Time Division Duplex (TDD) versus Frequency Division Duplex (FDD) and about what kind of waveform should be used in 5G are aiming to solve this issue.

In terms of hardware, challenges arise not only from the difficulty of the design itself, but also from the need to keep cost-effectiveness in a design that will be reproduced in large scale. Massive MIMO is demanding a completely new transceiver design philosophy where the PA, the antenna, the electronics and the processing unit should be integrated and operable like legos, in other words, transceivers must be modular ICs [4]. An issue that arises in large active antenna array design is coupling, especially when there is a need for integration, because this means that isolating components such as isolators and circulators must be removed [10]. This, allied with increased nonlinear effects, demands for complex compensation procedures, such as digital pre-distortion [10, 11]. A scalable solution demands low cost, low power and reliable components. The issue is finding components that balance these three features, particularly when the move to millimetre wave and the implementation of small-cell densification are important to unleash the full potential of the Massive MIMO proposal. The initial predictions about the use of lower quality hardware seem too optimistic, and the lowest quality hardware acceptable in term of I\Q imbalance, phase noise and quantization noise still imposes limitations in terms of cost and power consumption [8]. In summary, further hardware developments are required until a scalable integrated Massive MIMO solution is available in the market.

Although many challenges have to be overcome before companies decide to invest in this new architecture in detriment of the existing one, the transition seems unavoidable and it is of utmost importance that when that happens low cost, low power and reliable integrated hardware solutions are available, especially at millimetre wave bands.

1.3.3 Millimetre Wave

One of the most critical issues in the present day wireless communication scenario is spectrum shortage. This shortage in mobile bands is so problematic that it is usually referred to as the spectrum crunch [7]. Meanwhile, millimetre wave bands have a lot of available spectrum in frequencies ranging from 30GHz up to 300GHz [1]. This raises the following question: why haven't mobile services moved to millimetre wave bands? Part of the justification is technological while the remaining part relates with physical properties of millimetre wave. The major reason delaying the process is the lack of technological solutions that are both energy-efficient and cost-effective. The remaining reasons relate with propagation loss, atmospheric\rain absorption and blocking effects [1, 2] observed in the past for some implementations of traditional wireless communication architectures for non-mobile applications[3]. However, recent developments have addressed these issues and presented reasonable solutions for most of them, moving a step forward toward the use of millimetre wave in mobile applications.

Technological developments in semiconductor technology are the main propeller for the millimetre wave dream [1, 5, 6]. Those allowed for important cost and power consumption reduction. Thanks to these technological improvements, researchers now think it is plausible to implement large millimetre wave antenna arrays to keep antenna aperture constant with frequency [1, 2, 5, 12]. This eliminates the path loss dependence with frequency, thus eliminating the path loss problem in millimetre wave bands. Atmospheric and rain absorption effects become irrelevant in the small-cell densification paradigm, where ranges between cells are smaller than 1km [1, 5]. These phenomena actually improve small-cell performance be-

[3]Examples of this are satellite applications and terrestrial astronomical observatories.

cause they reduce inter-cell interference, and whenever absorption effects become more severe large antenna arrays will effectively overcome that by collecting and steering energy more efficiently [1]. With these advancements, the study in [12] already presents a functioning prototype operating at 28GHz carrier frequency, with 500MHz bandwidth divided in classical mobile 20MHz channels. The experience reveals good starting results in terms of range, data rate and mobility, even for Non-Line-of-Sight (NLoS) scenarios. These are promising results enabling the future of millimetre wave wireless applications.

Besides the obvious benefits in terms of bandwidth, data rate and miniaturization, millimetre wave brings several other not so obvious advantages. Among these is reduced interference [1, 2], that in millimetre wave has an on-off behaviour due to blocking. This might allow for the design of solutions mostly limited by noise, instead of interference. Another advantage of millimetre wave is its homogeneous behaviour when compared to present mobile bands [5]. Between 700MHz and 2.6GHz there is a total difference of three octaves. In millimetre wave a bandwidth of 2GHz represents marginal percentile variation over the carrier, this translates into similar characteristic over bandwidths larger than the total spectrum allocated to mobile in present day. In addition to the inherent gains related to these frequency bands, moving to millimetre wave brings the bonus gain of enhancing other technologies important in the 5G and beyond path, such as small-cell densification and Massive MIMO.

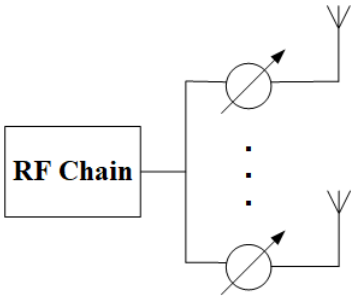

Figure 1.3: Analogue beamforming architecture.

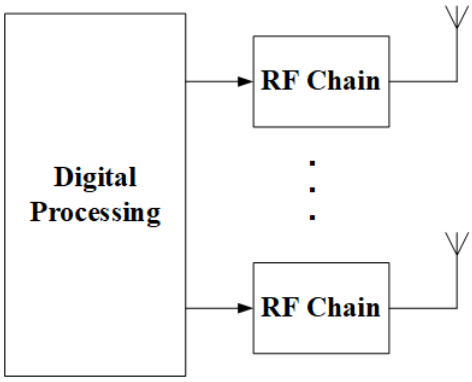

Figure 1.4: Digital beamforming architecture.

Even though millimetre wave is very promising and several hurdles have already been passed, there are still many challenges to be faced. Hardware impairments keep on bringing big challenges [1, 2, 12]. There is still a lack of cost-effective components for telecom

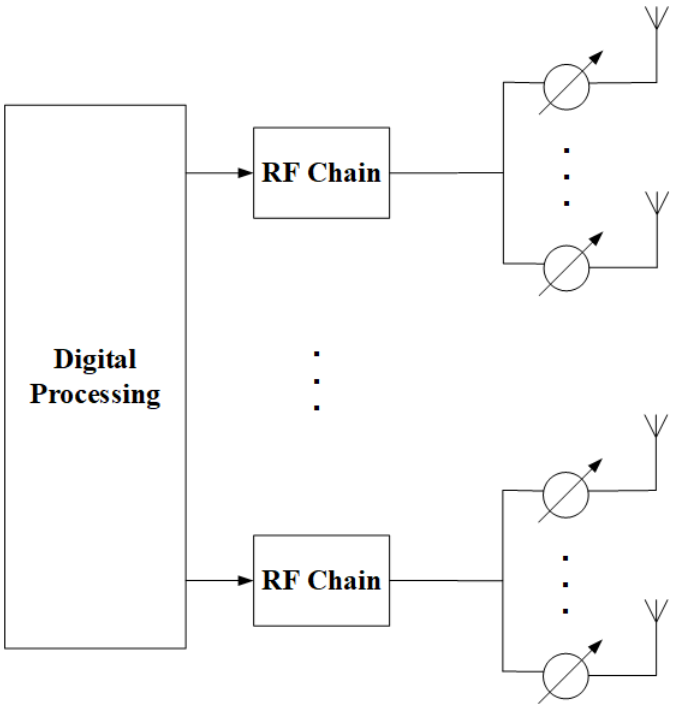

Figure 1.5: Hybrid beamforming architecture.

applications requiring massive globalized infrastructures. Low precision is a crippling defect of millimetre wave hardware which introduces high phase noise. This is very limiting when large phased arrays must be implemented because such arrays must be capable of performing beamforming, i.e. controlling the amplitude and phase of each element of the array in order to form the desired beam characteristics and aim it towards the desired direction. Traditionally this was implemented using an analogue architecture like the one presented in figure 1.3. This solution is of low complexity and low costs, since only one RF chain is required and the analogue components, like phase shifters, are more cost-effective than digital ones. However, such architectures rise rapidly in complexity when bi-directional communications are required or when multi-beam features are desirable [13, 14]. Therefore, digital architectures like the one presented in figure 1.4 have been proposed. Digital architectures implement one RF chain per antenna element, allowing for simple adjustment of the phase and power of each antenna. The higher degree of freedom brought by digital architectures allows flexible transmission and reception, simplifies the implementation of multi-beams and offer better control of large bandwidths than analogue architectures, making digital architectures highly desirable for implementing Massive MIMO solutions [13, 14]. However, when talking about millimetre wave applications, the cost and energy consumption of digital and mixed signal components, particularly of RF DACs, becomes prohibitive in the scenario of mobile communications, making digital beamforming architectures impracticable [1, 12, 13]. Therefore, hybrid architectures, like the one shown in figure 1.5, are the only viable beamforming solutions for millimetre wave applications. It has been shown that cost and energy consumption highly decrease when using this architecture, and that even though the number of implementable independent beams reduces in hybrid architectures they can still provide a good trade off between complexity and spatial multiplexing capabilities. The best way to balance and interconnect the analogue

and digital components in millimetre wave beamformers is still a state-of-the art debate and further improvements in semiconductor technology are mandatory to finally overcome these shortcomings.

On the list of major challenges, along with hardware impairments, are blocking effects. As said earlier, blocking effects aid in reducing interference. This happens because communication links become very directional with large arrays, and interference between links only happens when different terminals are in line or when moving terminals cross each other. On another hand, blocking effects absorb reflections and prevent transmission through obstacles. Therefore, if the desired communication link is obstructed by a given obstacle the signal will be blocked, aggravating the typical link transition from usable to unusable. This is so critical that sensitivity is expected to be mostly determined by blocking effects [1]. Workaround solutions might be required to circumvent blocking. Data showers, repeaters and access points in borders between indoor and outdoor environments are among the proposed workarounds [5]. Quick processing algorithms to detect blocking and correct beamsteering are another alternative [2]. While a definite solution isn't found, technologies like local-caching become evermore relevant in the millimetre wave scenario.

In short, there is a lot of work to be done in order to unleash the full potential of the millimetre wave solution that is so beautifully portrayed in reference papers.

1.3.4 Internet of Space

Internet of Space aims to make large bandwidth internet available everywhere in the world, particularly in remote locations and less developed countries. IoS is also anticipating a solution for the stress and congestion that wired and traditional wireless networks will suffer when IoT becomes massive.

The idea is the following: use low cost Low Earth Orbit (LEO) satellite constellations to cover the whole globe and provide internet services. The solution can be tailored toward specific regional goals. Deployments can be launched to space at high volume and low cost. This infrastructure will allow latencies to be reduced in some regions of the globe while providing an omnipresent home for IoT applications. Even though these are desirable features, IoS also brings some technical difficulties. Satellite tracking[4], synchronization and handoff mechanisms are among those challenges. Despite this, an encouraging fact is that some LEO constellations have already been projected for IoS, detailing electronic and economic requirements [15], giving good indications towards the deployment of IoS.

However, the major impediment of IoS implementation is hardware, like in most 5G key technologies. Developments in large phased arrays and CMOS technology for millimetre wave band are viewed as key enablers for the IoS implementation, as it requires these technologies to be affordable [3].

1.4 5G: Challenges & Shortcomings

In previous sections, both 5G demands and technological solutions have been presented. This section now addresses the 5G challenges and shortcomings, endeavouring to explain the most critical problems in a brief text, alerting, once again, for hardware issues, aiming to complement the previously presented information. A good overview of generic 5G implementation

[4]LEO satellites have fast orbits that must be tracked in order to communicate correctly.

challenges is presented in [1]. How to assure retro-compatibility in a multiple radio access technology scenario is one of the touched issues. Another issue is how to support mobility when fast vehicles, such as cars and trains, are introduced in networks while new principles are being considered. But in this section the focus will be on more transversal problems such as energy, cost, standardization and hardware.

The energy and cost problems are related. Considering the massive data rate increase in 5G, Joule per bit costs must be reduced a hundredfold in order to make 5G technologies affordable. Besides the need to reduce energy costs, there is also a need to increase energy efficiency. Existing power options wont be capable of powering the increasing data rates without more energy efficient technologies. This is particularly important in the BS hardware, because most of the 5G proposals are concerned with improving transmission efficiencies, neglecting the possibility of increasing power consumption in the BS due to increased data rates and increased processing complexity. Some ideas to reduce energy consumption have been presented, such as reducing data rates and switching off unused BSs, but these are non-ideal solutions. Ideally, hardware should be optimized to the point in which renewable energies could be considered a viable powering alternative.

The cost problem, however, goes beyond the energy problem. Costs rise up dramatically when the implementation of small-cell densification and Massive MIMO in millimetre wave appears to be the the best possible long-term infrastructure for the 5G implementation. This demands drastic cost reduction in millimetre wave hardware. Such cost reduction is one of the most challenging aspects of implementing 5G. While costs don't drop, joint ventures, like infrastructure sharing, seem to be the only alternative to allow the first test-bed BSs to be deployed. Another aspect in which costs can be shared is in the circumvention of licensing fees. This is important because exclusive channels and exclusive networks make present mobile communications very inefficient, and the open-access concept is an important enabler of the potential of small-cells, however, this will be one of the major bureaucratic issues to be overcome in 5G.

A crucial step toward the implementation of 5G is regulation and standardization. The completion of this step gives a sign that the technological proposals have matured enough so that detailed guidelines for commercial implementation can be defined. Even though this is an important step, the move towards regulation and standardization has come much later than the initial 5G proposals [1]. Among the most relevant institutions in this matter are the International Telecommunication Union (ITU) and the 3rd Generation Partnership Project (3GPP) [16]. While 3GPP mostly deals with 5G operation, ITU deals with spectrum allocation. 3GPP has divided its approach to 5G in two phases. By the end of phase 1, in September 2018, a stand-alone version of the first 5G guidelines will be available in release 15, the so-called 5G New Radio (5G-NR). Phase 2 will be concluded by the end of release 16 in 2019. ITU developed the International Mobile Telecommunication 2020 (IMT-2020) program to study the 5G hypothesis [17], and is now settling the agenda for the World Radiocommunications 2019 conference, where deliberations about 5G spectrum will take place. In these programs, several detailed guidelines have been produced for the implementation of reasonably well-developed technologies, most of them concern C-RAN and the allocation of new bands to mobile telecommunications. However, for more under-developed technologies, such as active antenna arrays for millimetre wave Massive MIMO, only very general guidelines were released. These technologies, in some articles, are already mentioned as beyond 5G technologies, and ITU already launched an IMT-2020 and beyond program [18]. This, once again, urges hardware engineers to speed-up their research on millimetre wave applications, as these

are an important part of future mobile communications and regulation and standardization procedures are slow and complicated challenges.

1.4.1 Hardware Challenges

The architecture designed for 5G brings new hardware challenges, including a new design philosophy, large active antenna arrays and densification. Some of the technological challenges have already been presented in previous sections. Here, more universal hardware hazards such as coupling, nonlinear behaviour and measurement, are addressed. This distinction is necessary because these problems are catalysed by the move to millimetre wave, especially in this new mobile architecture.

1.4.1.1 Coupling Effects

When an Electromagnetic (EM) wave impinges on an antenna it can be absorbed, reflected or partially absorbed and partially reflected. This depends on the antenna impedance, that can be matched, completely mismatched or slightly mismatched to the impinging wave. If multiple EM waves impinge on an antenna the same outcomes are possible, however, the antenna will only be matched if the superposition of the impinging waves causes matching, i.e. only an absorbed wave results from superposition, or if the receiving antenna generates a compensating EM wave to cancel the reflected wave resultant from superposition, thus forcing the antenna to be matched. When observed from the antenna terminal this can be interpreted as a variation of the antenna impedance. The impedance measured in a controlled environment is referred to as the passive antenna impedance, while the impedance seen from the antenna terminal when multiple EM waves impinge on it is called active or driving antenna impedance [19]. In an array this sort of multiple EM wave interference happens between array elements and is called mutual coupling. Mutual coupling exists both in transmitting and receiving mode, because leakage radiation will interfere in the surrounding elements when an element is transmitting, and reflections form each element will interfere on neighbouring elements when receiving. The coupling phenomenon is best explained in [19, 20].

Coupling changes the behaviour of the array, degrading directivity, side lobe level and radiation efficiency. However, the most jeopardizing effect of coupling in the array performance concerns scanning, because it creates the so-called array blindness [21], making some angles impossible to scan due to unitary reflection coefficients, causing all transmitted and received EM waves to be reflected in that particular angle. Besides the problems caused on the array it self, in a communication system, coupling degrades the performance of the complete transceiver chain, changing the point of operation of amplifiers, mixers and mixed signal components, causing efficiency loss and signal degradation.

The complexity of the coupling problem impedes it from being generally well understood theoretically, and usually application specific analysis is required because coupling will depend on the antenna elements used. The case of very large uniform arrays is a rare exceptions where coupling effects can easily be explained theoretically [19], because edge effects become irrelevant in this case. However, that is not the case in most practical scenarios, and because of this complexity, traditional wireless communication architectures avoid dealing with coupling effects by introducing isolators in the RF chain that "kill" the feedback effects of coupling, thus protecting the transceiver. However, in the millimetre wave 5G perspective solutions must be integrated, there is no place for bulky and expensive components such as isolators.

This forces RF engineers to deal with coupling effects and find alternative solutions, making coupling one of the major hardware problems to solve in the near future.

1.4.1.2 Nonlinear Behaviour

The major source of unwanted nonlinear behaviour in wireless telecommunication systems is the PA. PA design is projected based on well defined input and output loads in which PA performance depends; typically 50 Ω are considered as the reference load. As explained earlier, the need to use large active antenna arrays and remove isolators in 5G applications leads to significant coupling effects. Coupling will modulate the load seen from the PA output, thus changing efficiency, output power and nonlinear distortion; causing overall signal deterioration. This is manifested through EVM degradation.

The compensation of unwanted behaviours caused by coupling effects is a major challenge being addressed in current state-of-the-art RF research. The study in [10] presents a Digital Pre-Distortion (DPD) scheme to compensate coupling effects. However, DPD scales poorly with array size. To solve this issue [11] proposes a technique which reduces the number of required DPD blocks. Despite that, [22] shows that DPD cannot achieve maximum efficiency for advanced PA configurations. A characterization method using DC and RF models is also presented, analysing the extent of the impacts of coupling in transmitter performance. However, millimetre wave oriented research on this topic is scarce, being the study on [23] a rare example. This shortcoming must be addressed soon.

Beyond the added difficulty brought by coupling effects, 5G revolutionizes PA design by shifting toward a new philosophy. A single high power PA is replaced by several low power PAs attached to antenna array elements. This might not change the traditional design goals: high efficiency, high linearity and maximum output power; but will very likely change the way to achieve those goals. To add to this, if high PAPR OFDM waveforms are to be kept in 5G, these PAs must support them [1]. This implies designing PAs with high dynamic range, forcing the typical design trade-off between linearity and efficiency. A novel PA design challenge, however, is understanding and taking into consideration the impacts of signal distortion in antenna array metrics such as side lobe level, directivity and most importantly scan angle. This is relevant due to the central role of spatial multiplexing in 5G, so it is inadmissible to allow signal distortion to cause array pattern distortion. Noting the importance of this, the study on [24] already presents a model capable of predicting the far-field of arbitrarily sized active antenna arrays with low computational effort, but there is research shortage on this multidisciplinary problem.

The problems raised in this section and in the coupling section evidence the challenging interdependence of PA design and antenna design in this multidisciplinary 5G scenario. Giving an indication that PA designers and antenna designers will have to work more cooperatively in the future, or even merge their specialities.

1.4.1.3 Measurement

Measurement is crucial in design, certification and regulation activities. As with most hardware aspects, performing high quality measurements is getting harder in the perspective of millimetre wave 5G. The National Institute of Standard and Technology (NIST) of the United States explains exactly that on their overview article about the work they have been developing on millimetre wave characterization [7]. This paper stresses the importance of hav-

ing low uncertainty characterization of signals, devices and Over the Air (OTA) measurement procedures. This section, based on these studies, alerts the reader for the major measurement challenges in millimetre wave.

High reliability signal measurements are required to accurately characterize signal distortion. As with any measurement, signal measurements are susceptible to errors. Signal miss-characterization might occur due to the frequency response, impedance effects, interleave errors or nonlinear behaviour of the measurement equipment. These errors scale with frequency and are particularly critical in the large millimetre wave bandwidths aimed for 5G. This is portrayed in the NIST studies, where significant variations of an oscilloscope frequency response are verified in 1GHz of bandwidth at a 44GHz. In these millimetre wave bands, the quality of measurement hardware is similar to the quality of the hardware of a given design, thus demanding careful characterization and calibration of both measurement equipment and designs. Looking into signal characterization metrics, NIST considers EVM the most relevant metric, however, they alert for the difficulty of performing confident and traceable measurements, because DPD techniques are required to stabilize measurements, and because standard procedures for doing that don't exist, making measurements difficult to compare. The importance of EVM led NIST to propose an IEEE study group dedicated to solve EVM measurement challenges.

The availability of detailed transistor models, characterizing not only the transistor behaviour, but also its uncertainties, is fundamental to achieve first-pass PA designs. First-pass designs are even more crucial in millimetre wave, where production costs are exorbitant. However, large signal millimetre wave measurements must be performed to characterize the transistor and its uncertainties, so that transistor models and simulation tools to perform uncertainty analysis can be developed. Unfortunately, presently it is yet impossible to perform reliable millimetre wave measurements of the transistor's nonlinear behaviour. These measurements are the basis of traditional PA design. Device characterization is a big challenge that, if not overcome, will force PA designers to change their approach.

OTA characterization procedures gained relevance due to the increased importance of active antenna arrays in the 5G scenario. Therefrom emerged the need to acquire signal traceability from free space measurements, because now antenna terminals are no longer available. OTA characterization procedures are based on antenna metrics such as gain, polarization and far-field radiation pattern. These measurements are mostly performed in near-field. Near-field measurements are highly dependent on probe positioning, so there is a need to understand how to use OTA probes to minimize errors. To address this, NIST developed a robotic arm to position the antennas. This experimental apparatus is capable of performing OTA characterization, but antenna terminals are also accessible. By comparing OTA results with direct measurements NIST found that OTA characterization is highly dependent on the quality of the transmitted signal, the channel and coupling effects. To circumvent these issues NIST proposed using reference fields, however, they recognise that this is a sensitive issue that requires more work both on the OTA characterization systems and on channel modelling. Overcoming these challenges is mandatory for the implementation of future wireless telecommunication systems since OTA characterization will be the primordial means of understanding system performance.

1.5 5G: Manufacturers' Perspective

Until this point several research aspects related with 5G demands, 5G technological solutions and 5G challenges and shortcomings have been considered, giving special emphasis to the hardware problems of millimetre wave and Massive MIMO proposals. These are considered cornerstone technologies in the 5G scenario by researchers, but what about manufacturers? It is important to analyse their alignment with researchers and to understand to what path they will commit, because whatever manufacturers decide to do will inevitably influence the course of future wireless communication systems.

From a brief search, it is observable that renown manufacturers, such as Analog Devices, Huawei, Keysight, National Instruments, Qorvo, Qualcomm and Rohde & Schwarz, are very much aware of the 5G requirements and the importance of millimetre wave and Massive MIMO solutions in this scenario, having produced detailed documents explaining these theories to their costumers; there a typical 5G overview is usually presented. Some documents are mostly oriented toward designers, trying to provide them with useful design tools, while others are oriented toward measurement and calibration procedures.

In [25], Analog Devices presents an overview of the wireless telecom scenario, explaining the benefits and challenges of 5G, being aware of the tremendous work ahead and of the undergoing standardization programs. In the same document, they alert designers for the need to develop hybrid beamforming architectures for 5G applications due to cost and energy constraints. Challenges of such approach are explained, emphasizing the need for integrated transceivers that include both electronics and antenna in the same IC. In several documents, [6, 25], Analog Devices overviews millimetre wave semiconductor technologies available to design 5G Monolitic Microwave Integrated Circuit (MMIC) solutions, alerting for the need of powerful 3D modelling tools to achieve successful designs. Being aware of current developments and of the challenges ahead, Analog Devices promises to provide the required hardware solutions to designers. Analog Devices is also well aware of the urgency to develop measurement equipment for 5G, knowing that mere software improvements over existing equipment won't be enough [26]. They recognise the need to improve instrumentation hardware, which will be challenging without definite standard definitions, especially taking into consideration that the test and measurement industry recently invested heavily on the most recent LTE equipments [26]. To overcome this, they explain the importance partnerships have on the 5G implementation, giving as an example their strategic partnership with National Instruments (NI) [27]. Even though many challenges are to be faced, Analog Devices sees the evolutionary 5G environment as a highly exciting scenario to be a RF developer.

Huawei developed a website dedicated to their 5G accomplishments [28]. There they demonstrate awareness of 5G demands, benefits and challenges, showing their interest in being on the edge of developments by having renown researchers working on their teams and by integrating several worldwide collaboration projects to envision 5G. This way, Huawei hopes to be leading 5G innovation.

In [29], Keysight emphasizes the importance of reliable simulation data in cost-effective design and characterization of millimetre wave applications, compromising to develop simulation tools and real-time measurement tools to aid designers against challenges. In [30] and [13], Keysight and Rohde & Schwarz explain the OTA characterization techniques used to measure integrated active antenna arrays for Massive MIMO applications. Their major concerns are compliance with 3GPP guidelines and providing proper measurement equipment to characterize arrays OTA.

In the NI Trend Watch 2018 [31], National Instruments overviews 5G ambitions, evidencing the 3GPP effort to provide guidelines for 5G and the company effort to specialize in 5G fields of interest, denoting the increased complexity of 5G protocols, highlighting the architectural changes demanded by millimetre wave and Massive MIMO applications, and pointing out the importance of OTA characterization procedures and Software Defined Radio (SDR) in the 5G scenario. Their 5G Frequently Asked Questions (FAQs) page presents the evolution of mobile communication technologies, detailing the revolutionary aspects of 5G, revealing National Instruments' close contact to academic researchers [32]. NI reveals concerns in complying, understanding and spreading the 5G-NR releases, having several articles about 3GPP and ITU releases [33, 34], being aware of their standardization plan. NI also understands that the benefits of Massive MIMO outweigh the challenges, considering its implementation unavoidable in the 5G scenario [35]. Understanding the urgency of implementing Massive MIMO prototypes, NI developed hardware, systems and software to help designers in that sense [36]. To speed Massive MIMO even more, NI has partnerships with the universities of Bristol and Lund to develop Massive MIMO test-beds [37]. In another article [38], NI explains the heterogeneous 5G scenario, aware of the increased difficulty that the growing number of devices brings in terms of spectrum availability, making apparent the need for millimetre wave solutions. Comprehending the importance of millimetre wave in 5G, NI developed a modular millimetre wave transceiver based on SDR to help researchers in their prototype studies [38]. From this venture, NI understood the importance of SDR in the development of 5G solutions, so they compiled the most relevant SDR state-of-the-art in a single document to inform beginners and newcomers of its importance and potential [39].

Qorvo is concerned in presenting itself as an active part in the 5G scenario. In their website they evidence not only their technological solutions, but also their participation in standardization bodies [40]. Valuable information about semiconductor solutions for specific 5G applications can be found in this website. Qorvo's dedication to 5G is so great that they compiled 5G essentials in a textbook to introduce their costumers and newcomers to the 5G scenario [41]. Beyond the scenario explanation, this textbook explains how 5G will connect to 4G and lays out the main 5G milestones.

Qualcomm calls mobile the largest technology in human history, highlighting the transformative impact 5G will have on the society, comparing it to the impacts of the invention of the car and the invention of electricity [42, 43]. Because of this, Qualcomm alerts for the importance of global collaborations toward the 5G goal. The referenced documents present an overview of 5G, emphasizing the Qualcomm's role in the 3GPP standardization programs and their commitment to make 5G-NR a reality. In that sense, Qualcomm has developed the first 5G modem [44], focusing on IoT, millimetre wave and spectrum sharing as their major 5G-NR goals. For IoT, Qualcomm has developed documentation explaining how 5G-NR will improve the LTE support for massive IoT, announcing their chipset solutions for 5G-NR IoT [45]. Qualcomm is also leading the 3GPP meetings on spectrum-sharing policies, having detailed documents explaining spectrum allocation modalities and explaining the new opportunities of horizontal and vertical spectrum-sharing introduced in 5G-NR [46]. Qualcomm wants to make 5G-NR millimetre wave available in 2019, however, they are aware that the complexity of the design might delay commercial deployments. On the other hand, they are also aware of their chances due to technological advancements in silicon. To make 5G-NR millimetre wave a reality, Qualcomm performed major network coverage simulations and developed a smartphone prototype [47].

From this small snapshot, it is already perceptible that the vision of manufacturers seems

to align with the vision of researchers. This is a good indicator that in the near future the idealized 5G technological solutions might become a reality, even though there are still many challenges and shortcomings to be solved.

1.6 Workplan

1.6.1 Interpretation

In what concerns RF design for 5G applications, it can be stated that the presented solutions place active antenna arrays in the spotlight, elevating the importance of antenna arrays in the optimization of the RF transceiver, relegating the PA to a more secondary role in that regard when compared with previous mobile generations. The most relevant\capable solutions seem to be a combination of Massive MIMO, millimetre wave and small-cell densification, however, these solutions must become cost efficient, energy efficient and readily available in a short period of time. This seems rather unlikely because active antenna array transceiver design is very far from being a trivial problem, having several layers of complexity concerning antenna design, amplifier design, integration and characterization.

In 5G scenarios the antenna design is hampered by the move to higher frequencies, where expensive dielectric materials and more advanced techniques are required to achieve high reliability designs. This allied with the need for larger bandwidths makes the antenna design achievable only to a few designers. Beyond this, 5G antennas require the implementation of additional complex functions like phase and amplitude control to perform the multiple beamforming, beamsteering and adaptive beamforming features demanded by 5G solutions. These functions besides making the antenna array design more complex, also increase costs because expensive phase shifters are required to implement them.

The amplifier design must adapt to the new design philosophy planned for 5G solutions, having to support high PAPR signals while dealing with the additional challenges of higher frequency and larger bandwidth designs.

The integration of PAs and antenna arrays in a MMIC causes behavioural problems in both the amplifier and the antenna. While antenna coupling effects cause variations in PA performance, the PAs nonlinear behaviour also changes antenna array pattern properties. Besides functional problems there are technological problems associated with integration because the development of MMICs is a very specialized, complex and long procedure with considerable associated costs.

Before active antenna array transceivers can be deployed there is the need to further improve characterization methods, particularly OTA characterization procedures. OTA alone must be capable of accurately attesting the array performance and detecting malfunctions because with integration traditional characterization methods won't be available.

Besides these design and characterization challenges, the existing technologies also require further developments to allow energy efficiency to increase and costs to decrease.

From a careful analysis of the 5G scenario one can conclude that the shortcomings stated above are the most urgent issues that RF engineers must address. Otherwise it will be very unlikely that RF hardware will be available for future mobile communications.

1.6.2 Long-Term Vision

It has become apparent that there is a need to understand how active antenna array design can be improved to satisfy modern mobile communication requirements. Accurate characterization of all the integrating parts of the active antenna array as well as the capability to characterize and optimize its overall performance are essential to acquire this knowledge. With such knowledge it will be possible to define more informed design guidelines and to develop real-time optimization tools for the RF transceiver.

The awareness of the aforementioned led to the definition of several goals dedicated to the characterization of active antenna arrays, constructing a long-term vision to address the 5G issues at hand. These goals are now briefly stated:

- Research characterization methods for power amplifiers, antennas, antenna arrays and active antenna arrays.
- Study the impacts of the removal of isolators in active antenna arrays, focusing on the impacts of coupling in amplifier performance and on the impacts of nonlinear behaviour in array performance, aiming to understand how these effects limit active antenna array capabilities such as adaptive beamforming and multiple beamforming, striving to develop optimization methods to minimize these effects.
- Define guidelines to improve active antenna array design.
- Explore optimization techniques to enhance overall active antenna array transceiver performance.
- Understand how OTA characterization techniques can be used to characterize and optimize active antenna array transceivers in real-time based on system level metrics such as EVM.

1.6.3 Short-Term Approach

The mentioned goals must be broken down into smaller and more achievable milestones in order to reach the ambitions portrayed by the long-term vision. The time constrains imposed by the framework of a MSc dissertation forced the milestones to be more focused than the broader scope of the long-term vision. Because of this, and because of the crucial role of antenna arrays in next-gen wireless communications, the developed work was directed toward the design and characterization of nonlinear antenna arrays. The selection of this path was also influenced by the lack of state-of-the-art research on nonlinear antennas. Therefore, the short-term approach presented in this dissertation encompasses every step taken since the definition of the long-term vision until the validation of the nonlinear antenna array model.

This path contemplates both the understanding of basic concepts and the research of state-of-the-art topics, having the following major objectives:

- Understand the most important performance metrics of antennas and antenna arrays.
- Study, design and measurement of microstrip antennas and microstrip antenna arrays.
- Explore how antenna arrays can decrease sensitivity, increase selectivity and reduce interference, thus increasing channel capacity.

- Research how the introduction of an amplifier per element in antenna arrays can make them nonlinear, paying special attention to the impacts this might have on radiation pattern.

After having these milestones defined the experimental work could begin. Designs were tailored for the 5GHz band, a 5G interest band. Millimetre wave designs were desirable, but several limitations impeded such a path to be taken. The following chapters are dedicated to the portrayal of the developed work as well as a critical analysis of the obtained results.

Chapter 2

Antennas: Studies & Experiments

2.1 Introduction

Several 5G solutions have pointed out that the BS antenna must dramatically improve in the next mobile generation to comply with 5G demands, being Massive MIMO the major exponent of this idea. The ability to create statistically independent channels, the ability to reuse time-frequency resources through spatial multiplexing, and the ability to circumvent channel noise floor and fast fading are among the presented arguments toward the use of large antenna arrays in the next mobile generation. This would allow for greater selectivity, lower interference, lower sensitivity, which, as a consequence, allows for the transmission of lower power signals while increasing overall network capacity. However, these arguments are presented in an information theory perspective that is disconnected from the antenna itself. It is therefore difficult to understand how the antenna design might limit such gains. This reveals the need to understand what these buzzwords mean in antenna terminology; this is the goal of chapter 2. Here antennas are studied not only for the sake of understanding antenna theory and practice, but also to better understand the role of antennas in future wireless communications. To achieve this, the Balanis' introductory book on antennas, referenced in [20], was used as the main antenna theory reference, while the connection between antenna theory and 5G was established by comparing what was learned from Balanis to what was learned during chapter 1.

The antenna is the transducer between guided environment and free space, being the key component that actually allows wireless communications to exist. Antennas are therefore used to both transmit EM waves into free space and receive them back into a guided environment. Proper antenna design is fundamental as it allows other system requirements to be relaxed while keeping good overall transceiver performance. Improper design, on the other hand, can lead to energy storage instead of energy transportation. This can seriously limit range of operation and SNR. The importance of having good antennas was never neglected in mobile communications, however, in previous generations the antenna had the major goal of covering with the same signal as much of its surrounding area as possible, leaving the job of increasing capacity to higher levels of abstraction. Now antennas are viewed as a means to acquire capacity gains, therefore the concept of what is a good antenna design changes in 5G when compared with previous generations.

Chapter 2 now follows with a physical interpretation of important antenna metrics, aiming to understand the practical consequences of their values. Next microstrip antennas are

discussed. These are the most used antenna elements in mobile communications. Then the study moves to array theory where the aforementioned potential gains of antenna arrays are interpreted through the lens of antenna theory.

2.2 Antenna Theory: Important Concepts

Until this point antennas and their abilities have been mentioned countless times. However, what is an antenna? How can it be modelled? What are the metrics to evaluate its performance? These questions haven't yet been seriously addressed in this document. In truth, it has already been stated in the introduction that an antenna establishes the connection between guided environment and free space, being a means to transmit and receive EM waves. Physically an antenna is a combination of a metallic structure with some kind of dielectric material. Conceptually this constitutes the essence of what an antenna is, so lets start addressing modelling.

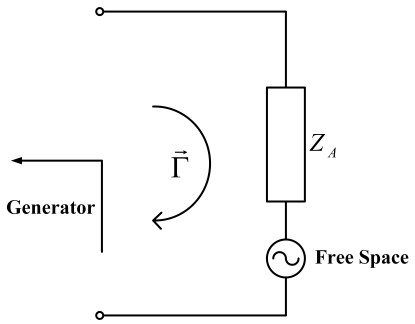

Figure 2.1: Basic Antenna Model.

The simplest, but yet more insightful[1], way to model an antenna is to interpret it as an impedance, as shown in figure 2.1 and as mathematically expressed by equation (2.1).

$$Z_A = R_A + jX_A \tag{2.1}$$

$$R_A = R_r + R_L \tag{2.2}$$

As evidenced by expression (2.2) the antenna resistance R_A is divided into two components, R_r and R_L. R_r represents the part of the power delivered to the antenna that is radiated, while R_L denotes the part of the power delivered to de antenna that is dissipated through dielectric or metallic losses. The reactance X_A represents the energy storing capabilities of the antenna. This simple model is elucidative of the fact that when using an antenna it must be matched so that the transmission\reception efficiency is maximum, making clear that the idealized maximum power that can be delivered to the load by the antenna is half of the available power at the source. In this case antenna efficiency is considered to be 100% as there are no losses due to reflection, e_r, or metallic and dielectric losses, e_{cd}. Antenna efficiency can be determined through expression (2.3).

$$e_o = e_r \cdot e_{cd} \tag{2.3}$$

[1] At least for an electronics engineer.

$$e_r = 1 - |\Gamma|^2 \tag{2.4}$$

This model also indicates the design goals: minimize losses, $R_L \to 0$, minimize energy storage, $X_A \to 0$, and optimize energy radiation, $R_r \to Optimum$, while matching the antenna, $|\Gamma| \to 0$. It should be stated that this is a rough approximation that doesn't consider important phenomena like dielectric and metallic losses in the ground plane, but it constitutes the perfect example to understand what is important in antenna design.

The model denotes an important antenna metric, input impedance, however, radiation properties aren't properly visualized through a modelling resistance, therefore, more comprehensive metrics exist to express them. The radiation pattern is a representation of the antenna radiation properties as a function of spatial coordinates in far-field. In mobile communications antennas usually operate in this field region.

Before further addressing the radiation pattern it is important to understand what is meant by far-field. As is known from EM theory, EM fields are distance dependent. This dependence is usually represented by a power series inversely proportional to distance, r. Therefore field configurations near and away from the antenna will differ. Equation (2.5) expresses this idea for the sake of visualization[2].

$$Total\ Field = \sum_{n=1}^{\infty} \frac{1}{r^n}\ Field\ (n) \tag{2.5}$$

In far-field high-order terms tend to zero, the EM field becomes proportional to $\frac{1}{r}$ and the field distribution only varies by a scaling factor, preserving its shape within any circumference taken along the same plane. This greatly simplifies the evaluation of antenna radiation metrics.

$$r > \frac{2D^2}{\lambda} \tag{2.6}$$

Equation (2.6) is used to determine the minimum radius away from the antenna in which far-field behaviour is dominant. D stands for the largest antenna dimension, while λ stands for the free-space wavelength in which the antenna operates. For this expression to be valid D must be greater than λ. It must be stated that perturbations of the EM source in near-field can change the far-field pattern and that different EM sources can generate the same far-field pattern.

Lets get back to the radiation pattern. From EM theory one can determine the average radiation power density generated by an antenna by evaluating the Poynting vector of its fields, as expressed in equation (2.7).

$$\overrightarrow{W_{rad}}(\theta,\phi,r) = \overrightarrow{W_{av}}(\theta,\phi,r) = \frac{1}{2}\ Re(\overrightarrow{E}(\theta,\phi,r) \times \overrightarrow{H}^*(\theta,\phi,r)) \tag{2.7}$$

The total power radiated by the antenna is found by integrating the radiation power density over a sphere, as shown in (2.8).

$$P_{rad} = \frac{1}{2} \oiint_S Re(\overrightarrow{E}(\theta,\phi,r) \times \overrightarrow{H}^*(\theta,\phi,r)) \cdot d\vec{s} \tag{2.8}$$

[2]This concept is extensively explained in the articles available in [48] and [49].

If an antenna radiates equally in all directions its radiation power density will be given by the ratio of the radiated power over the sphere surface area, this is expressed in (2.9). Such an antenna is an important reference metric in antenna theory and is called an isotropic source.

$$\overrightarrow{W_o}(\theta, \phi, r) = \hat{a_r} \left(\frac{P_{rad}}{4\pi r^2} \right) \tag{2.9}$$

If the radiation power density is multiplied by r^2 radiated power per solid angle is obtained. Such operation eliminates distance dependence while maintaining angular dependence. This makes sense since in far-field distance only accounts as a scaling factor and the field distribution shape is preserved along any plane. Radiated power per solid angle in antenna theory is referred to as radiation intensity and is related with electric field distribution in the far-field region. When talking about radiation pattern it is radiation intensity, or some other directly derived metric, that is implied. The idea portrayed in this paragraph is depicted in equation (2.10).

$$U(\theta, \phi) = r^2 \; W_{rad}(\theta, \phi, r) \tag{2.10}$$

As previously alluded, there are several reference radiation patterns in antenna theory. The one already mentioned is the isotropic source whose radiation intensity is expressed by equation (2.11) and figure 2.2.

$$U_o = \frac{P_{rad}}{4\pi} \tag{2.11}$$

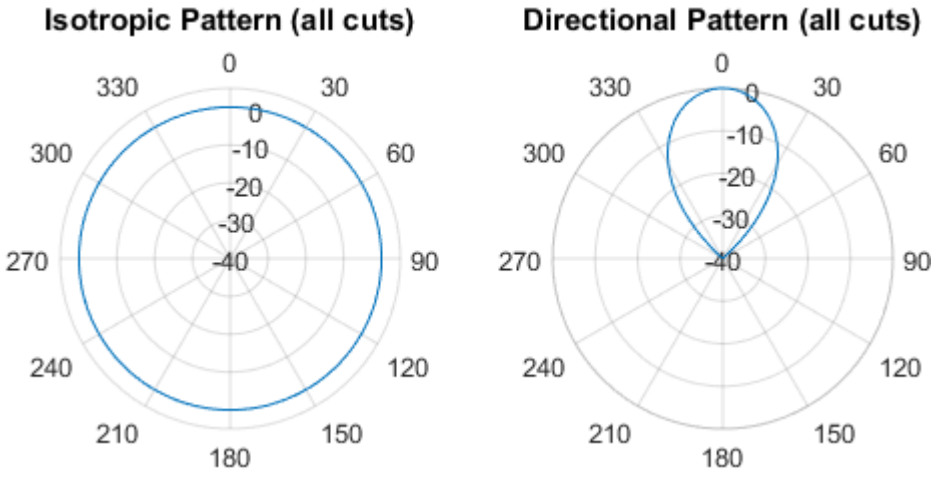

Figure 2.2: Radiation Patterns of isotropic and directional antennas.

Some reference radiation patterns are related with the idea of directionality, i.e. they take into consideration whether the antenna directs radiated power toward a given angle[3] or whether it radiates evenly in all angles[4]. A relevant pattern is one that is directional in a plane and non-directional in a given orthogonal plane, this is called an omnidirectional pattern. Examples of such patterns are shown in figures 2.2 and 2.3.

[3] Directional pattern.
[4] Non-directional\Isotropic pattern.

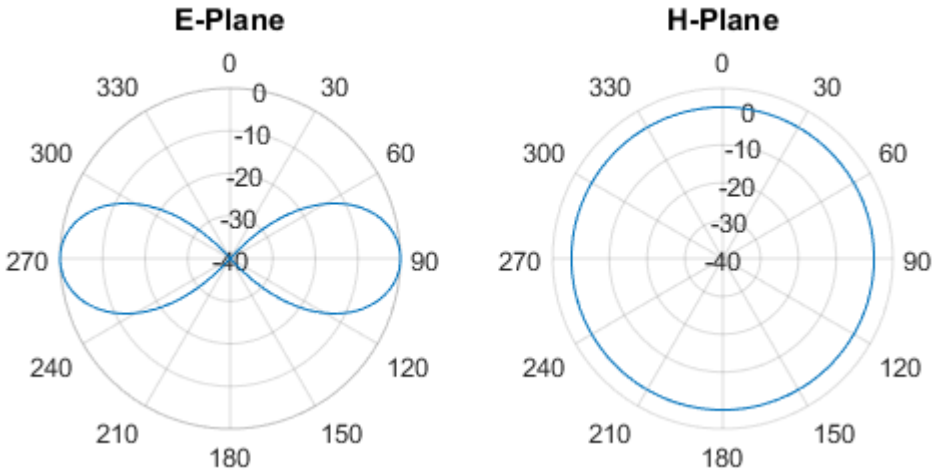

Figure 2.3: Omnidirectional Radiation Pattern

The directionality idea is accounted for by directivity. This metric compares the radiation intensity produced by an antenna in a given direction with the radiation intensity of the isotropic source. Directivity is defined by (2.12).

$$D(\theta,\phi) = \frac{U(\theta,\phi)}{U_o} = U(\theta,\phi)\frac{4\pi}{P_{rad}} \tag{2.12}$$

However, a more realistic metric to evaluate this is gain because, contrarily to directivity which evaluates radiated power, gain, expressed in (2.13), evaluates input power, thus considering metallic and dielectric losses. Even though gain is a more rigorous metric, realized gain, expressed in (2.14), is what is typically measured because it also considers mismatch loss. Realized gain measurements can then be corrected to gain with reflection coefficient measurements. It should be stated that gain metrics assume polarization match, so the measured and reference antennas must be aligned in a manner that allows maximum power transfer between them when measuring gain.

$$G(\theta,\phi) = U(\theta,\phi)\frac{4\pi}{P_{in}} = e_{cd}\ D(\theta,\phi) \tag{2.13}$$

$$G_{re}(\theta,\phi) = e_r\ G(\theta,\phi) \tag{2.14}$$

As already evidenced the radiation pattern is taken along a sphere centred at the antenna location, therefore it is best visualized in 3D. However, 2D cuts along the principal planes, the E-plane and the H-plane, are enough for a complete characterization. The E-plane contains the electric field vector and the direction of maximum radiation. The H-plane contains the magnetic field vector and the direction of maximum radiation. The field cuts can either be plot in a linear or polar graphs and are usually expressed in logarithmic units.

The most important features of these graphs are the maxima lobes, the nulls, as well as the angles in which they occur and their magnitude. From these values other interest metrics, such as beamwidth and Side Lobe Level (SLL), can be defined. The most used beamwidths are the Half-Power Beamwidth (HPBW), which indicates the angular separation between the two directions neighbouring the major lobe that have half of its radiation intensity value,

and the First-Null Beamwidth (FNBW), which indicates the angular separation between the first pair of radiation intensity nulls that surround the major lobe. SLL is the ratio between the radiation intensity of the secondary lobes and the radiation intensity of the major lobe. Figure 2.4 provides visualization of the aforementioned metrics.

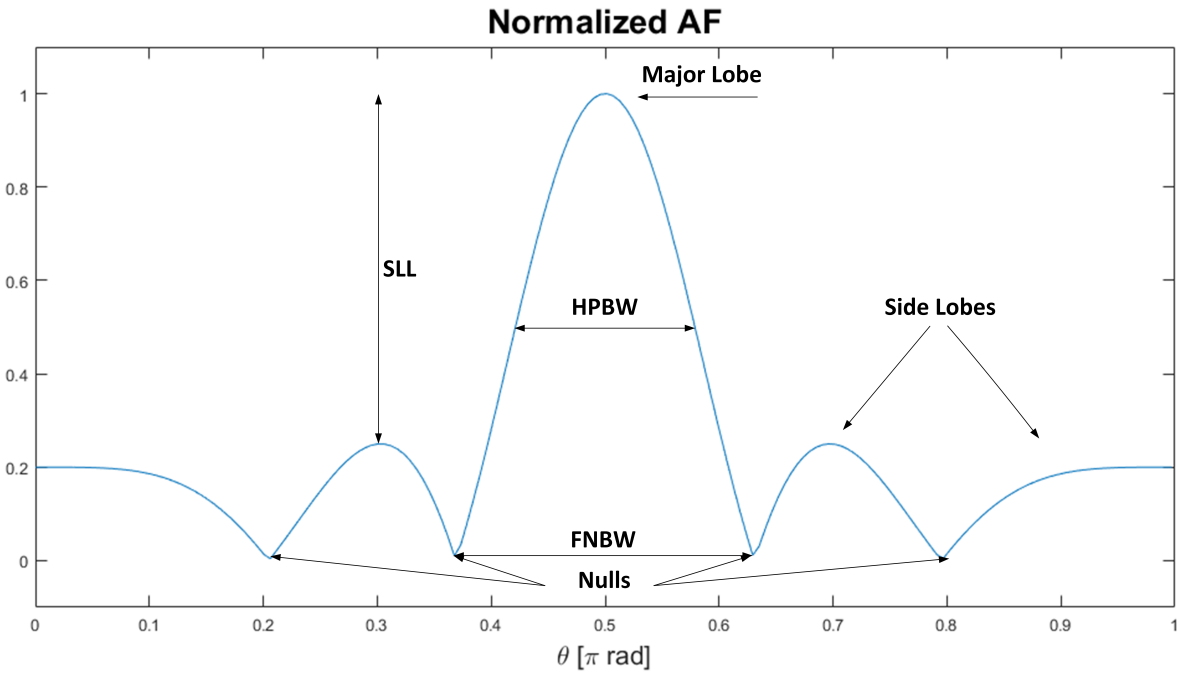

Figure 2.4: Important Radiation Pattern Metrics

Another metric worth mentioning is bandwidth. Antenna bandwidth is usually divided in two components: pattern bandwidth and input impedance bandwidth. Pattern bandwidth is the range of frequencies for which the radiation pattern properties respect project requirements, therefore being an application specific definition. Input impedance bandwidth is practically defined as the range of frequencies in which the antenna presents reflection coefficient bellow $-10dB$. The narrowest intercepting range of frequencies between these bandwidths defines the antenna bandwidth.

This section has presented an overview of important antenna concepts. There is much more to say than what was presented, however, here the focus was on limiting the discussion to the aspects most relevant to the developed work.

2.3 Microstrip Antennas

Microstrips can be broadly defined as structures constituted by a 3D dielectric material with metallic sheets laying on its top and bottom faces. Microstrip antennas are the most widely used antenna elements in mobile communications. What makes them so desirable?

In reality its wide use is no surprise, the simplicity of the microstrip structure makes it inexpensive and eases production procedures and costs, allowing almost all production steps to be automated. Besides this, microstrips are very versatile, being adjustable to a large range of requirements. Behavioural adjustments can be performed dynamically, by using varicaps

or active components, or statically by changing the microstrip shape or by tuning passive components. Microstrips support multiband design and can be compressed to fit into small electronics, this is very desirable in mobile applications. The compatibility with MMIC design is probably the feature that makes them most attractive for 5G applications.

2.3.1 Rectangular Microstrip Antenna

As previously mentioned, the number of possible microstrip antenna configurations is immense, however, the rectangular microstrip antenna is the most widely used and most alternative configurations derive from it. Therefore, it makes sense to start microstrip studies with the rectangular microstrip antenna.

There are several methods to analyse this structure, among them are the cavity model, the transmission line model and full-wave analysis. The cavity model is a comprehensive physical interpretation of the rectangular microstrip antenna behaviour, thus it is presented in this document due to this comprehensive aspect, however, mathematical aspects are left aside. The simpler transmission line model, for the particular case of the studies developed in the presented work, provides a good first approximation that can be optimized toward the desired goals in a full-wave simulator. Therefore it is the used method for initial design. Full-wave methods, based on Maxwell's equations, are the most rigorous and general EM analysis tools. These methods can be used to accurately tailor the desired response, however, the learning curve is very steep, so they are only used indirectly, through CST simulation and optimization.

2.3.1.1 Concept

The cavity model states that a rectangular microstrip antenna can be ideally approximated by a resonating cavity bound by two Perfect Electric Conductors (PECs), the rectangular patch and the ground plane, and four Perfect Magnectic Walls (PMWs), the dielectric walls along the perimeter. As known from EM theory, no electric field propagates through a PEC and no magnetic field propagates through a PMW.

This model can be further simplified by using the Huygens' principle. Thus the rectangular patch is represented by an electric current density source, and PMWs are represented by an electric current density source and a magnetic current density source. The electric current density source associated with the PEC patch is null as there is no current path within the patch. The electric current density and the magnetic current density on the dielectric walls are respectively obtained by equations (2.15) and (2.16), where $\overrightarrow{E_s}$ represents the tangential electric field and $\overrightarrow{H_s}$ represents the tangential magnetic field along the microstrip antenna edges.

$$\overrightarrow{J_s} = \hat{n} \times \overrightarrow{H_s} \tag{2.15}$$

$$\overrightarrow{M_s} = -\hat{n} \times \overrightarrow{E_s} \tag{2.16}$$

The edges of the rectangular microstrip antenna are open circuited and no electric current flows in the dielectric, thus there is no current density along the dielectric walls, so $\overrightarrow{J_s}$ is null and, as a consequence, there are no tangential magnetic field components within the cavity. $\overrightarrow{M_s}$ is the only non-zero field source. Therefore, the rectangular microstrip antenna can be

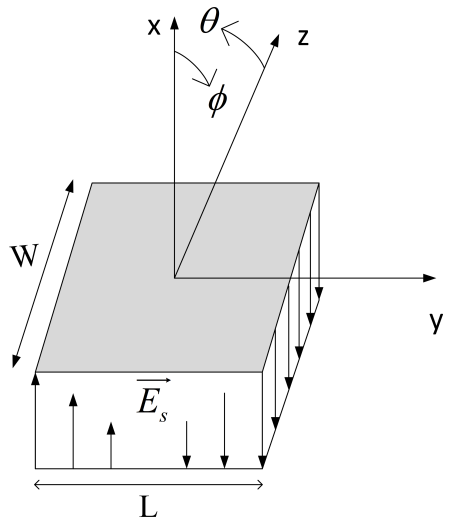

Figure 2.5: Rectangular Microstrip Antenna in mode TM^x_{010}.

modelled by four magnetic current density sources, one along each dielectric wall. Image theory can be used to account for the presence of a ground plane, this doubles the magnitude of the magnetic current density on each wall as expressed in (2.17).

$$\overrightarrow{M_s} = -2\hat{n} \times \overrightarrow{E_s} \tag{2.17}$$

When considering rectangular microstrips in this scope only TM^x propagation modes are considered. This means that the EM wave propagates along the x-axis and no magnetic field component exists tangential to this direction, agreeing with what was previously mentioned. Rectangular microstrips are mostly designed to propagate dominant TM^x_{010} mode, which only propagates a tangential electric field component and a transversal magnetic field component as expressed in (2.18)[5]. The distribution of the tangential electric field along the rectangular microstrip cavity in this propagation mode is represented in figure 2.5.

$$TM_{010} = \begin{cases} E_x(y) = E_o \cos\left(\frac{\pi}{L}y\right) \\ H_z(y) = H_o \cos\left(\frac{\pi}{L}y\right) \\ E_z = E_y = H_x = H_y = 0 \end{cases} \tag{2.18}$$

The resonant frequency of TM_{010} mode is given by expression (2.19), thus dictating $L_e = \frac{\lambda}{2}$.

$$f_{r_{010}} = \frac{1}{2L_e\sqrt{\mu\epsilon}} \tag{2.19}$$

To better understand how a rectangular microstrip antenna radiates it is best to analyse sources in opposing walls together.

As seen from figure 2.6 and as can be determined by expression (2.17), the sources separated by L, $\overrightarrow{M_1}$ and $\overrightarrow{M_2}$, have the same phase, same magnitude and are separated by $\frac{\lambda}{2}$.

[5]For proof consult [20].

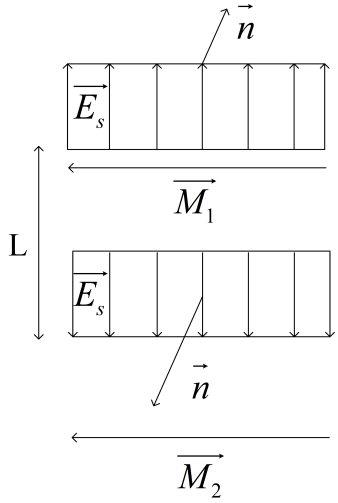

Figure 2.6: Radiating Sources.

Thus they can be analysed as a two-element antenna array separated along the y-axis whose radiated power intensity is given by expression (2.20).

$$U_{total}(\theta,\phi) = U_{source}(\theta,\phi) \times \left[1 + e^{j(kd\sin(\theta)\sin(\phi)+\beta)}\right] \tag{2.20}$$

The terms in square brackets represent each element of the array; k is the the wave number $\frac{2\pi}{\lambda}$, therefore the product kd represents the phase difference between sources due to spatial separation between elements; β represents the phase difference between sources due to source excitation; $\sin(\theta)\sin(\phi)$ is the far-field observation point. As already stated the distance between elements is $\frac{\lambda}{2}$ and the phase difference between sources is zero, so expression (2.20) can be transformed into expression (2.21), giving a clear indication that the radiation pattern maximum is normal to the rectangular patch surface, in other words along $+x$ because the ground plane acts as a shield towards $-x$, preventing backwards radiation.

$$U_{total}(\theta,\phi) = U_{source}(\theta,\phi) \times \cos\left(\frac{\pi}{2}\sin(\theta)\sin(\phi)\right) \tag{2.21}$$

Around the magnetic current density source circulates an electric field. Using the right-hand rule it can be concluded that the electric field radiated by the microstrip antenna must propagate along x[6], therefore the $x-y$ constitutes the principle $\overrightarrow{E}$-plane. From the aforementioned and using (2.7) it becomes apparent that the magnetic field must propagate along z, making the $x-z$ the principal $\overrightarrow{H}$-plane.

By analysing the sources separated by W, $\overrightarrow{M_3}$ and $\overrightarrow{M_4}$, represented in figure 2.7, it can be seen that their magnitude is null for $y = \frac{L}{2}$, thus cancelling radiation along the principle $\overrightarrow{H}$-plane. It is also noticeable that $\overrightarrow{M_3}$ and $\overrightarrow{M_4}$ have equal magnitude and opposite phase, therefore their combined effects also cancel radiation along the principle $\overrightarrow{E}$-plane, i.e. at $\frac{W}{2}$. In non-principal planes the radiation of these sources is also small when compared with the sources separated by L. Therefore sources separated by L are called radiating-sources while

[6]If this isn't obvious, analyse figures 2.5 and 2.6 to arrive to this conclusion.

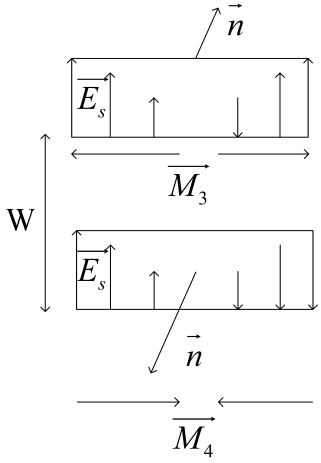

Figure 2.7: Non-Radiating Sources.

sources separated by W are called non-radiating sources. This means that the radiation pattern cuts of the rectangular microstric antenna dominantly exhibit a broadside pattern[7].

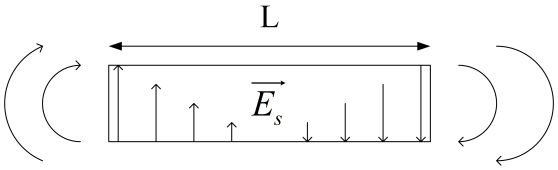

Figure 2.8: Fringing fields in rectangular microstrip antennas.

The perfect conditions described would contain all fields within the structure, not allowing any radiation to occur. But radiation indeed occurs due to loss effects and small perturbations on the field distribution that cause fringing fields to propagate away from the cavity into free-space, this is shown in figure 2.8. These phenomena, however, keep field distribution very similar to what was described, therefore the presented analysis is a valid comprehensive model of the rectangular microstrip antenna, eventhough it is just an approximation.

It should be evidenced that magnetic current densities used in the cavity model don't physically exist. This concept is used to aid with the visualization of the patch behaviour by analogy with familiar electrical properties. What is meant by this approach is that the macroscopic behaviour of the fields radiated by the rectangular patch antenna can be modelled by an hypothetical magnetic current density source, assuming its existence.

The transmission line model of the rectangular microstrip antenna is a much more practical approach than the cavity model. It starts by stating that the rectangular microstrip antenna can be modelled by a microstrip transmission line with non-stationary surface-waves propagating in its structure. These waves, however, partially propagate in its dielectric and partially propagate in free-space, therefore, to take this into account, the dielectric permit-

[7]Meaning that most radiation is normal to the rectangular patch.

tivity must be corrected by expression (2.22).

$$\epsilon_{reff} = \frac{\epsilon_r + 1}{2} + \frac{\epsilon_r - 1}{2}\left[1 + 12\frac{h}{W}\right]^{-\frac{1}{2}} \tag{2.22}$$

Then the explanation proceeds by stating that fringing fields responsible for radiation elongate the patch length, therefore length must be corrected by expression (2.23) to equal $\frac{\lambda}{2}$.

$$\begin{cases} \Delta L = 0.412h\frac{(\epsilon_{reff}+0.3)\left(\frac{W}{h}+0.264\right)}{(\epsilon_{reff}-0.258)\left(\frac{W}{h}+0.8\right)} \\ \\ L = L_e - 2\Delta L \end{cases} \tag{2.23}$$

Finally, a method to determine the rectangular patch width is required to complete the design process. For that expression (2.24) is typically used. This expression is mostly empirical and is known to give good practical radiation efficiency results.

$$W = \frac{c}{2f_r}\sqrt{\frac{2}{\epsilon_r + 1}} \tag{2.24}$$

The directivity of the rectangular microstrip antenna can be obtained from expression (2.25).

$$D = \left(\frac{2\pi W}{\lambda_o}\right)^2 \frac{\pi}{I} \tag{2.25}$$

$$I = \int_0^{\pi}\int_0^{\pi}\left[\frac{\sin\left(\frac{k_o W}{2}\cos(\theta)\right)}{\cos(\theta)}\right]^2 \sin^3(\theta)\cos^2\left(\frac{k_o L}{2}\sin(\theta)\sin(\phi)\right)\, d\theta\, d\phi \tag{2.26}$$

The presented expressions assume that the rectangular patch dimensions are greater than the dielectric height, which for practical cases is usually true. This method provides tools to rapidly start a crude design of a rectangular microstrip antenna that can then be further optimized in a full-wave simulator.

2.3.1.2 Experiments

Now, with the basic theory explained, a rectangular microstrip antenna design for $5.64GHz$ is presented. The design is developed in ISOLA ASTRA 3 dielectric[8]. With the frequency of operation and dielectric selected the determination of W and L consists in direct application of formulas 2.22, 2.23 and 2.24.

However, besides dimensioning, antenna design also requires feeding. There are several methods to feed the rectangular microstrip antenna, but the selected method was the coaxial feed because it is simple and allows decoupling between antenna structure and any circuitry connected to the antenna. This is useful for future designs. This feeding mechanism consists in inserting a probe through the antenna structure exactly in the point where it is matched,

[8]For details about the dielectric please refer to appendix A.

thus forming a matched connection. This point is empirically determined for $\frac{W}{2}$ and a distance of x_f from the patch edge. x_f is expressed in 2.27[9]. For visual aid please refer to figure 2.10.

$$x_f = \frac{L}{2\sqrt{\epsilon_{re}(L)}} \tag{2.27}$$

$$\epsilon_{re}(L) = \frac{\epsilon_r + 1}{2} + \frac{\epsilon_r - 1}{2}\left[1 + 12\frac{h}{L}\right]^{-\frac{1}{2}} \tag{2.28}$$

With this knowledge the design is now complete and the results are presented in table 2.1.

Dielectric Brick [mm]	L [mm]	W [mm]	Feed Point [mm]
25.6	15.37	19.64	2.9

Table 2.1: Theoretical rectangular microstrip antenna dimensions.

With these values two antennas are built in CST[10], one with an ideal feed directly connected between ground plane and the rectangular patch, and the other using a real SMA connector, as shown in figure 2.10. The connector was designed with the datasheet information available in [51]. Note that only the real feed is implementable. As can be seen in figure 2.9 both designs are shifted within 10% of the desired operation frequency, being that the real feed drifts more from the desired result. This means that the design must be optimized toward the desired goals. Usually this is corrected by simply moving the feed point, since expression 2.27 is an ideal empirical approximation that doesn't consider losses. But for the time being lets use these designs to make some interesting observations.

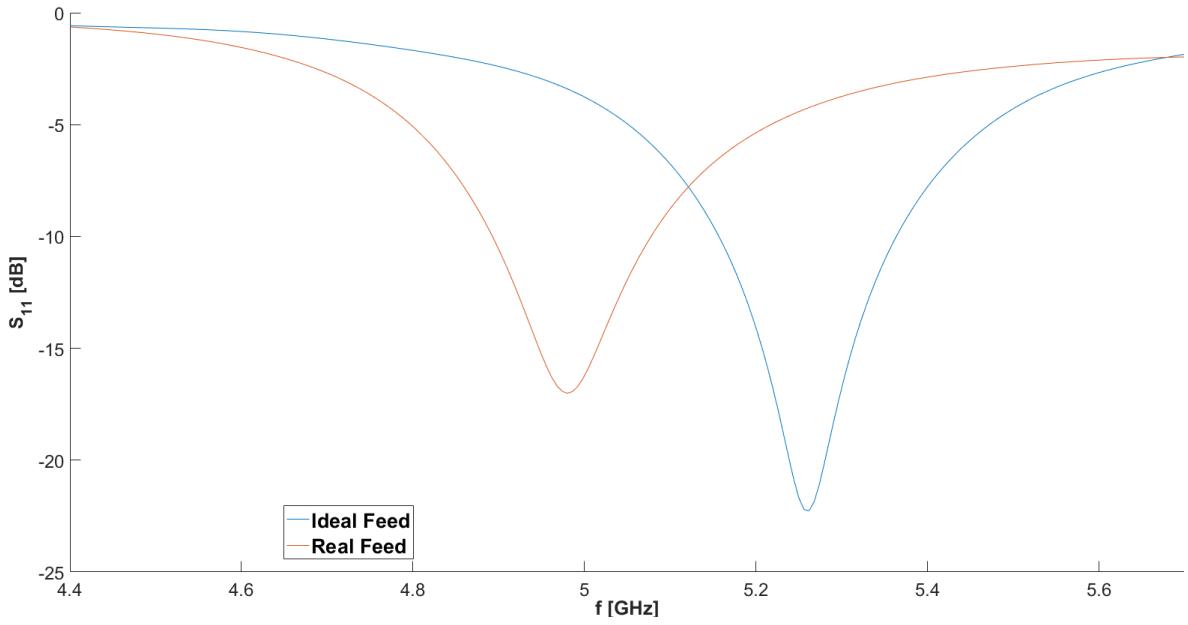

Figure 2.9: S-Parameters of theoretical rectangular microstrip antenna design.

[9]This expression was obtained empirically and it provides good radiation characteristics. The studies that lead to such conclusion are explained in more detail in [50]

[10]When in doubt about any simulation procedure please refer to appendix A.

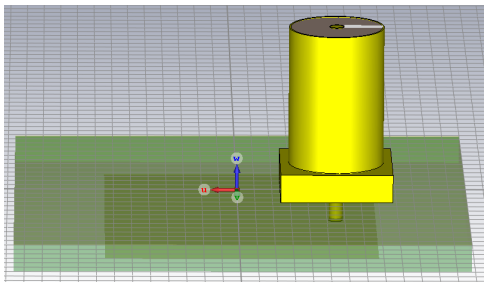

Figure 2.10: Real coaxial feed in rectangular microstrip antennas.

The advantage of using powerful full-wave analysis tools is that they allow for the validation of conceptual models, so now some thought will be given to the verification of the cavity model with CST. Figures 2.11 and 2.12 show the electric field simulated by CST at the radiating and non-radiating sources. It is interesting to observe that this simulation perfectly matches the model described in figures 2.6 and 2.7. Near the edges of figures 2.11 and 2.12 the fringing effects portrayed in 2.8 are also observable.

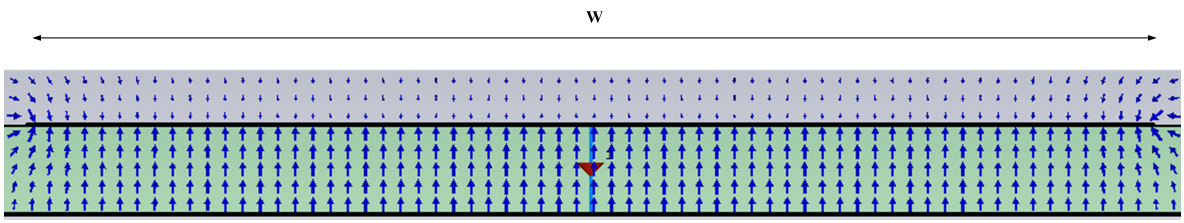

Figure 2.11: Electric field in radiating sources.

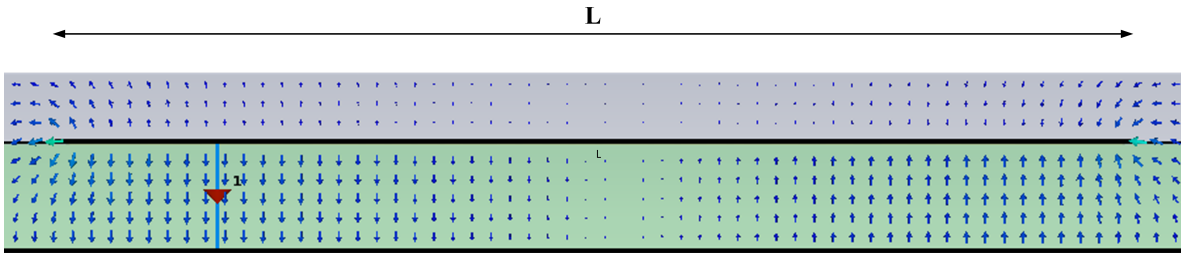

Figure 2.12: Electric field in non-radiating sources.

Figure 2.13 shows the simulated tangential magnetic field within the rectangular microstrip antenna. The blue represents null values in the colour bar, once again agreeing with model predictions.

Figures 2.14 and 2.15 show the maximum radiated electric and magnetic field from the rectangular microstrip antenna sources simulated by CST. These results evidence that the principal E-Plane cuts W in half while the principal H-Plane cuts L in half, thus agreeing with what was previously stated.

Even though the previously evidenced points are somewhat obvious, they were very important in the learning process and enabled a proper understanding of the rectangular microstrip antenna, so they were deserving of this renewed highlighting.

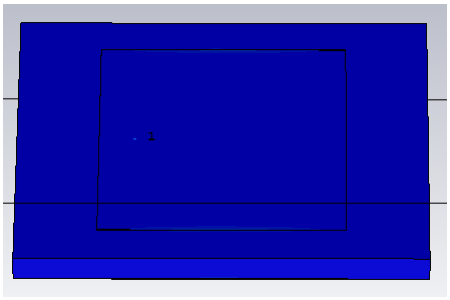

Figure 2.13: Tangential magnetic field in rectangular microstrip antenna.

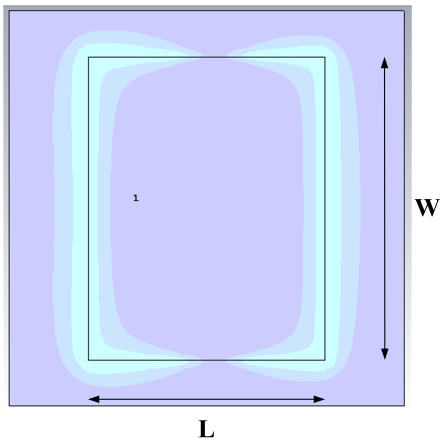

Figure 2.14: Maximum electric field in rectangular microstrip antenna.

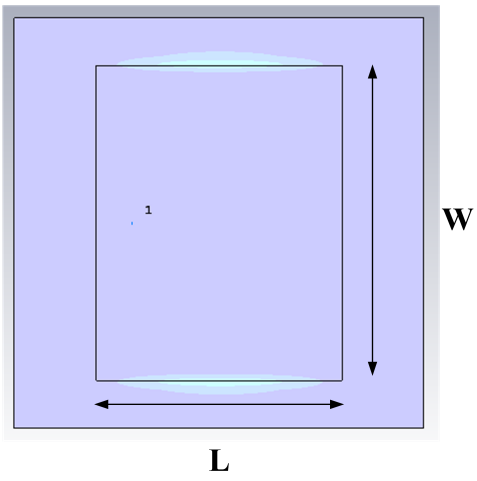

Figure 2.15: Maximum magnetic field in rectangular microstrip antenna.

Now it is time to optimize the rectangular microstrip antenna for the desired response. Several parametric sweeps and optimizations were performed over the previous design until a coaxially fed rectangular microstrip antenna operating at $5.4GHz$ was obtained. The resulting dimensioning is presented in table 2.2. This design was then produced and measured. The final board can be view in figure 2.16.

Dielectric Brick [mm]	L [mm]	W [mm]	Feed Point [mm]
25.6	14.10	16.29	4.08

Table 2.2: Final rectangular microstrip antenna dimensions.

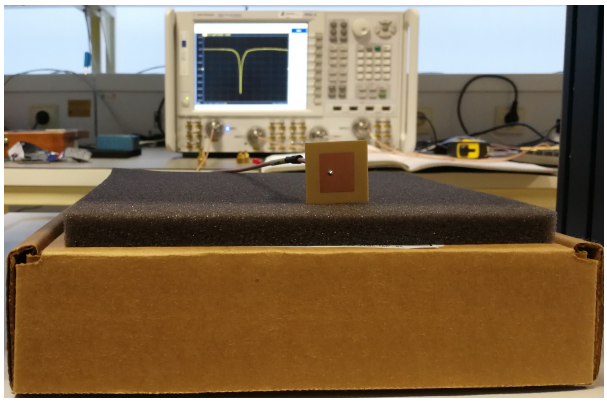

Figure 2.16: Final rectangular microstrip antenna design.

As can be seen in figure 2.17, the optimized and measured results[11] are shifted about $262MHz$. To find the source of such simulation error several parameters were swept in CST. Variations of $tan\delta$ only changed adaptation values, but didn't change the frequency band. Variations of L obviously shifted the resonant frequency toward the desired value, but physical measurements of the patch antenna agreed with the initially simulated values. Therefore, the only parametric value whose variation made sense was the dielectric ϵ_r. It was found that if ϵ_r equal to 2.7 was considered the simulated values would approximate the measured values. This is portrayed in figure 2.17. If finer optimizations adjusting both ϵ_r and $tan\delta$ were performed it would be possible to obtain a perfect match between results, but such process would be too time consuming and providing little benefit to the conceptual experiments being performed, especially considering that ϵ_r slightly varies form batch to batch. Variations between measurement and simulation are often reported in literature for the used feed type as it is said to be hard to modulate properly, however, changing any of the feed parameters arbitrarily didn't seem to produce any significant variation in frequency band.

Besides these S-Parameters variations, the radiation patterns in figure 2.18 show good agreement between simulation and measurement. The measured results show some oscillation due to non-ideal measurement conditions, but the tendency of the curve evidences the aforementioned agreement.

As a final remark, lets look to table 2.3 and evaluate the final design. As stated the design is shifted $262MHz$. The bandwidth is approximately 5% of the carrier, which is typical in

[11] Any doubts about measurement procedures please refer to appendix B.

coaxial feed designs. The realized gain is $6.4dBi$, which is close to the expected value of directivity given from expression 2.26 that results in $D = 6.54dBi$.

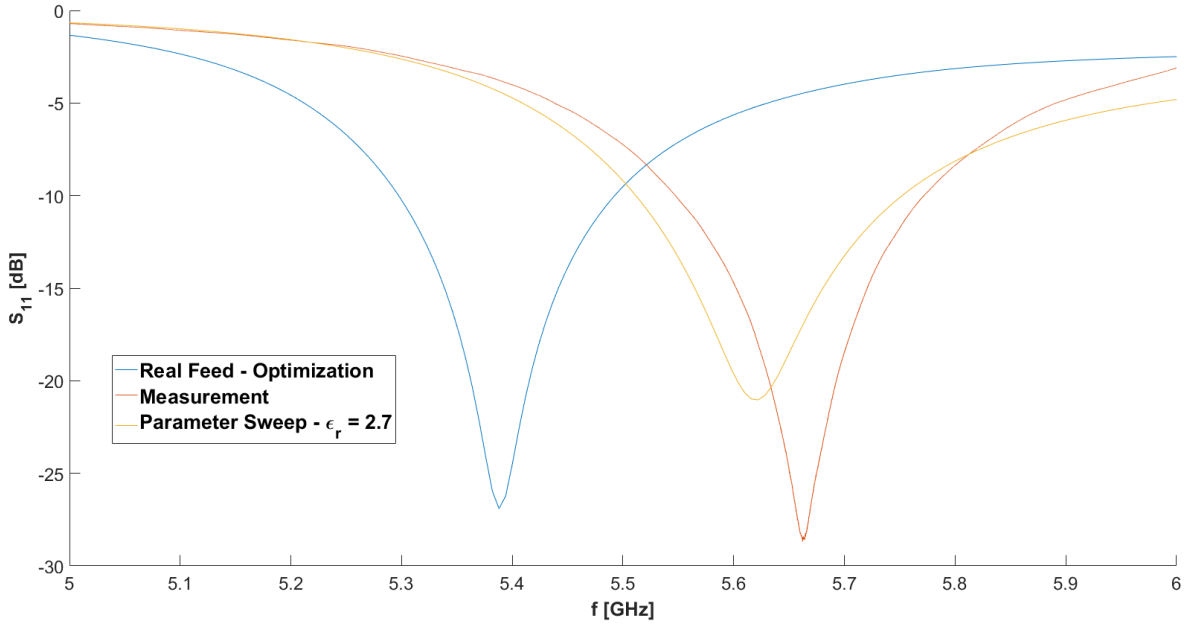

Figure 2.17: S-Parameters of real rectangular microstrip antenna design.

Carrier [GHz]	Bandwidth [MHz]	G_{re} [dBi]
5.662	225	6.4

Table 2.3: Summary of rectangular microstrip antenna characteristics.

Even though the presented design is very academic, it was an interesting example of how in RF theory, simulation and measurement procedures might be accurately adjusted and still provide slightly different results. But overall, it was a good effort to validate old theories through simulation and experiment.

2.4 Antenna Arrays

Antenna arrays can be defined in a broad sense as a group of antennas operating in coordination. There are several array types, but all fit into three general categories: 1D, 2D and 3D arrays, depending on along how many dimensions its elements are distributed. This document focuses, without loss of generality, on 1D[12] arrays.

Arrays gained popularity due to the need to increase directivity in a simple manner, avoiding complex antenna designs such as parabolic, lens and other types of reflector antenna configurations. To simplify the analysis equal element arrays are usually considered and it is assumed that no coupling exists between them. In these conditions there is no perturbation of the near-field EM source and the far-region electric-field can be given by expression (2.29). In this expression the Array Factor (AF) is a function descriptive of the impacts that source

[12] Also called linear arrays.

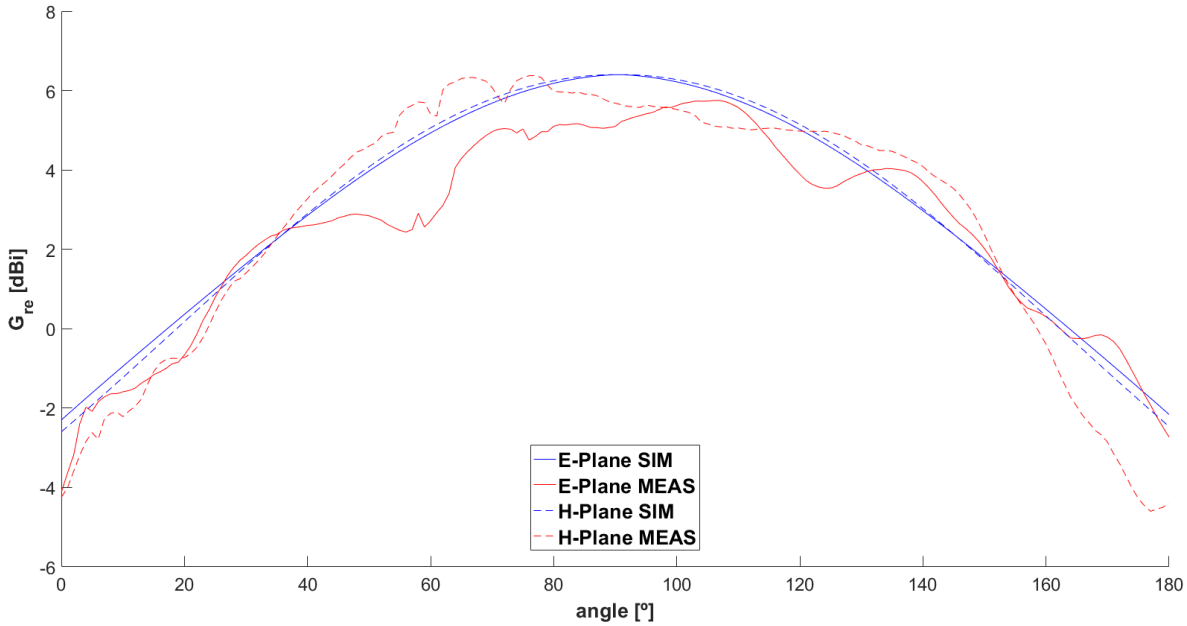

Figure 2.18: Rectangular Microstrip Antenna - Simulated versus Measured G_{re}.

spatial distribution and excitation have on the radiation intensity produced by the antenna array[13]. The AF can intelligently be controlled to obtain the desired array response.

$$\overrightarrow{E}_{total}(\theta,\phi) = \overrightarrow{E}_{element}(\theta,\phi) \times AF(\theta,\phi,d_n,\beta_n) \tag{2.29}$$

When observing the array in far-field the distance to the centre of the array is almost equal to the distance to any of the array elements because array dimensions are very small when compared to the far-field radius. Therefore the magnitude and angular orientation of the vectors that connect each array element to a point in far-field can be considered equal, this is represented in figure 2.19 and expression (2.30). This means that AF is independent of the spatial propagation vector e^{-jkr}.

$$\text{Far-Field} \rightarrow \begin{cases} Angle & \rightarrow \ \theta \approx \theta_1 \approx \theta_2 \approx \cdots \approx \theta_{N-1} \approx \theta_N \\ Magnitude & \rightarrow \ |r| \approx |r_1| \approx |r_2| \approx \cdots \approx |r_{N-1}| \approx |r_N| \end{cases} \tag{2.30}$$

However, in far-field the components radiated from each element present a small phase-shift due to their spatial separation in near-field. This can be accounted for by expression (2.31) where d_n is the distance of the nth element to the centre of the array.

$$\text{Phase Shift} \rightarrow r_n = r - d_n \cos(\theta) \tag{2.31}$$

Excitation sources can also control phase shift, β_n, and power radiated, a_n. Therefore the AF of a linear array is generally given by expression (2.32)[14]. From this expression it can be

[13] It should be highlighted that $U(\theta,\phi) \propto |AF(\theta,\phi,d_n,\beta_n)|^2$.

[14] When analysing linear arrays sources are aligned along the z-axis to simplify mathematical description.

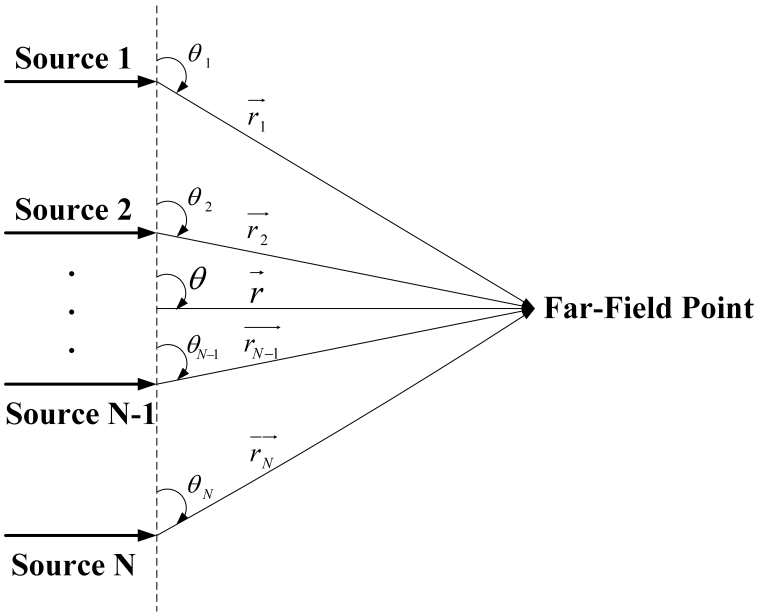

Figure 2.19: Array element distance to far-field point.

perceived that the AF is described by a real sinusoid if distance, phase shift and power are symmetrically distributed about the centre of the array.

$$AF = \sum_{n=1}^{n} a_n e^{jkd_n \cos(\theta)+\beta_n} \tag{2.32}$$

The directivity gains obtained by using a broadside[15] uniform array[16] are expressed by equation (2.33)[17]. This is an important array design evaluation metric.

$$D_o = 2N\frac{d}{\lambda}D_{element} \tag{2.33}$$

Such directivity gains increase selectivity and allow transmitters to reduce power or to serve lower sensitivity receivers. This evidences the importance of antenna arrays in acquiring capacity gains for future mobile communications.

Besides increasing directivity, antenna arrays can be manipulated to perform other functions of interest for 5G applications such as scanning, source synthesis and adaptive beamforming. Now it is explored how these functions are realized and how they help to achieve the capacity gains claimed by 5G solutions. In the presented analysis it is assumed that the symmetry conditions previously mentioned are always met.

2.4.1 Rectangular Microstrip Antenna Array

From the presented array theory an 8-element linear rectangular microstrip antenna array was designed based on the developed element design. The selected element spacing was

[15] Boardside means $\theta_o = 90^o$, in other words, radiation maximum normal to the array plane.
[16] Uniform arrays have equal spacing, equal amplitude distribution and progressive phase shift.
[17] Consult [20] for proof.

$25.6mm$ which is approximately $\frac{\lambda}{2}$ at $5.662GHz$[18]. This spacing allows full scan without the appearance of undesired maxima. The elements are aligned along W because this reduces coupling for the same centre-to-centre distance[19] [20]. The developed antenna array is portrayed in 2.21 where it is connected to the power splitter developed in appendix C.

The measured S-Parameters observed in figure 2.20 show that the element adaptation slightly drifted from the microstrip element. This behaviour is explained by coupling effects between neighbouring elements of the array in the report in [19]. These coupling effects change element impedance even when the antenna array is not excited. Regardless of that, the array is matched for most of the measured frequencies.

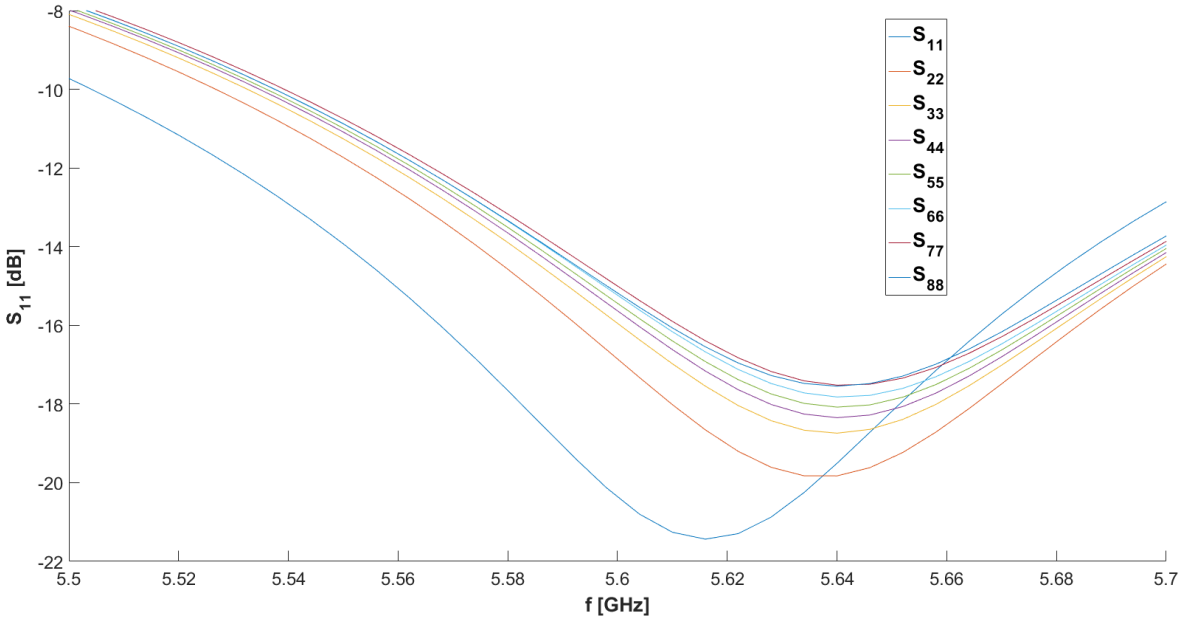

Figure 2.20: Measured S-Parameters.

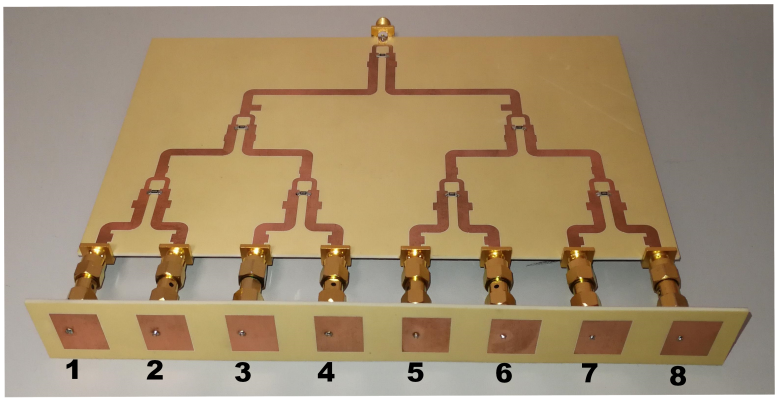

Figure 2.21: Designed rectangular microstrip antenna array.

[18]Initially designs were considered for $5.85GHz$. At this frequency $\frac{\lambda}{2}$ equals $25.6m$. Then the design frequency was changed and this parameter was forgotten.

[19]This happen because the distance between the closest metal is larger in this configuration.

By observing figure 2.22 the resemblance between measured and simulated results is evident. The simulated and measured H-Plane are almost coincident, apart from a small gain difference. In the E-Plane there is a very precise match between array maxima and nulls until the third null. The difference for the angles near 0^o and 180^o is probably due to setup hazards because the measurement manifests an oscillatory behaviour around the simulated value. Note that the designed antenna array is an omnidirectional antenna because the E-Plane is directional while the H-Plane is non-directional. This is typical in linear antenna arrays. For the design to be fully directional the array dimensions should be increased to at least a planar array.

The main difference between simulation and measurement is G_{re}. The simulated array presents G_{re} equal to $14.06dBi$ while the measured array presents G_{re} equal to $12.04dBi$. This variation can be justified by how difficult it is to properly account for copper and dielectric losses in simulation and by inaccuracies of the feed structure model. Despite that, the obtained results aren't far from the expected directivity given by expression 2.33 which is $15.43dBi$. These results also differ in terms of SLL in the principal E-plane. While the simulated antenna holds $13dB$ of SLL the measured antenna has an improved SLL of $15dB$. Thus, the designed antenna array produces less spurious radiation than expected from full-wave simulation. The differences in the null level, however, aren't so clarifying because they might be caused by the limited sensitivity of the experimental apparatus.

In summary, the rectangular microstrip antenna array design successfully matched the expected results. Once again proving old theories by experimentation.

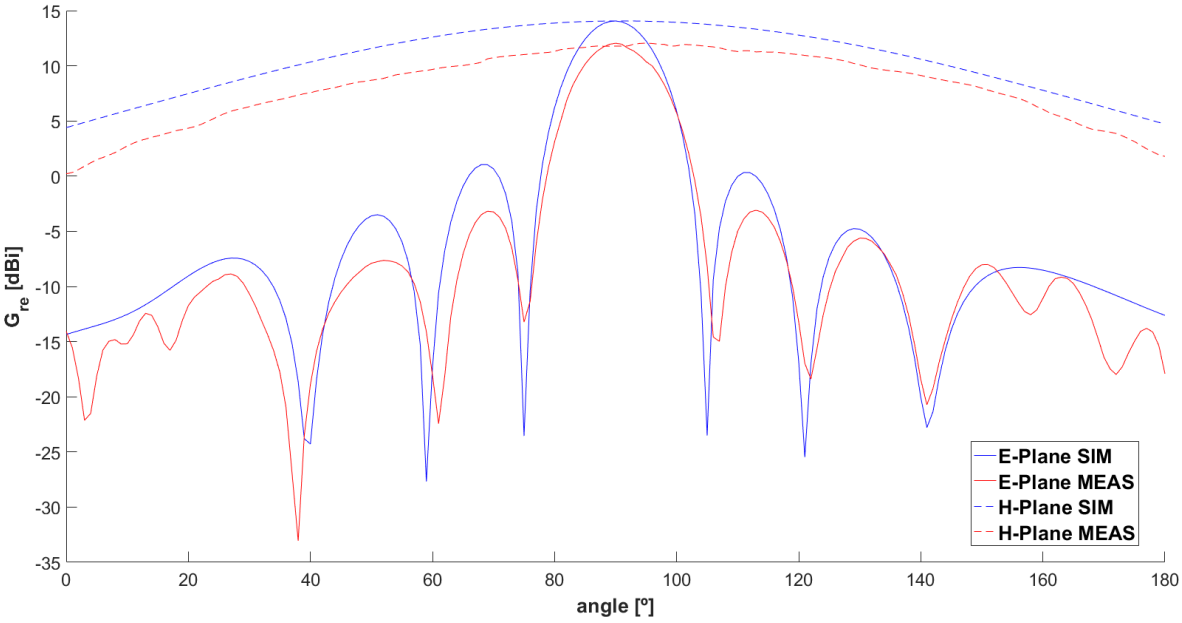

Figure 2.22: Simulated versus Measured radiation pattern.

2.4.2 Array Functions: Scanning

2.4.2.1 Concept

Scanning is the capacity to direct the major beam towards the desired direction. By manipulating expression (2.32) into expression (2.34)[20] it becomes rather evident how to control excitation phase to orient the maximum AF towards the desired angle, θ_o.

$$AF = \sum_{n=1}^{n} a_n e^{jkd_n[\cos(\theta)-\cos(\theta_o)]} \tag{2.34}$$

Therefore, beyond the improvements brought by higher directivity, scanning arrays also support terminal mobility. This capacity is a great asset for future mobile communications.

$$d_{max} = \frac{\lambda}{1 + |\cos(\theta_o)|} \tag{2.35}$$

The array design, however, must take into consideration that excessive element spacing might cause unwanted AF maxima to appear. The maximum element spacing that avoids this for the case of the uniform array is expressed by (2.35), indicating that, for a full-range scanning array, spacing must not exceed $\frac{\lambda}{2}$.

2.4.2.2 Simulation

To test scanning a MATLAB script was developed[21] considering isotropic source,i.e. it is in fact an AF simulator. This script generates the desired phase excitations. Then, these coefficients are introduced in CST to excite the previously designed 8-element linear array. Table 2.4 presents a record of those excitation vectors.

Angle	β_1	β_2	β_3	β_4	β_5	β_6	β_7	β_8
30	-150.9	-301.7	-92.5	-243.4	-34.2	-185.1	-335.9	-126.8
45	-123.2	-246.3	-9.5	-132.7	-255.8	-19.0	-142.2	-265.3
60	-87.1	-174.2	-261.3	-348.4	-75.5	-162.5	-249.6	-336.8
90	0.0	0.0	0.0	0.0	0.0	0.0	0.0	0.0

Table 2.4: Scanning phase excitations.

Figures 2.23 to 2.26 show the normalized radiation patterns of the designed scanning excitations. As can be seen the, results from MATLAB and CST are very similar in terms of major lobe behaviour and scan towards the desired direction. However, as the scan direction tends to zero the SLL increases much faster in CST than in MATLAB because the rectangular microstrip antenna array has much higher gain toward broadside than toward end-fire. Nevertheless, the CST results validate proper algorithmic implementation.

[20] This is done by merely substituting β_n by $-kd_n\cos(\theta_o)$.
[21] This is available in appendix D

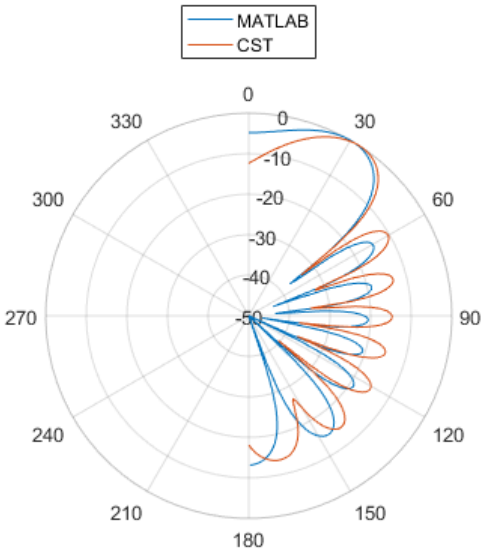

Figure 2.23: Scan 30.

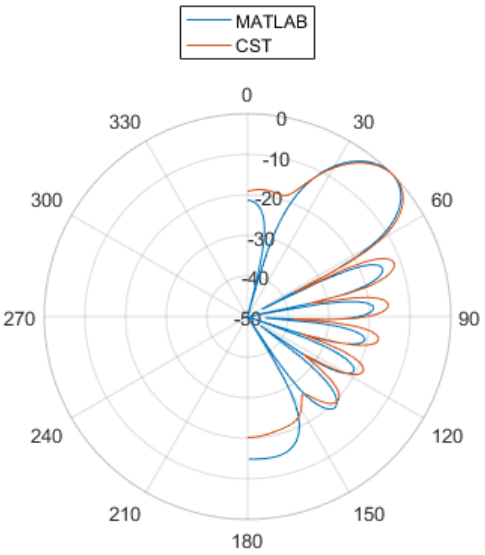

Figure 2.24: Scan 45.

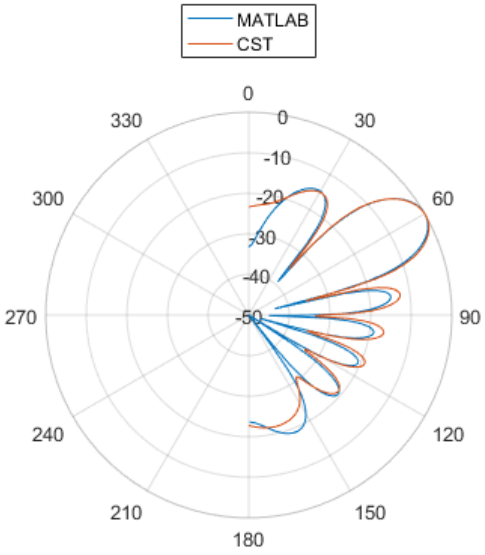

Figure 2.25: Scan 60.

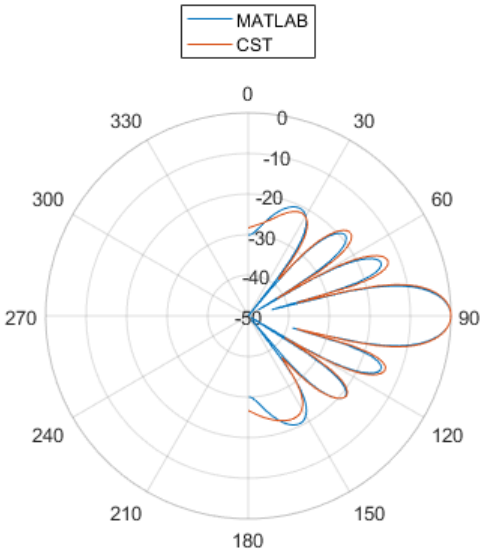

Figure 2.26: Scan 90.

2.4.3 Array Functions: Source Synthesis

2.4.3.1 Concept

Source synthesis techniques[22] control array element spacing, power and phase distribution. The major aim is to design an array pattern with desired properties in terms of nulls, SLL, directivity, among other important antenna metrics. In array design it is desirable to reduce interference on both transmission and reception while keeping high directivity and scanning capacity. This is achieved by controlling SLL and by forcing array pattern nulls toward the

[22] Also referred to as beam-shaping.

direction of interferers, being an important interference reduction mechanism integrated in 5G solutions.

The Dolph-Tschebyscheff array, based on the Tschebyscheff polynomials in (2.36), is one the proposed methods to control SLL.

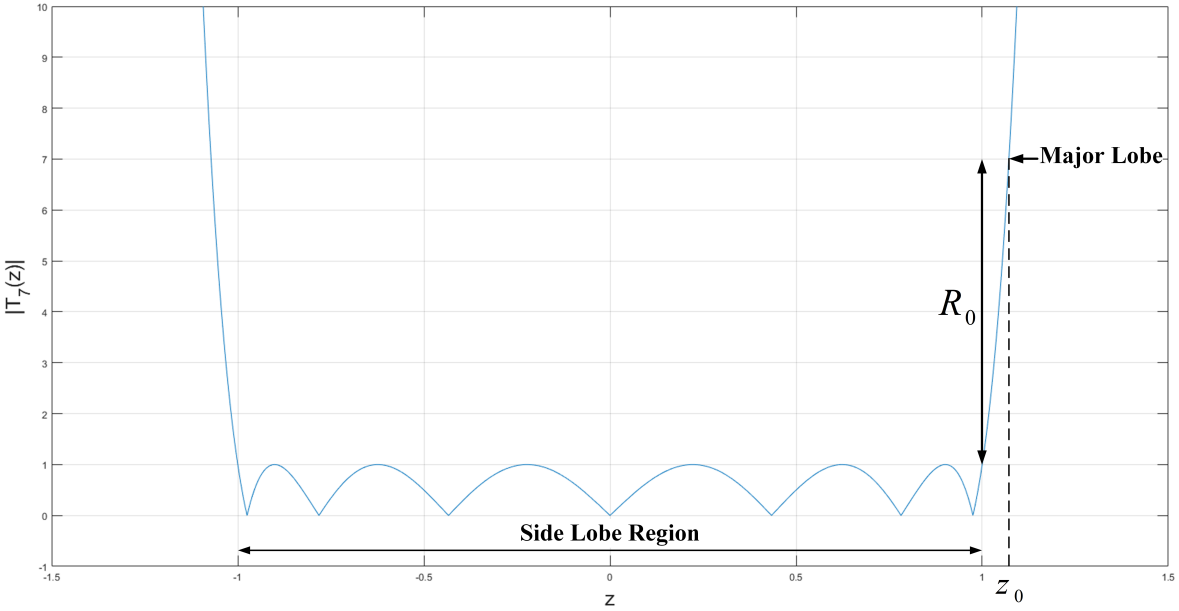

Figure 2.27: Example of Dolph-Tschebyscheff array design.

$$T_m(z) = \begin{cases} \cos[m\cos^{-1}(\frac{z}{z_o})] & -1 \leq \frac{z}{z_o} \leq 1 \\ \\ \cosh[m\cosh^{-1}(\frac{z}{z_o})] & -1 < \frac{z}{z_o},\ \frac{z}{z_o} > 1 \end{cases} \tag{2.36}$$

$$\frac{z}{z_o} = \cos(u) \tag{2.37}$$

$$T_m\left(\frac{z}{z_o}\right) = 2\frac{z}{z_o}T_{m-1}\left(\frac{z}{z_o}\right) - T_{m-2}\left(\frac{z}{z_o}\right) \tag{2.38}$$

The AF in expression (2.34) can be described by the sum of several harmonic cosines. Each harmonic can be represented by a Tschebyscheff polynomial while the total AF can be manipulated to equal T_{n-1}. Tschebyscheff polynomials have well known coefficients[23], so AF power coefficients can be determined by solving the equation relating T_{n-1} with the AF in its Tschebyscheff polynomial form. In such case, the region where Tschebyscheff polynomials are represented by cosines corresponds the minor lobes while the region described by hyperbolic cosines corresponds to the major lobe. In a Dolph-Tschebyscheff array to z_o is corresponds the AF maxima, therefore it is selected to obtain the desired voltage ratio between major and side lobes[24], this is expressed in (2.39). In this method it is assumed that element spacing is

[23] Coefficients can easily be determined by expression (2.38).

[24] To help with visualization please refer to figure 2.27.

uniform.

$$T_{n-1}(z_o) = R_o \tag{2.39}$$

One of the existing techniques to force nulls in desired directions is the Schelkunoff method. This method assumes that elements are equally spaced and that phase shift between elements is progressive. Given the number of desired nulls and their location the Schelkunoff method determines number of required elements as well as their excitation to produce the desired response. To achieve this the expression (2.32) is rewritten in a clever way, expressed in (2.40).

$$\begin{cases} AF = \sum_{n=1}^{N} a_n z^{n-1} \\ \\ z = e^{kd\cos(\theta)+\beta} \end{cases} \tag{2.40}$$

Through this representation it becomes rather evident that AF can be described by a polynomial of order $n-1$. A polynomial can always be represented by the product of its roots, as shown in (2.41).

$$AF = \prod_{n=1}^{N} \alpha_n (z - z_n) \tag{2.41}$$

Therefore, by properly selecting the z_n values the AF will present nulls towards the desired directions. Excitation coefficient can be determined by expanding expression (2.41) into expression (2.40). It should be noted that the variable z travels within the unity circle in an angular range defined by $kd\cos(\theta) + \beta$ called visible region, so to produce AF nulls z_n must be in the unity circle within the visible region.

2.4.3.2 Simulation

In this section the Dolph-Tschebyscheff and Schelkunoff source synthesis algorithms are implemented and tested. These algorithms were implemented in MATLAB simulators available in appendix D. The simulation procedure followed are similar to those presented in the scanning experiments, following the MATLAB simulation with EM validation.

Table 2.5 presents the excitation coefficients for an 8-element Dolph-Tschebyscheff array with SLL bellow $-28dB$.

a_1	a_2	a_3	a_4	a_5	a_6	a_7	a_8
0.3743	0.5826	0.8417	1.0000	1.0000	0.8417	0.5826	0.3743

Table 2.5: 8-element Dolph-Tschebyscheff Array - SLL = 28dB.

As can be viewed in figure 2.28 the task of controlling the SLL bellow $-28dB$ is successfully achieved, with MATLAB results agreeing well with CST EM simulation. Note that the SLL improvement in this scenario is of almost $15dB$ when compared to the scenario presented in figure 2.26.

Now moving into Schelkunoff source synthesis. Table 2.6 presents the list of desired nulls and the Schelkunoff excitations. Figure 2.29 evidences how the theoretical MATLAB simulator can force the desired nulls. The CST result also presents accurate nulls in the

nulls	-	0	30	45	60	120	150	180
a_n	1.00	4.26	8.64	11.45	11.45	8.64	4.26	1.00
β_n	-56.83	-45.52	-36.21	-30.37	-26.46	-20.62	-11.32	0.00

Table 2.6: Schelkunoff Source Synthesis - Nulls and Excitation

angular range between 30^o and 150^o, but beyond that limit the rectangular microstrip antenna array isn't capable of forcing the desired nulls. This is related with the lack of gain toward end-fire. However, it should be noted that the power levels obtained are bellow $-40dB$ for every desired null. This power level is typically used as a null reference in antenna design. It should also be pointed out that the imposition of so many nulls has caused the major lobe to broaden. To achieve this source excitations have a maximum variation of a order of magnitude such variation can lead to inefficient antennas.

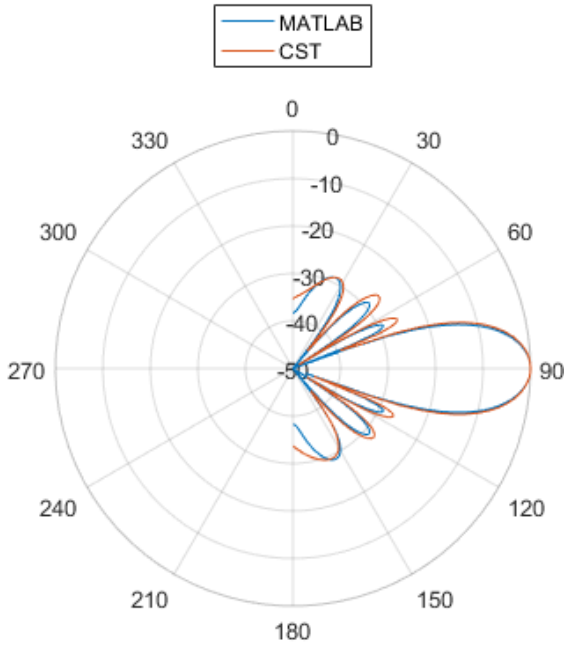

Figure 2.28: Dolph-Tschebyscheff.

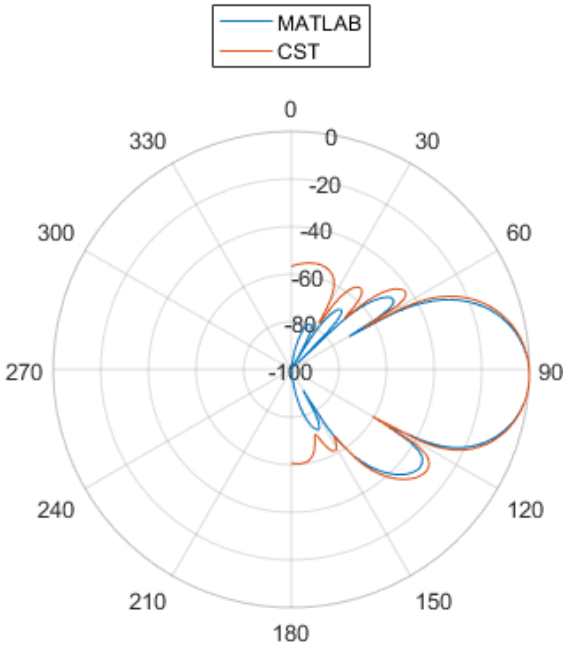

Figure 2.29: Schelkunoff.

The presented results validated the algorithmic implementation of the Dolph Tschebyscheff and Schelkunoff source synthesis techniques. An interesting step further would be to implement them in an active antenna array and experimentally validate them, but there were no such arrays available to test.

2.4.4 Adaptive Beamforming

2.4.4.1 Concept

The ability to control major lobe direction, SLL and null placement reveals the incredible utility of the previously mentioned techniques, particularly in low dynamic applications where the alignment between transmitter, receivers and interferers is almost constant. However, as the number of users, interferers and their dynamic increase it becomes very hard to comply

with AF requirements using those classical techniques, calling for the implementation of dynamic methods. This is the case of real-world mobile communications applications, especially 5G oriented, that have high mobility and high number of users.

In such applications there is a need to automatically distinguish Signal of Interest (SoI) and interferers, Signal Not of Interest (SNoI), and to cancel SNoIs while amplifying SoIs. This can either be done by analysing the Direction of Arrival (DoA) and time delay of each signal or by using optimization techniques based on training sequences. The later approach, called adaptive beamforming, is simpler and more broadly used. One way to do this is to optimize the AF excitation so that the squared error between the desired and the computed AFs is minimized. In such case, the optimum result is the Wiener solution, that for a linear array with equally spaced elements is expressed by (2.42). In expression (2.42) the AF is given by (2.40), z equals $e^{kd\cos(\theta)}$ and the vector $\overrightarrow{a}_{opt}$ contains information on both amplitude and phase excitation. This optimization is usually performed using the Least Mean Square (LMS) algorithm[25].

$$\overrightarrow{a}_{opt} = \overrightarrow{R}_{zz}\overrightarrow{r}_{zAF} \tag{2.42}$$

Adaptive beamforming is therefore capable of conjugating gains of classical methods, obtaining the optimum balance between scanning, SLL control and interference cancellation. This technique allows mobile communications to operate in larger ranges due to increased signal strength, to have a system mostly limited by noise, to overcome channel fading due to reduced multipath and to increase security because a dedicated link is created for the user. Through this lens it is now understandable how adaptive beamforming allows antenna arrays to increase capacity gains in future mobile communications, but there is still an answered question: how is spatial multiplexing achieved?

Spatial multiplexing is achieved through multiple adaptive beamforming, where the array generates a dedicated beam per terminal, each carrying different information. This makes communication channels orthogonal as each beam only accepts a SoI. This can either be done by operating the array in different frequencies or by dividing the array in sub-arrays that are operated independently. The first approach limits signal bandwidth, not allowing time-frequency resources to be reused, therefore in a Massive MIMO scenarios sub-arraying must be implemented[26]. Arrays capable of performing such multiple adaptive beamforming techniques are called active antenna arrays.

[25]For better explanation of LMS method please refer to [20] and its references.

[26]Minimization of coupling effects in sub-arrays aggravate the demand for large arrays in Massive MIMO.

Chapter 3

Nonlinear Antennas

3.1 Introduction

The PA is a device whose major function is to provide power gain to input signals. Power gain, described in (3.1), varies depending on input power, starting to compress as input power increases, as shown in figure 3.1. This reveals the intrinsic nonlinear behaviour of this device. The high powers managed by PAs make them the major nonlinear source in wireless communication systems.

$$G_p = 1 + \frac{P_{dc} - P_{diss}}{P_{in}} \tag{3.1}$$

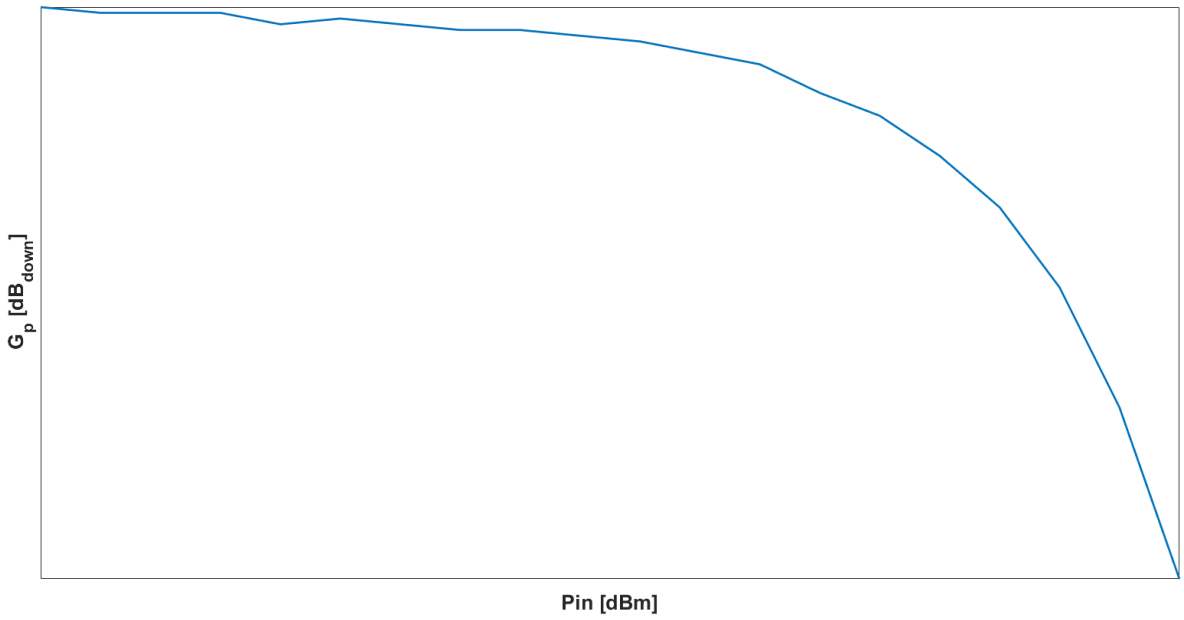

Figure 3.1: Representation of gain compression versus input power.

Due to these nonlinearities the input signal induces Amplitude Modulation (AM) and Phase Modulation (PM) on the output signal . These are respectively referred to as AM-AM and AM-PM conversions. For proper system operation these conversions must be accurately

characterized and corrected. The study of methods to achieve this has been an important research topic since the existence of wireless communications. Therefore the need to connect PAs and antenna arrays without isolation in 5G applications led researchers to study the impacts of coupling on PA linearity. However, the impact PA nonlinearities have on antennas is an issue seldom addressed. This issue wasn't very relevant in previous mobile generations because antennas were non-directional and only one signal was broadcast, but in 5G applications it becomes crucial because AM-AM and AM-PM conversions change amplitude and phase excitation of active antenna arrays, making them nonlinear. This can potentially lead to increased interference and in extreme cases might even cause connection loss on all communication channels.

There is therefore a need to comprehend the impacts PA distortion has on array pattern and to understand what boundaries must be respected to preserve proper spatial multiplexing operation. Only recently has research with this intent been developed. Chapter 3 is dedicated to the study of this state-of-the-art issue. It starts with a brief overview of PA oriented nonlinear theory, following with a discussion of the state-of-the-art. Then a comprehensive theoretical model built on basic nonlinear concepts and on basic antenna theory is presented, aiming to predict the nonlinear effects on array pattern from a basic principle approach. In this endeavour [52] was the main nonlinear theory reference guide.

3.2 PA Nonlinearity: Important Concepts

Signal distortion is the modification of the original signal characteristics. Distortion is said to be nonlinear whenever the distorted signal contains components uncorrelated with the original signal, for example new frequency components. Weakly nonlinear memoryless behaviour can be approximated by a third order polynomial like the one in (3.2).

$$y_{NL}(t) = a_1 x(t) + a_2 x^2(t) + a_3 x^3(t) \tag{3.2}$$

As a first approximation PAs can be considered weakly nonlinear memoryless devices[1] and the typical telecommunications signals can be described by (3.3).

$$x(t) = A(t)\cos(w_c t + \theta(t)) \tag{3.3}$$

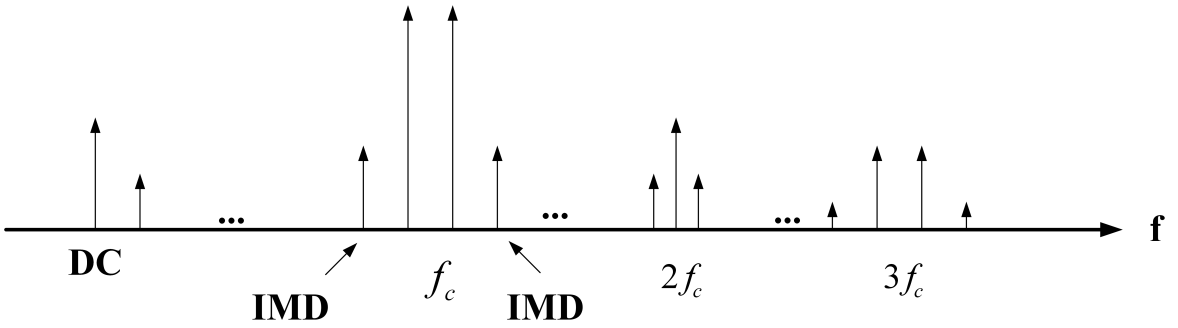

Figure 3.2: Signal distortion components.

[1] This is only valid for the range of operation where weak nonlinearity is exhibited!

As deductible from expressions (3.2) and (3.3), when a telecommunication signal passes through a PA it generates uncorrelated components at DC, at the harmonics, at the fundamental and near the fundamental frequency as shown in figure 3.2. These respectively constitute bias point distortion, harmonic distortion, co-channel distortion and adjacent channel distortion. In wireless communication systems co-channel and adjacent channel distortion constitute the most critical nonlinear components as they both degrade own and neighbouring communication channels, this cannot simply be allowed. Therefore such distortion components must be properly characterized and corrected to maintain expected PA behaviour. The one-tone test and the two-tone test are classical PA characterization approaches geared toward that goal.

As suggested by the name, the one-tone test consists in feeding a sinusoidal tone to the amplifier input and measuring the output signal power and phase. This allows for the characterization of AM-AM and AM-PM conversion behaviour. This method also characterizes PA gain compression, defining an important metric in nonlinear characterization, the $1dB$ compression point, which is the input power for which gain has compressed $1dB$ from its small signal value. However, single tone tests don't generate non-harmonic frequency components and therefore don't provide information about co-channel and adjacent channel interference, giving no indication about the device tendency to generate spectral regrowth, therefore leaving no margin for the implementation of compensation techniques.

To address these shortcomings two-tone tests place two similar sinusoidal tones symmetrically distributed about the fundamental frequency at the PA input. In these conditions the PA generates the components in (3.4) at the fundamental frequencies and the components in (3.5) at Intermodulation (IM) frequencies.

$$P_{fund} \rightarrow \begin{cases} \left[a_1 A + \frac{9}{4} a_3 A^3\right] \cos(w_1 t) \\ \\ \left[a_1 A + \frac{9}{4} a_3 A^3\right] \cos(w_2 t) \end{cases} \tag{3.4}$$

$$P_{IMD_3} \rightarrow \begin{cases} \frac{3}{4} A^3 \cos[(2w_1 - w_2)t] \\ \\ \frac{3}{4} A^3 \cos[(2w_2 - w_1)t] \end{cases} \tag{3.5}$$

By measuring the output power of the tones and of the Intermodulation Distortion (IMD) components it is possible to define two important PA characterization metrics: the Intermodulation Ratio (IMR) in (3.6) and the Third Order Intercept Point (IP3). The IP3 is defined as the point where the small signal $P_{tone}(P_{in})$ and $P_{IMD}(P_{in})$ curves would intercept each other if distortion components of order higher than three were negligible in the large signal region. This simple metric is usually enough to describe weakly nonlinear devices.

$$IMR = \frac{P_{fund}}{P_{IMD}} \tag{3.6}$$

It should be stated that neither the presented model nor the presented methods rigorously characterize PA behaviour because in reality higher order distortion terms are relevant, the PA presents some memory effects and for proper nonlinear characterization input signals must resemble as much as possible real operation scenarios. More complex multi-tone characterization techniques that allow the implementation of complex compensation techniques such

as DPD were developed with this rigour in mind. However, as the realized studies are based on a comprehensive basic principle approach the less rigorous presented tools are enough.

3.3 State-of-the-Art

Even though the impacts of nonlinear distortion in antenna arrays are seldom researched it is empirically known that they degrade antenna pattern[2], change channel noise and spectral properties, and that AM-AM and AM-PM conversions limit beamforming functions, thus lowering signal quality [53, 54]. In the meantime between the first observations of nonlinear antenna performance degradation and present day some research fields had to delve into this problematic, being the most relevant examples of this satellite and mobile applications. This section now gives an overview of the main ideas proposed to address the impact of nonlinear distortion in antenna arrays, analysing their evolution across time.

An article from 1999, [53], evidences the importance of active antennas and states that analysis and simulation of nonlinear effects in active antennas wasn't a well-established field, alerting for the need of a joint analysis of antenna and circuit, considering radiation effects. By this time the study of PA nonlinearities was already very well established. In the same article a behavioural model for the characterization of active antenna arrays is presented. It is claimed that this model can predict large signal array pattern, array pattern interference and intermodulation pattern, however, no proof, neither simulated nor measured, is presented and no insightful understanding of the phenomenon seems to be acquired with this study.

As active antennas became increasingly relevant in satellite applications research geared toward the understanding of the impacts of IMD products on active antenna array radiation pattern using third-order memoryless PA models. The study in [55] shows that the IM3, IM5 and IM7 products typically scan toward the carrier major lobe. Then an IM controller to eliminate IMD is proposed. This is done by cleverly adjusting phase excitation to radiate IMD products away from the major carrier beam without signal degradation. To experimentally validate this model a 6−element linear phased array powered by a single high-power PA and a MMIC IM controller were developed. The obtained results matched with predictions leading authors to claim that their technique increases SIR. The study in [56] follows a similar approach and presents comparable results and claims, however, these studies seem to be neglecting the impacts in-band distortion has on SIR. This idea, even though very interesting in the satellite application scenario, cannot be extended to modern 5G scenarios because it would increase adjacent channel interference in spatial-multiplexing environments. As satellite requirements got stricter and moved to multibeam applications there was a need for a better characterization of PA nonlinear behaviour. As described in [57], the more accurate Shimbo model[3] started to be used to describe PA nonlinearity as it allowed for simple integration with antenna array models. The study in [57] characterized all the active antenna array PAs and proved that the Shimbo model provides good IM characterization, claiming once again that arrays improve SIR .

With the rise of Massive MIMO in 5G applications the attention shifted once more toward the study of the impacts of PA nonlinearity on array pattern. In such scenario in-band distortion as well as scanning and source synthesis impacts can no longer be ignored.

An article from 2016, [54], studies the impacts of PA nonlinear behaviour on BER in

[2]Gain, beamwidth, SLL, among other metrics.

[3]This model is based on AM-AM and AM-PM conversion curves. For more details consult [54].

adaptive antenna systems, aiming to prove that nonlinearities cause nulls to shift in the array pattern. In the analysis it is assumed that amplifiers have no memory[4]. The Shimbo model is used to describe PA nonlinearity. Simulation results showed that nonlinearities radiate co-channel interference in several directions, causing null shifting. To compensate this a LMS algorithm was developed, automatically taking into account distortion effects through a distorted weight vector extractable from Shimbo model. Simulation showed that LMS optimization is capable of minimizing distortion effects, but a slight null shift always occurs. A two-element array test-bed then proved experimentally that PA nonlinearity causes null shifting. This simulation\optimization approach provides interesting results, being a good tool to predict expected nonlinear behaviours in the array pattern, but lacks comprehensive analysis. Besides mere observation, it isn't clearly stated why these null shifts occur. The algorithm doesn't seem to give insight about the problem, looking incapable of predicting special cases.

Recent research developments have specifically addressed nonlinear impairments on active antenna arrays in 5G Massive MIMO scenarios. The proposals of such studies are now presented and scrutinized. The aim is to explain the improvements brought by these theories toward the 5G vision while evidencing where improvements are still required.

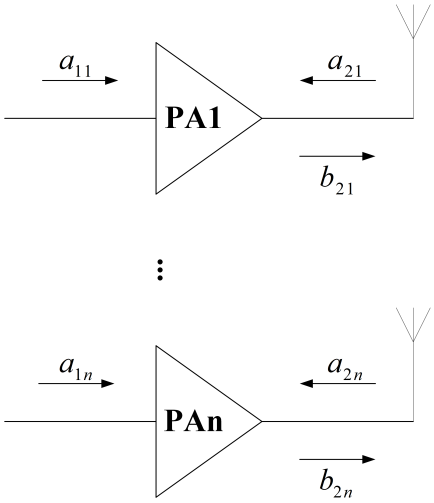

Figure 3.3: PAs in the multiple transmitter scenario described in [24].

The foreseen wide bandwidth communication channels that will be used in 5G Massive MIMO technologies bring added challenges to nonlinear characterization researchers. The study presented in [24] starts by pointing out some nonlinear characterization shortcomings of the existing state-of-the-art that cannot prevail in wide bandwidth applications. Among the highlighted points are the need to consider memory effects, the need to consider multiple antenna constrains and the need to view PAs as Multiple Input Single Output (MISO) devices. The article then follows with the presentation of a characterization model for wideband active antenna arrays. The presented model is based on Volterra memory polynomials and power wave analysis, being power waves described by Finite Impulse Response (FIR) filters. As seen in figure 3.3, this model uses a_{1i} and a_{2i} power waves to represent the PA inputs while b_{2i}

[4]Meaning that AM-AM and AM-PM conversions are frequency independent.

power waves represent the PA output signal[5]. With this approach authors claim that they can accurately represent PA nonlinearity in multiple transmitter scenarios; that they can consider antenna coupling effects, adjacent mixing effects and mismatch effects with a_{2i}; and that they can predict MIMO output, array far-field and beamforming functions with b_{2i}. This model therefore constitutes an excellent tool to simulate and optimize active antenna array systems to tailored goals. For this, accurate characterization of both PAs and antenna array is required. This technique has the potential to reduce design time and costs, allowing first-pass designs and minimizing the risk of damaging expensive components in extensive experimental tests. However, as is always the case, this study has its shortcomings. First of all, the presented analysis is excessively centred around PA characterization and often neglects the impairments the antenna array might pose. For example, stable array operation is assumed without taking into consideration that this implies: equal elements, equal current distribution, no coupling between elements and far-field analysis. Another example: it is assumed that b_{2i} are the radiated power waves by each antenna element, but this isn't completely true because it is the interference between a_{2i} and b_{2i} that actually impinges on each antenna element. It is also stated that S-Parameters completely characterize the antenna array[6], that the model generally predicts far-field, even though no experimental proof is presented under the simplifications made, and that array fabrication isn't required to attest the functionality of the model. Far-field measurements are required to support these claims, otherwise they seem unfounded. Secondly, it is hard to make good assumptions about the model variables to realistically operate the simulator because, like PA nonlinearities, coupling effects depend on operation mode, therefore a_{2i} and b_{2i} are interdependent. This makes it very hard to predict and measure a_{2i} without changing system operation point. Finally, the transmitter model is tested with different OFDM signals on each PA. This isn't a general 5G MIMO scenario because no sub-arraying operation is performed and because signals are completely uncorrelated. In 5G adaptive arrays, even though signals are uncorrelated, some element excitations are correlated, this scenario must be tested to realistically portray 5G scenarios.

The study in [22] presents a similar approach of [24], but it is even more focused on the PA nonlinear characterization, addressing the array as a coupling source, not aiming to understand the radiation behaviour of the active antenna array transmitter. This assumption once again reveals the disregard for antenna array impairments. Despite that, this study adds upon previous research by stating that coupling effects will not only change RF behaviour, but also its DC behaviour. This must be modelled for proper PA characterization, particularly in terms of efficiency. Therefore, the article proposes and experimentally validates a DC current model, adding another valuable tool to accurately characterize nonlinear active antenna arrays. In the presented multiple transmitter analysis it is assumed that all PAs present similar nonlinear behaviour. The authors are aware this is an ideal approximation that might lead to loss of generality, but use it to make the simulation model useful. In this analysis, besides testing OFDM signals, the study also considers a scanning array scenario. The results show that even though a non-general coupling analysis is used, for the particular case studied, experimental results and model predictions validate each other for both scenarios. However, small variations observed in error shape for the scanning array might be

[5]Thus representing the PA as a MISO device.

[6]Cross parameters are typically used as coupling metrics. However, coupling effects are dependent on excitation and environment, being most sensitive to scanning [19, 20, 21]. Therefore, typical S-Parameters characterization doesn't generally account for coupling in 5G scenarios. As nonlinear effects change array excitation they are also likely to change real-time array coupling effects.

a manifestation of non-considered effects. To complement the interesting results presented it would be important to accurately address coupling, to test a more realistic 5G MIMO scenario where both OFDM and array function are considered simultaneously, and to analyse the impacts on array pattern.

The article in [58] is probably the closest study to 5G Massive MIMO presently available in state-of-the-art research. Contrarily to the previously presented articles, which are mostly based on power wave analysis, this study builds its proposal upon information theory and signal processing. It addresses Massive MIMO theory concerns[7] while taking into consideration circuit level impairments of PAs and antenna arrays. Therefore, this study is one of the few examples of a full-range top-down approach to the 5G Massive MIMO problem. By starting from a Massive MIMO perspective this study assumes that signals follow Gaussian distributions and that channels are orthogonal. This orthogonality condition allows for the separation of linear and distorted signal components. As in the previously presented studies, these distorted signal components are obtained through Volterra memory polynomial description of PA nonlinearity. From the presented model the article then follows with the demonstration of how maximum directivity of distortion can be used as a pessimistic metric for distortion level, also showing that corrections must be made in multiple transmitter applications to properly account for SIR at the receiver, evidencing some miss interpretations presented in older satellite oriented research. With this model the authors are capable of extracting several interesting conclusions of which the most relevant are now listed:

- Distortion is beamformed in more directions than signal.
- Third-order distortion is the dominant distortion component.
- The model is capable of predicting distortion direction.
- Distortion direction depends on precoding weights[8].
- It is possible to steer distortion away from users.
- Direction of distortion is affected if different amplifiers distort differently, otherwise distortion direction isn't affected[9].
- Distortion doesn't vanish as the number of antennas tends to infinity, contradicting initial Massive MIMO assumptions.
- Distortion approximates isotropic radiation as the numbers of channels increase.
- High delay spreads improve distortion behaviour[10].

Some of these conclusions are in conformity with what was already presented in previous state-of-the-art studies, giving credibility to ones that are new. This is an important asset for this study that presents a theoretical model without EM simulation or experimental validation. It should be noted that even though the presented analysis is mathematically heavy, the authors endeavoured to present a comprehensive analysis of their work. This is a

[7] Issues like: channel fading, precoding, prefixes, signal modulation...
[8] Precoding weights are relatable with beamforming weights.
[9] This raises concerns about approximations made in some state-of-the-art works.
[10] This degrades other communication metrics.

major advantage in comparison with other state-of-the-art articles. However, it also has its downsides. First of all, it makes several optimistic assumptions like orthogonality and negligible coupling effects. These assumptions limit the generality of the model. Starting from an orthogonality premise is particularly difficult to support without experimental validation, being hard to accept that linear and distorted signal components are separable in practice. Secondly, it often imposes restrictive conditions on array operation, like equal amplitude and phase excitation in each element[11], to draw conclusions without evidencing that this isn't a generalizable scenario. In this analysis authors also seem to only be concerned with effects on major lobes, neglecting other important radiation pattern metrics like SLL. Finally, some odd assumption are made given the presented model. For example, it is assumed that amplifiers have equal distortion characteristics and provide equal power, even though it is stated that different amplifier distortion characteristics impact radiation properties and that power variations can change nonlinear behaviour. This is rather strange when it is also stated that in multiple beam scenarios different powers can be radiated by each beam. The most perplexing statement, however, is claiming, without presenting any proof, that the presented model expresses the same radiation pattern effects that would be observed if non-gaussian signals were considered at the input, even though this would require model redefinition. In summary, the study in [58] presents an interesting top-down approach to 5G Massive MIMO, giving comprehensive insights about the impacts nonlinear distortion has on the radiation properties of active antenna arrays, but sometimes lacks rigour in its statements. Experimental validation is therefore very important to clarify the presented concerns and more studies addressing the 5G Massive MIMO from this perspective are required.

As portrayed, across time several interesting approaches have been presented to address the impacts of nonlinear distortion in active antenna arrays. The mentioned characterization and optimization techniques evidence enormous potential, providing tools to test new scenarios and optimize designs considering real word limitations. However, the complexity and multidisciplinary nature of this problem seem to be causing difficulties in the definition of the complete set of premises that truthfully characterize real world behaviour. This seems to be caused by the focus on optimization, not aiming to understand the complete set of basic principles that govern the multiple disciplines, which sometimes are well-bound approximations. Such approach makes it hard to distinguish between the premises that are flexible from the premises that aren't. This also impedes the comparison between simulation and conceptual visualization, which forces the designer to blindly believe in the simulator until the final experimental test. This might be very problematic. Another problem seems to be the imprisonment of present approaches to classical PA characterization techniques that often neglect the influence the antenna might have on the results. Therefore, the presented tools are very promising, but seem to still require some fine tuning.

The following work aims to fight this tendency by presenting a very simplified analysis of the problem at hand. The goal is to understand the basic principles governing both antenna design and PA characterization, and then use them to predict some of the presented results in literature from a comprehensive basic principle approach.

[11] This imposes broadside radiation.

3.4 Theoretical Model: Concept

In state-of-the-art articles it is often stated that nonlinear distortion causes, among other radiation pattern distortion phenomena, SLL degradation and null shifting. However, the motives for the manifestation of such effects are often omitted or not clearly understood. This study consists on a comprehensive basic principle model of array pattern distortion that tries to understand why such effects are manifested.

The developed nonlinear antenna array model is said to be a basic principle approach because it makes the most basic assumptions possible about the PA, the antenna array and the excitation signal. The PA is represented by a 3_{rd} order model and memoryless conditions are assumed. The antenna array is described by array factor theory, neglecting coupling effects, and it is assumed to have narrow bandwidth[12]. The excitation signal is a sinusoidal tone[13].

This approach doesn't aim to be general, making several invalid assumptions for 5G scenarios, but it tries to balance the influence of the antenna array and of the PAs on radiation pattern. The aim is rather on the ability to predict and explain array pattern distortion using basic principles while confronting the obtained results with more complex state-of-the-art studies. A major goal of this study is to make a clear distinction between signal distortion and array pattern distortion.

3.4.1 3_{rd} Order Nonlinear Antenna Array

The signal present at the output of a 3_{rd} order nonlinear PA when a sinusoidal signal is presented to its input is given by expression 3.7.

$$y_{NL}(t) = \frac{1}{2}a_2A^2 + \left(a1A + \frac{3}{4}a_3A^3\right)cos(\omega t) + \frac{1}{2}a_2A^2cos(2\omega t) + \frac{1}{4}a_3A^3cos(3\omega t) \tag{3.7}$$

The antenna array is narrow band, therefore, the harmonics and the DC component are filtered and only the fundamental frequency component is radiated. The radiated signal by each antenna element consists in a linear component of the input signal and a third order amplitude distortion of that same signal. This radiated signal gives the amplitude excitation of each element as shown in 3.8.

$$a_n = a_{1_n}A + \frac{3}{4}a_{3_n}A^3 \tag{3.8}$$

$$AF = \sum_{n=1}^{N} a_n e^{j(n-1)kd[\cos(\theta)-\cos(\theta_o)]} \tag{3.9}$$

Therefore, the AF function for the case of an equally spaced N-element linear antenna array is given by expression 3.9.

[12] This is often the case in classical mobile communications.

[13] This excitation is seldom studied in research because of its simplicity, but it provides interesting insights.

3.4.2 Phasor Diagram Representation

By observing expressions 3.8 and 3.9 it can be noted that the AF function is complex if distortion components don't distribute symmetrically about the centre of the the array. This is a major difference from traditional signal distortion where real signals are represented in complex form to simplify analysis. Therefore, the most intuitive way to observe and understand radiation pattern distortion is to represent the AF terms in a phasor diagram[14].

To better understand this now consider the case of a two element array. If the pattern is normalized to the first element the total AF is given by 3.10.

$$AF = 1 + ae^{jkd[\cos(\theta)-\cos(\theta_o)]} \tag{3.10}$$

If there is no distortion this expression merely represents the AF of a two element array. However, the presence of distortion causes AF distortion. As shown in figure 3.4, if both phasors are aligned along the same direction distortion doesn't change the resultant phasor angle, but distorts amplitude, thus causing SLL distortion.

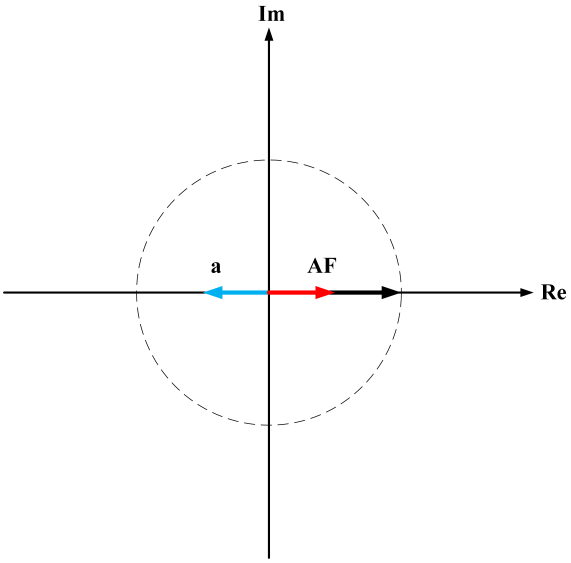

Figure 3.4: Radiation pattern distortion in phasor alignment scenarios.

If the two phasors aren't phase aligned both angular and amplitude distortion will occur. This is portrayed in figure 3.5.

As shown in figure 3.5, if distortion is such that one phasor has much larger amplitude than the other, the resultant phasor will tend to the larger amplitude phasor and array pattern will be mostly determined by element pattern because AF will tend to isotropic. Such thing happens when one amplifier distorts less than the other and power starts to increase.

For the case of a N-element array the phasor diagram distribution is more complex and it is hard to predict the worst case scenarios, but the possible observable effects are the same. Also note that distortion doesn't shift the array pattern major lobe because for the angle θ_o the exponent is equal to one and all the amplitudes of 3.9 add up, resulting in the maximum possible AF.

[14] This clever idea was inspired in the study presented in [59].

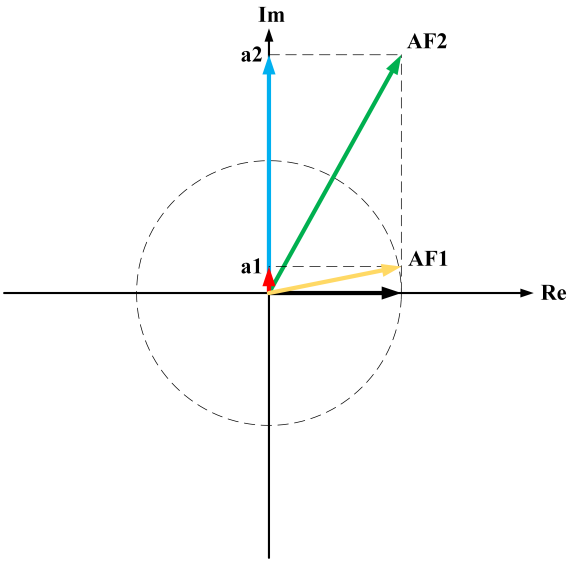

Figure 3.5: Radiation pattern distortion in phasor misalignment scenarios.

3.4.3 Interpretation

Now that the theoretical model is presented and visualized it is time to summarize its implications and draw some conclusions. Lets first review the total radiated electric field by an antenna array.

$$\overrightarrow{E}_{total}(\theta,\phi) = \overrightarrow{E}_{element}(\theta,\phi) \times AF(\theta,\phi,d_n,\beta_n) \tag{3.11}$$

This expression tells us that any factor that is common to every term of the AF of expression 3.9 can be extracted from the AF and considered as a scaling factor of the element pattern. Therefore, the AF is merely a function of what is different in each element excitation and only this difference will influence the configuration of the radiated field[15]. This leads to the following very interesting observation: if signal distortion in each element is equal no array pattern distortion will be observed. This agrees with some observations made in [58].

If the signal distortion distribution is symmetric about the centre of the array the AF is a real function and its phasor sum is always aligned. As previously stated, this will cause SLL distortion, but won't change the angular distribution of the AF. Therefore, this type of signal distortion distribution is incapable of changing the number of nulls nor the number of maxima.

Other signal distortion distributions cause both SLL degradation and null shift, but the extent of the impacts of such signal distortion in the array pattern is greatly dependent on the resultant phasor for a given mode of operation, being some signal distortion configurations more damaging than others. Extreme cases can potentially deform the array pattern to the extent of changing the number of maxima and nulls.

The most interesting thing to note, however, is that for the case under study the array pattern major lobe won't be shifted away from the desired angle, independently of the distortion distribution configuration.

[15] Assuming array theory is valid!

3.5 Theoretical Model: Simulation

In the previous sections the proposed theoretical model has been presented and visualized. There is, however, the need to validate it. A good way to start is by demonstrating that the predicted radiation pattern distortion observations are also inferable from a full-wave simulator like CST. To aid with this task the theoretical model is implemented in MATLAB and a test program is developed to generate random distortion components[16]. From this program the distorted amplitude excitations can be extracted and used to feed the linear antenna array designed in chapter 2[17].

The random distortion generation program was run several times until an extreme signal distortion distribution case occurred. This extreme case was then used to feed the linear antenna array. Table 3.1 presents the amplitude excitation of one of such cases. Figure 3.6 presents the distortion effects predicted by the theoretical model in MATLAB while figure 3.7 presents the results returned by CST for the same amplitude excitation. The results are normalized because this representation highlights radiation pattern shape distortion and because there is no interest in absolute gain values.

a_1	a_2	a_3	a_4	a_5	a_6	a_7	a_8
21670	2342	8404	13343	30895	678	1713	6437

Table 3.1: Example of asymmetric amplitude excitation distortion.

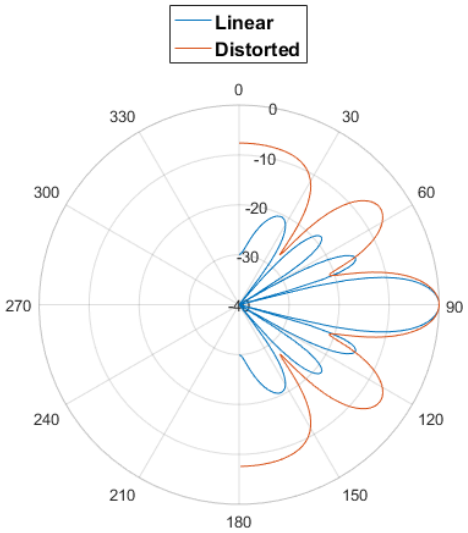

Figure 3.6: Theoretical Model.

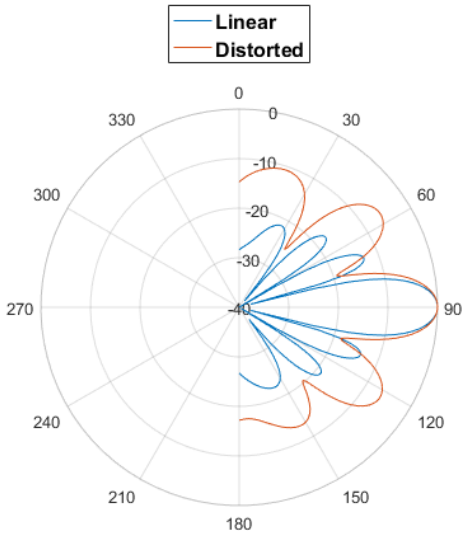

Figure 3.7: EM simulation.

As evidenced by figures 3.6 and 3.7, the results hold by the theoretical model are very similar to those obtained through EM simulation. A slight divergence is observed toward 0^o and 180^o because the rectangular microstrip antenna radiates poorly toward end-fire.

Besides the similarities between results it is important to highlight that these results are in accordance with the expectations: when distortion components are non-symmetric about

[16] These programs can be consulted in appendix D.
[17] Appendix A explains how to do this.

the centre of the array the radiation pattern is distorted, but the major lobe doesn't change direction. The presented example evidences both SLL distortion, null level distortion and radiation pattern shift. The radiation patten shift is reflected in the variation of the number of maxima and nulls. It should be noted that to evidence these phenomena it was given a very extreme example. More subtle variations are expected in real applications.

Through this simulation process it was also observed that array pattern distortion doesn't occur for uniform signal distortion distributions and that symmetric signal distortion distributions only cause SLL variation, not altering the number of maxima and nulls. However, these results will be more accurately and reliably explored in the following section. Therefore, such discussion is excluded from this section as the presented results already gave confidence to the developed theoretical model. Note that the observations made are limited to single tone excitations of the antenna element!

3.6 Theoretical Model: Experimentation

Now there is some confidence in the developed model. Therefore, it must be proved that PAs behave as described and that arrays respond accordingly to the model. To achieve this a experimental test-bed was developed.

3.6.1 Single Amplifier Test-Board

Before designing a multiple PA board it is important to understand the behaviour of a single PA. Therefore, a PA test-board inspired on ERA-2+ datasheet was designed for $5.67GHz$[18]. The test-board schematic is presented in figure 3.8.

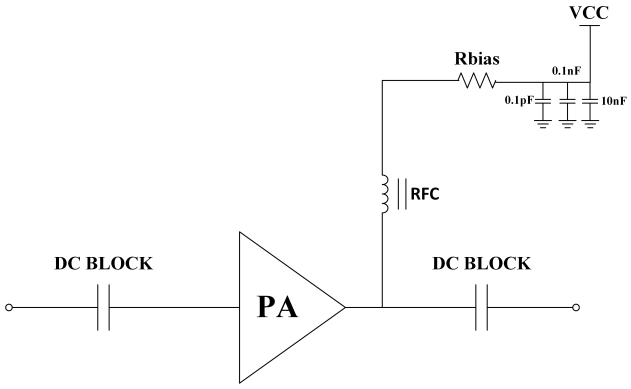

Figure 3.8: PA board schematic.

The components used for the testboard are listed in table 3.2. For this particular board a 100Ω resistor was used for bias. A high-Q capacitor of $2.4pF$ from Murata was selected as DC block because its datasheet indicated very low impedance for the interest band. Signal path lines are $3.83mm$ wide, which is the 50Ω line width for $5.67GHz$. Spacing was left in the layout for proper soldering of each component in accordance with the respective datasheets. The DC path was designed in a manner that allows all components to be properly soldered

[18]This is the operating frequency of the power splitter designed in appendix C

while respecting the $2cm$ available between power splitter branches[19]. The resultant PCB is shown in figure 3.9.

Component	Reference	Datasheet
PA	ERA-2+	Available at [60]
RFC	TCCH-80+	Available at [61]
DC Block	GJM 1555	Available at [62]
Trimmer	TSM4 YJ	Available at [63]

Table 3.2: List of components used.

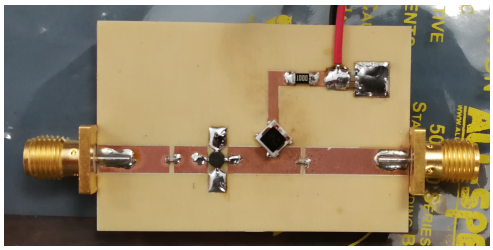

Figure 3.9: Developed single PA board.

The main goal with this design is to get familiarized with classical nonlinear characterization methods and to understand how different gain compression characteristics can be obtained in order to validate the proposed theoretical model. The ERA-2+ datasheet gives good indications in this regard, showing that drift in bias current causes changes in gain compression characteristics. To practically achieve this in the developed board one only has to adjust polarization voltage. Table 3.3 shows the required voltages to achieve 4 interest bias points and figure 3.10 shows the measurements of gain compression obtained through one-tone characterization[20].

IQ [mA]	VCC [V]
20	5.25
30	6.30
40	7.34
50	8.40

Table 3.3: Voltages that force desired polarization points

The results of figure 3.10 clearly prove that different gain compression characteristics are indeed obtained, particularly when bias current drops. This is expected because as current drops the conduction angle also reduces, thus increasing nonlinearity. Note that the maximum variations observed between feed points for a given value of P_{in} are about $1dB$.

Figure 3.11 shows the two-tone characterization of the design PA for several frequency spacings between tones for a polarization of $30mA$. Observe that all curves show the same

[19] This was done in antecipation to the multi-PA board design that must be integrated with the power splitter.

[20] Nonlinear characterization procedures are explained in appendix B.

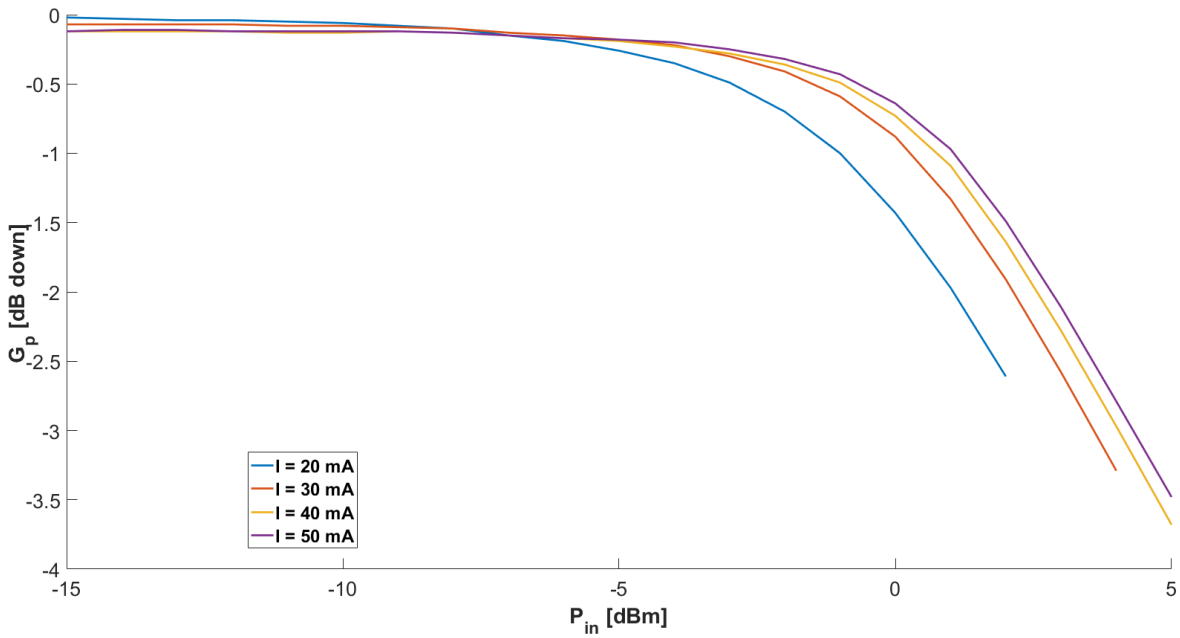

Figure 3.10: Normalized gain compression versus polarization current.

tendency independently of tone spacing. This was also verified for other polarizations. Such behaviour indicates that for the narrow band design considered memory effects can be ignored.

3.6.2 Multiple Amplifier Test-Board

The multiple PA board is built with a power splitter module described in appendix C and with 8 single PA modules like the one described in the previous section. The board is designed in a way that perfectly aligns with the linear antenna array designed in chapter 2. In this board the bias resistor is a 47Ω resistor plus an 100Ω multi-turn precision trimmer[21]. The idea is to use the trimmers to change R_{bias} and control current feed. This, as a consequence, controls the distortion characteristics. Such alternative had to be implemented because it would be impractical to use 8 independent power supplies. The resultant board is shown in figure 3.12 connected to the 8-element antenna array in an anechoic chamber measurement setup.

Before testing the multiple PA board all R_{bias} are set to 50Ω and then the board is feed. Voltage is increased until each amplifier draws $30mA$ in this configuration[22]. This is the maximum current drawn by each amplifier of the multiple PA board. Current was kept this low because it was previously observed that faster gain compressions occur for smaller current feeds. The voltage that provides $30mA$ per amplifier in the described condition is $5.13V$. After this initial calibration the voltage source is fixed and the bias resistors are changed in order to force gain compression. Figure 3.13 shows how resistor variation is capable of changing gain compression characteristics in a similar manner to the single PA board.

[21] This trimmer is listed in table 3.2.
[22] This means the total current is $240mA$

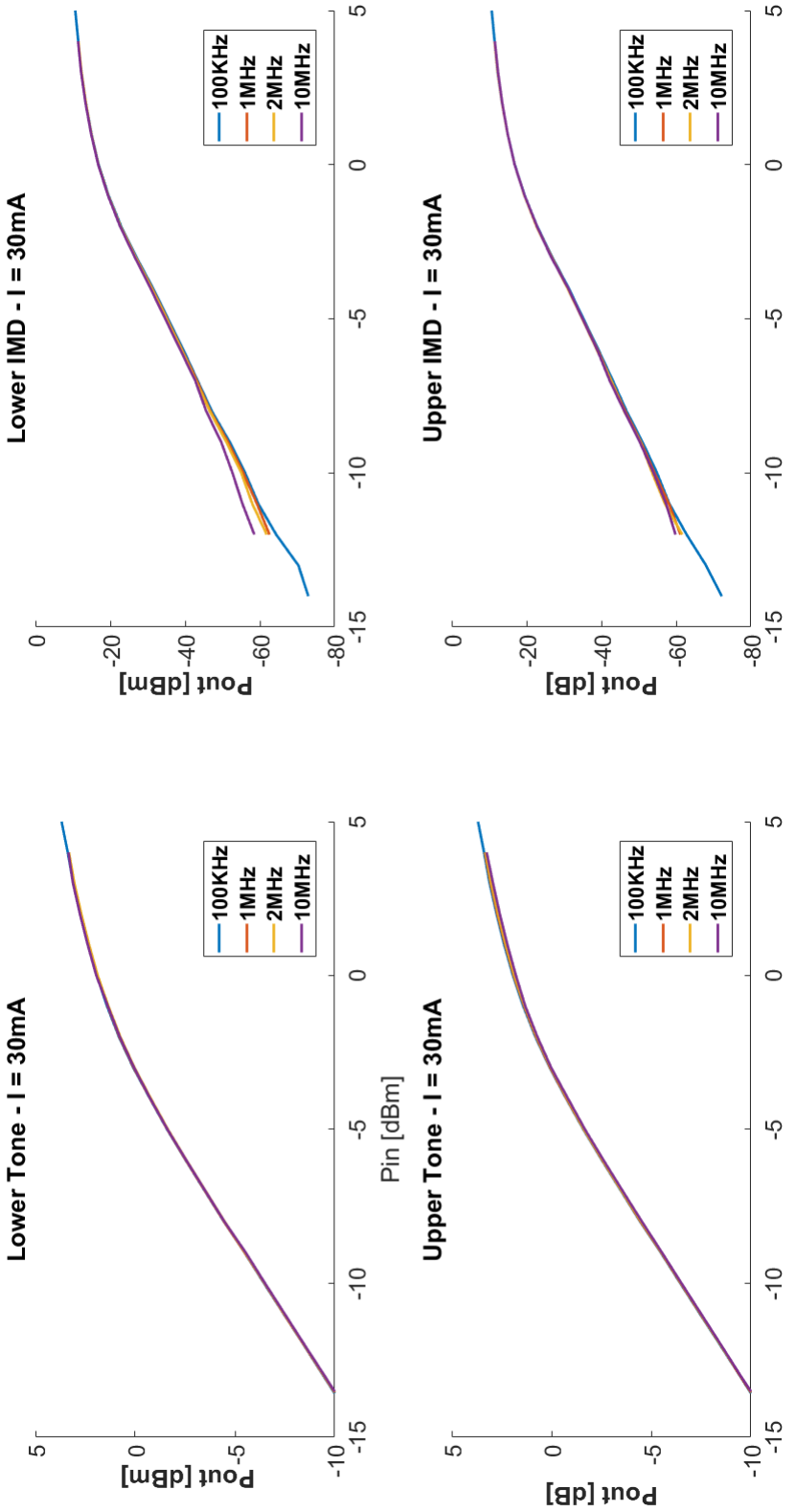

Figure 3.11: Two-tone characterization test.

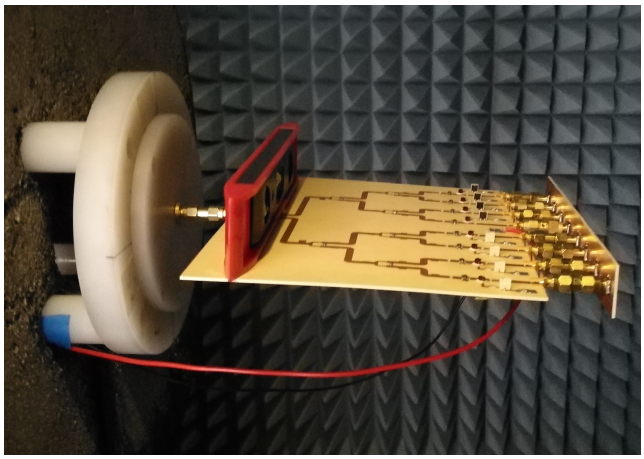

Figure 3.12: Developed multiple PA board.

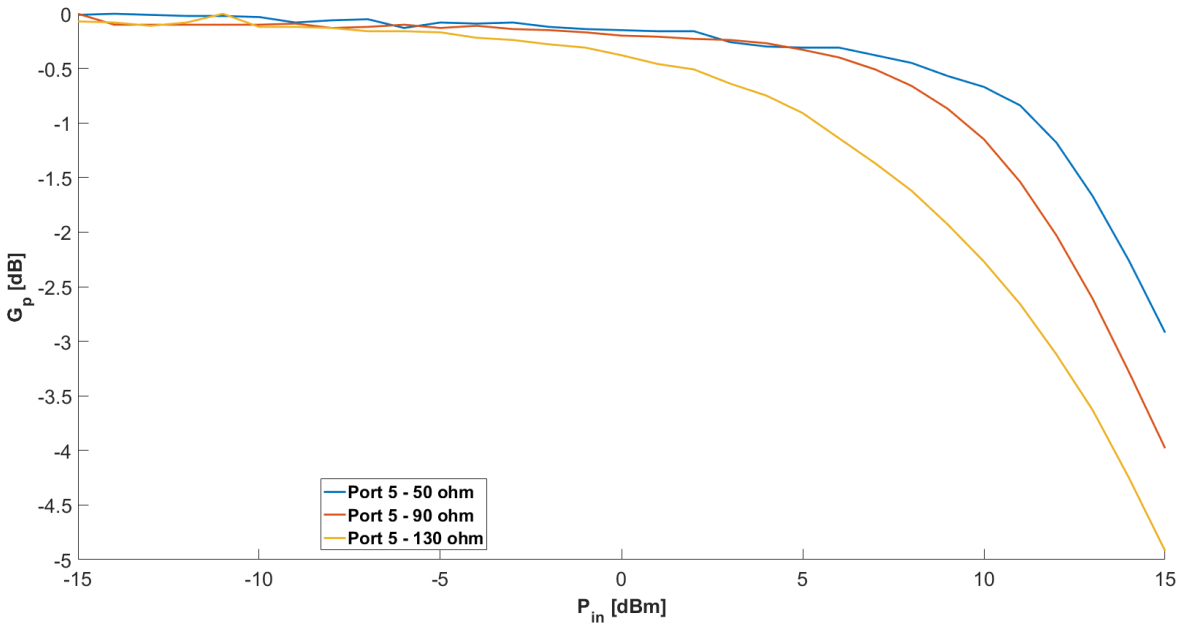

Figure 3.13: Normalized gain compression versus R_{bias}.

3.6.3 Nonlinear Antenna Measurement

After knowing that the conceived experimental apparatus works from the point of view of signal distortion it is time to test the nonlinear antenna array in an anechoic chamber environment. To do this several experimental test settings were defined contemplating both uniform, symmetric and asymmetric signal distortion distribution. These settings are listed in table 3.4 and the corresponding measured current consumptions are shown in table 3.5. The bias resistor values presented in table 3.4 are selected between 50Ω and 130Ω so that the compression characteristic at a given PA varies between the blue and yellow curves shown in figure 3.13. The selection of bias resistors thus dictates the distortion distribution in the array. Tests 1 and 2 contemplate uniform distortion distributions with different signal compression. Non-uniform distortion distribution is studied in tests 3 and 4. Finally, test 5 studies a symmetrical distortion distribution scenario. The variation of measured current consumption for each test scenario, observed in table 3.5, gives a good practical indication that the distortion characteristics seen in figure 3.13 are preserved in the presence of the array.

R_{bias} [Ω]	R_1	R_2	R_3	R_4	R_5	R_6	R_7	R_8
Test 1	50	50	50	50	50	50	50	50
Test 2	130	130	130	130	130	130	130	130
Test 3	130	120	90	50	130	50	130	50
Test 4	130	50	130	50	130	50	130	50
Test 5	130	110	90	50	50	90	110	130

Table 3.4: Tested experimental configurations.

Config	Test 1	Test 2	Test 3	Test 4	Test 5
I [mA]	241	106	153	176	156

Table 3.5: Experimental configurations - Bias Current.

For each test setting the array pattern measurements were performed for the two input powers: $0dBm$ and $8dBm$. The compression correspondent to these input powers is observable in figure 3.13. As can be seen, for $0dBm$ not all amplifiers are linear and at $8dBm$ not all amplifiers are significantly compressed. It would be of interest to explore these two extremities where all amplifiers are linear and where all amplifiers are compressed, but that wasn't possible due to experimental setup dynamic range limitations[23].

Lets now look into the awaited results. Figure 3.14 proves that uniform signal distortion distributions don't distort radiation pattern. Note that the radiation pattern shape doesn't change for: equal PA polarization at different compression points; different PA polarizations at different compression points; and even for low power symmetric signal distortion distribution. Don't forget that gain is normalized!

Figure 3.15 shows that increased signal distortion in symmetrical signal distributions cause SLL and null level variation, but don't cause array pattern shift nor do they change the number of nulls and number of lobes.

Figure 3.16 shows how asymmetric signal distortion distributions can cause array pattern shift. This is particularly visible near 0^o and 180^o where the blue and red line drift apart.

[23]For more details on the experimental apparatus please refer to appendix B.

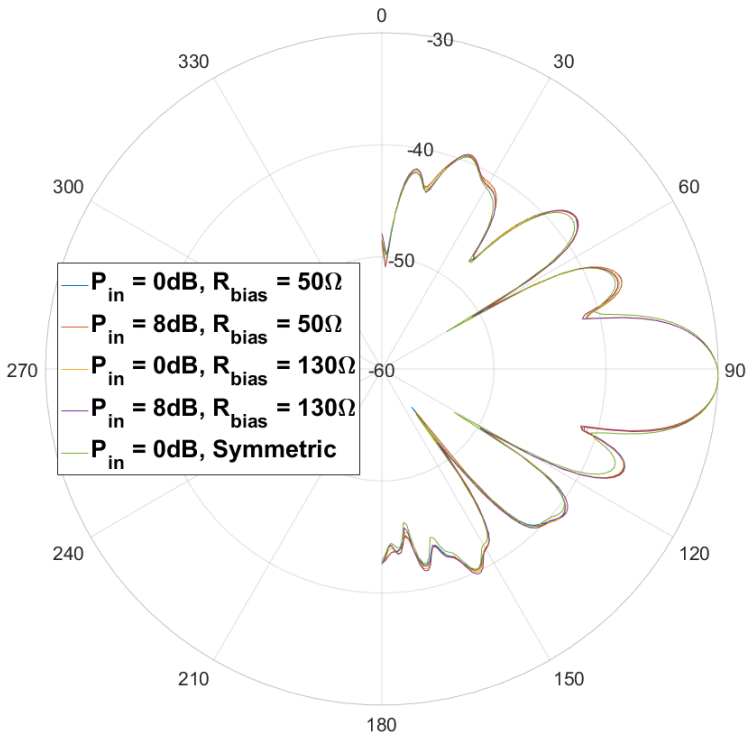

Figure 3.14: Pattern Distortion in real AF functions.

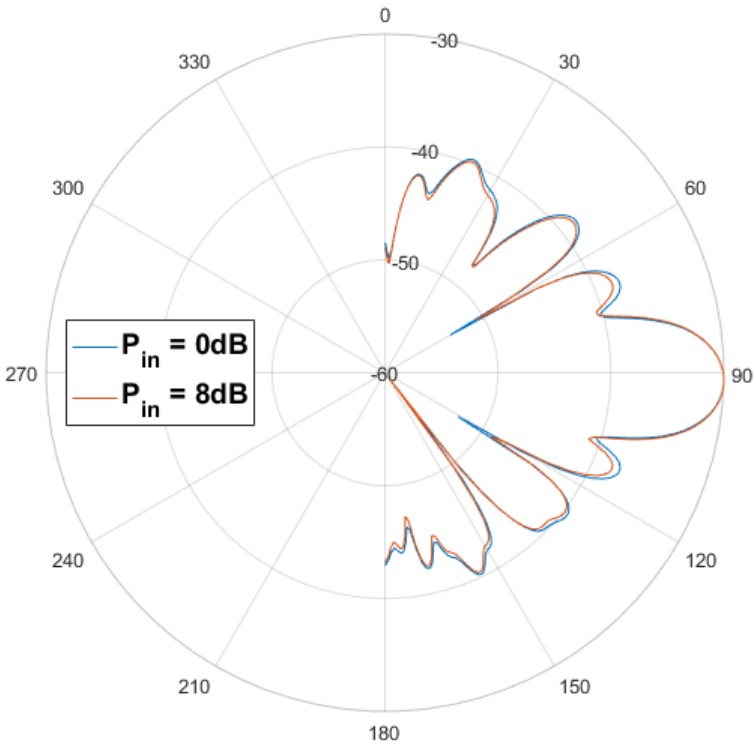

Figure 3.15: Pattern Distortion - Symmetric signal distortion distribution.

Figure 3.17 shows how asymmetric signal distortion distributions can cause SLL distortion. This is visible in the degradation of the second nulls as gain compression increases. This configuration in particular gives the idea that if signal power was further increased it would result in the elimination of the second nulls of the array pattern. With these results it is therefore proved experimentally that asymmetric signal distortion distributions can cause radiation pattern shape distortion.

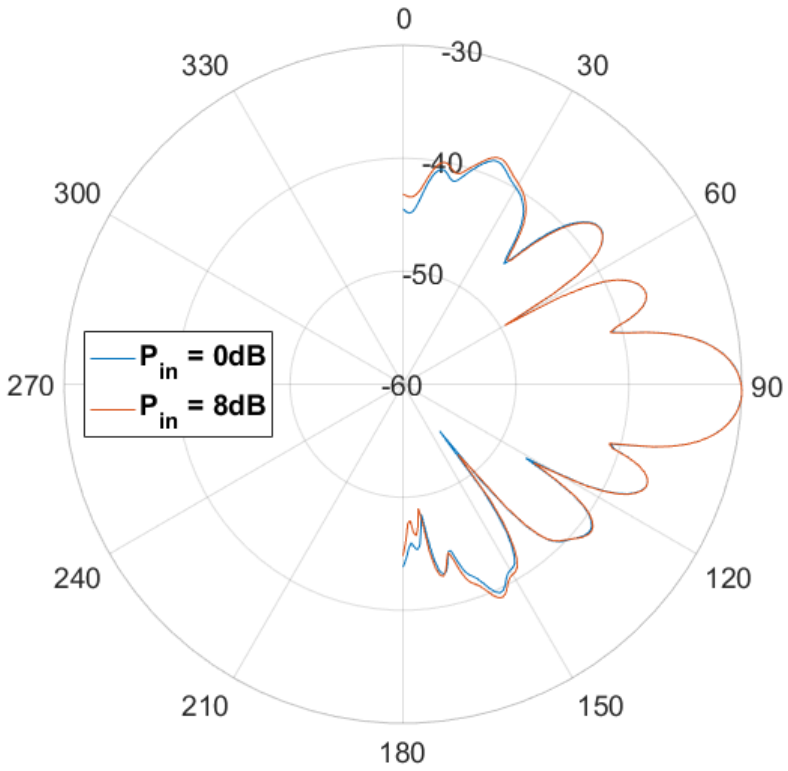

Figure 3.16: Pattern Distortion - Asymmetric signal distortion distribution - config 1.

The most interesting thing to prove, however, is that independently of the distortion components the major lobe direction doesn't shift. This is further evidenced in figure 3.18 where the results obtained from all testing scenarios are overlapped in the same graph.

The obtained results are encouraging for future studies on nonlinear antenna arrays, but it should be noted that the presented results were limited by the short dynamic range of the experimental setup which did not allow nonlinear effects to manifest more expressively. Allied to this is the empirical nature of the experiment, i.e. it isn't known a priori what configuration will cause the most degrading resultant AF phasor, therefore the selected configuration might not be significantly expressive of the array pattern distortion phenomenon. It would therefore be interesting to merge this more conceptual approach with the more rigorous approaches available in state-of-the-art. This would allow a more evident observation of array pattern distortion.

Regardless of its simplicity, this model arrives at several conclusions presented in state-of-the-art while providing some additional contributions, particularly for the simple case of single tone array excitation. For this particular topic no other study was found in state-of-the-art. The advantage of the presented approach is the intuitive connection between model and

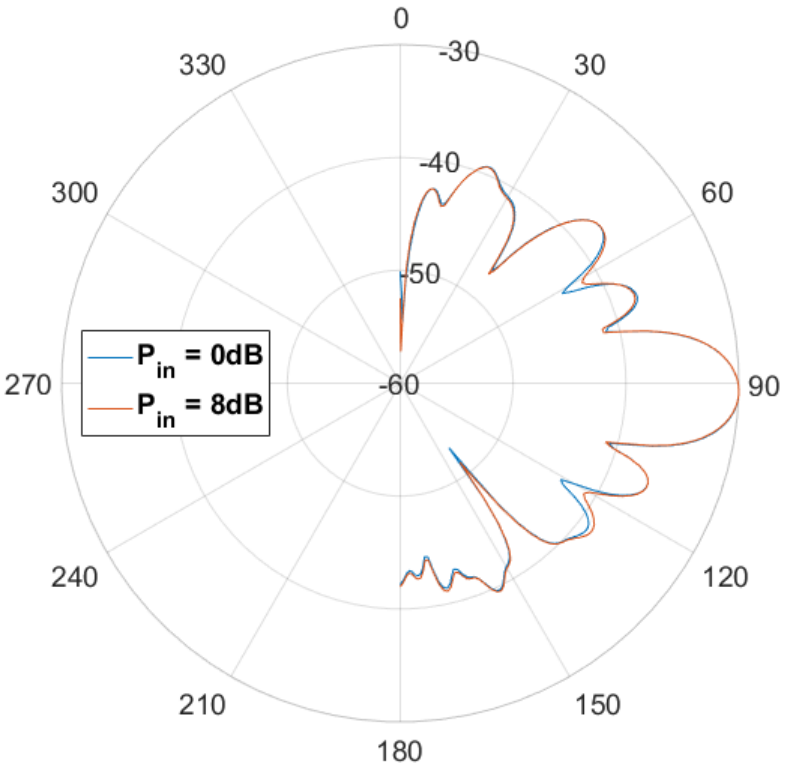

Figure 3.17: Pattern Distortion - Asymmetric signal distortion distribution - config 2.

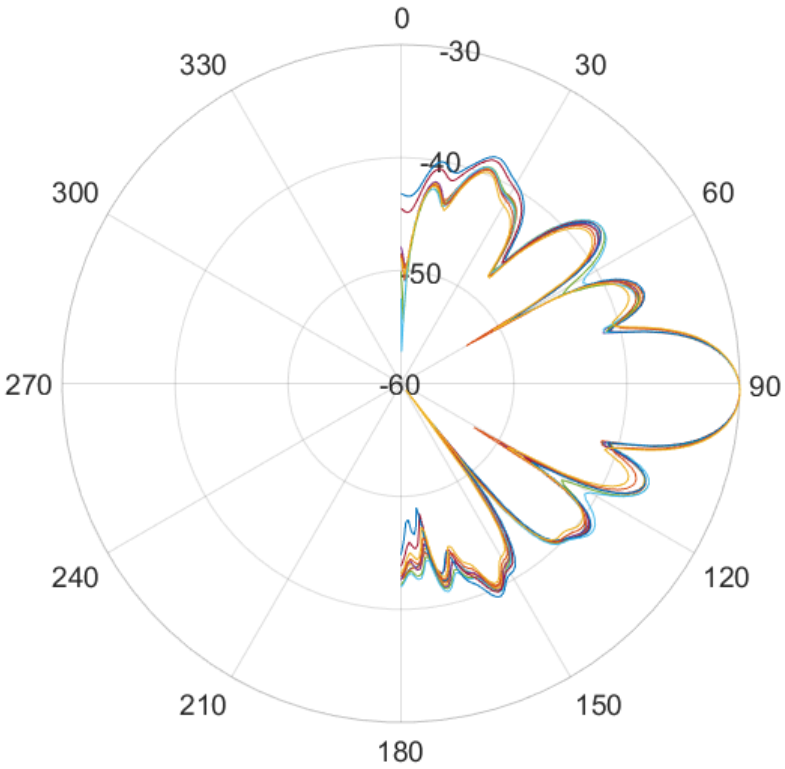

Figure 3.18: Pattern Distortion - all tested scenarios.

expected result. This allows us to be reluctant when faced with experimental observations of undesired effects as well as being critical of the results given by more complex models. The most important contribution of this work, however, is the clarification of the difference between signal distortion and array pattern distortion.

Chapter 4

Final Remarks

This chapter overviews what was accomplished with the develop work during this MSc dissertation. Initially, the major contributions of this work are evidenced. Then, a critical analysis is presented where some shortcomings and alternative paths are explained. Finally, possible future developments are portrayed.

4.1 Contributions

This section now presents the major contributions of this work by the order of their presented in the document.

Chapter 1 provides a good overview of the present mobile communication scenario, presenting the envisioned solutions for 5G as well as their benefits and shortcomings. This overview doesn't simply present the scenario, it looks carefully to the available documentation in order to understand what are the major RF hardware problems and explores those problems in detail. This chapter tries to be general by including both research and industry perspectives. Therefore, chapter 1 is a good resource for contextualization in the present mobile scenario, especially for people aiming to understand what are the RF hardware issues. At the end of this chapter a plan of action to solve the most critical RF hardware issues in 5G is given. This might be interesting for people looking to understand where to start their work toward the solution of these problems.

Chapter 2 presents an overview of antenna theory supported by several designs and experiments. Besides presenting theory, this chapter also makes the important connection between antenna theory and the central role of antenna arrays in future mobile communications. Chapter 2 thus constitutes a good resource for beginners learning antennas and for people trying to understand how antenna arrays can enhance mobile communications.

Chapter 3 explains the currents state-of-the-art knowledge about nonlinear antenna array transmitters. The state-of-the-art analysis goes beyond the presentation of the articles and tries to point out shortcomings and possible improvements to state-of-the-art studies. The most relevant contribution of this work, however, is the alternative method proposed to study nonlinear antenna arrays presented in this chapter. This method is more concerned with the impacts signal distortion has on radiation patterns than some of the most recent state-of-the-art articles. The proposed model was validated both by simulation and experiments. This model makes a clear distinction between signal distortion and array pattern distortion, providing insights about the expected array pattern distortion given a certain signal distortion

spatial distribution. This last point is the major contribution of the developed model.

The appendices provide information about simulation and measurement procedures. This information might be helpful to beginner designers.

4.2 Critical Self-Reflection

Now that the positive aspects of the developed work were presented this section considers its downsides. The following criticisms refer to the document structure in order to clearly identify potential future improvements in each phase of work development.

A criticism that can be made to chapter 1 is that it is too focused on RF hardware problems and because of this it might not provide useful information to people exploring other 5G issues. It might also be said that the presented overview is too extensive given the range of applications that are explored afterwards in the document. The path presented to solve RF issues in 5G applications is given from the perspective of a beginner with yet small understanding of the field. Thus, even though the presented plan is supported by research it might be in the wrong direction. Its simplistic and disperse nature might require more detailed tuning to give fruitful results in the resolution of the complex issues at hand.

A shortcoming of chapter 2 is that it only explored well-known antenna theory topics, not exploring any state-of-the-art issue. In the presented discussion it would also have been interesting to consider different antenna elements, explore antenna polarization and design an active antenna array to test source synthesis applications and explore adaptive beamforming. However, in this MSc dissertation framework there was no time to address the aforementioned points. It should be noted that even though the presented study didn't explore state-of-the-art antenna topics, it was a crucial learning step which enabled the implementation of the experimental test-bed of the theoretical model presented in chapter 3.

Chapter 3 presents a modest contribution to the ambitious goal of understanding how nonlinear antennas behave. Even though interesting results are presented there are also some shortcomings. These are now listed bellow.

- The presented model only considers the single tone excitation of the antenna array. This is a case of reduced practical value in mobile communications.
- No scanning or source synthesis functions are explored in the presented results.
- Important multiple adaptive beamforming functionalities aren't tested.
- The developed model doesn't provide tools to exactly determine the resultant AF phasorial distortion in a practical scenario. Being therefore difficult to empirically test the worst case array pattern distortion scenario.
- The model was tested in small signal distortion scenarios. It would be important to test this model in higher distortion scenarios to more clearly evaluate their impacts in array pattern distortion.

4.3 Future Work

The future work consists in further developing the presented work by following the path presented in chapter 1.

First there is a need to mathematically connect the presented approach with more accurate PA and antenna characterization techniques available in state-of-the-art. Once this is done there is room to test worst case array pattern distortion scenarios and to explore compensation techniques. It would then be interesting to incorporate coupling effects in the developed model and evaluate how results might vary.

Another interesting path is to explore how OTA characterization techniques can be used to characterize array pattern distortion phenomena.

There is therefore plenty of possibilities to expand on the developed work, but before doing this it is important to further test the developed test-bed until more severe array pattern distortion phenomena are observed. Then, with those results a scientific paper will be produced to spread the developed model into broader horizons.

Future studies should also test important antenna functions in 5G scenarios like scanning and multiple adaptive beamforming.

Appendix A

Simulation Procedures

In the course of the developed work several simulation and optimization procedures had to be extensively performed to complete distinct tasks that eventually culminated in the manufacturing of a final design or in a conceptual proof. This appendix aims to provide a good understanding about the general simulation approach followed while alleviating the main text of repetitive simulation procedure descriptions.

A.1 Dielectric Information

It makes sense to leave here the dielectric characteristics before advancing into any simulation procedures because the same dielectric material was used in every design.

Reference	ISOLA ASTRA 3
Thickness [mm]	0.035
Height [mm]	1.52
ϵ_r	3
$tan\delta$	0.0016

Table A.1: Dielectric properties.

A.2 Circuit Simulation

The selected RF circuit design tool was Keysight's ADS 2016. The following sections evidence the followed simulation procedures and alert for important simulation concerns. The guidelines described mostly follow Keysight's ADS documentation orientation[1] and personal experience.

A.2.1 Design and Optimization

The circuit design was split into three stages: the circuit optimization stage, the EM simulation stage and the co-simulation validation stage.

[1] The most used reference guide was the example book available in [64].

Initially a schematic of the desired circuit is defined and parametrized. Several design goals are then defined. Finally the optimization engine searches the best fit for the design goals through parameter adjustment. The ADS optimizer was configured to use the hybrid and gradient algorithms.

After optimization a layout is automatically generated, placing all transmission lines with proper physical displacement[2]. Then an EM simulation is performed to attest the radiation properties of the design. This was done using ADS Momentum Microwave simulator. To properly configure this simulation the dielectric structure, mesh and ports must be adequately defined. The dielectric must be correctly characterized in height, dielectric constant, loss tangent and, if existent, in via structure. For reliable results the mesh simulation frequency should at least double the maximum simulated frequency and cells per wavelength must be adjusted to create a sufficiently fine mesh; in the developed EM simulations 60 cells per wavelength were used. Ports are placed where components are to be soldered to allow co-simulation tests, these ports are calibrated using the ADS TML calibration standard. Besides this, the frequency range must be adjusted to cover the bands of interest with sufficient resolution.

Finally the resultant EM model is placed in a schematic along with discrete components. Then a co-simulation attests the validity of the design considering radiation effects.

Complex circuits must be broken down into modules and the aforementioned steps must be performed several times. This approach leads to better results because on each iteration circuit level optimizations take into consideration the radiating effects found in previous steps, allowing for a more reliable representation of the RF circuit.

For the developed designs only S-Parameters simulations were required to achieve the desired goals.

A.2.2 Reference Guide Design

For circuit design based on design guides no simulations were performed because typically relevant data wasn't available to perform accurate simulations. Therefore, for such designs ADS was only used as a layout design tool to produce the final circuit board while the design itself is inspired on design guide heuristics[3].

A.3 Antenna Simulation

The antenna design tool used during this MSc dissertation was CST Studio Suite 2017, most specifically the CST Microwave Studio and CST Design Studio tools. The following sections explain important concerns that must be taken into account while using this EM simulator as well as the chosen simulation path. The presented procedures are mostly based on personal experimentation and on guidelines given in CST Studio Suite 2017 documentation and design guides.

A.3.1 Solver Selection

An important step while using a powerful EM simulator is the selection of an appropriate numerical solver for the specific problem studied.

[2] All developed designs were based on planar microstrip lines.
[3] This was the case of the PA boards.

The CST time domain transient solver was always used in the developed antenna designs because it was the most general solver available, scaling well with the larger meshes required for antenna array simulation, performing well when integrating nonlinear devices. These were desirable features for the developed work. However, using this solver requires some attention.

First of all the simulation bandwidth must be at least 30% of the carrier frequency for the simulator to allow the excitation response to stabilize and present reliable results. Therefore a frequency range between $3GHz$ and $9GHz$ was selected to guarantee accurate simulations near the $5GHz$ band

Secondly, whenever the obtained results present unexpected oscillatory behaviour the solver accuracy must be increased. In final designs this parameter was set to $-60dB$.

Finally, at the first solver iteration the adaptive mesh refinement option must be on, so that the mesh is optimized to present low variance results.

To further assure correct mesh generation the number of cells per wavelength can also be adjusted. This parameter was set to 60 cells per wavelength.

A.3.2 Ports and Monitors

CST offers several tools to excite antennas and evaluate their performance. In CST antenna port excitation can either be emulated by discrete ports, waveguide ports or plane waves. The selected method was the discrete port because even though it is simpler and less accurate this method is easier to control while providing trustworthy results.

The results of most interest for the developed work are S-Parameters, field distributions and far-field pattern. To acquire this data CST provides ports and E-field, H-field and Far-Field monitors.

A.3.3 Optimization

Optimization in powerful EM simulators must be carefully controlled as brute-forcing approaches can lead to very extensive simulations resulting in nothing like the desired goals. Therefore, a method where parametric variations were combined with pure optimization techniques was preferred.

Initially the key design parameters are individually varied and simulated for a sensible range of values. From these results potential interest value regions are defined. Only then is the optimizer set up.

In the optimizer setup the parameters to be optimized are bound within the interest region and specific design goals are defined to help the optimizer to converge to the desired response. The optimization algorithm used was the Trust Region Framework.

A.3.4 Array Simulation

Besides the aforementioned metrics of interest, in antenna array design it is also relevant to test amplitude and phase excitations to test source synthesis techniques and to study the impacts of PA nonlinear behaviour in array pattern. To perform these studies in CST all element ports were simulated separately and combined with the “combine results” post-processing tool.

This tool allows rapid manipulation of source amplitude and phase excitation, giving immediate results of the array pattern with the considered excitation.

A.4 Manufacturing

Once simulated designs are in accordance with requirements they are ready for manufacturing. Since the developed designs are planar only three cuts of the device are required to fully describe the design: the top layer, the bottom layer and the via layer. This information is directly exportable from the EM simulators through gerber files. The developed boards were all manufactured in Instituto de Telecomunicações of Aveiro using a milling process.

Appendix B

Measurement Procedures

During the developed work many were the occasions where designs had to be validated experimentally. This validation demands for the execution of several detailed measurement procedures. This appendix aims to provide a good understanding about the procedures followed while alleviating the main text of repetitive descriptions.

B.1 S-Parameters

S-Parameters characterization is probably the most on demand measurement in RF engineering. Agilent Technologies' PNA-X N5242A Vector Network Analyzer (VNA) was the measurement equipment used to perform such characterization because it has 4 ports available. This speeds-up the measurement of multiple port devices. Whenever the number of ports was higher than 4 the excess ports were matched to 50Ω loads and several measurements were performed in different port configurations until a complete device characterization was achieved.

Before performing measurements the PNA-X was calibrated for the interest band using Agilent Technologies 85052D calibration kit. The guided calibration procedure was followed.

B.2 Antenna Pattern

To perform array pattern measurements far-field conditions are required. Therefore, these measurements were performed in an anechoic chamber. In such environment the walls are covered with RF absorbers and very directive probe antennas are used to impinge a direct illumination of a plane wave into the test antenna, thus emulating far-field conditions. The test antenna is characterized by measuring the S_{21} between the probe and test antennas. Probe antennas are linearly polarized to allow accurate characterization of both direct and cross polarizations.

Radiation pattern measurements are performed along the principal $\overrightarrow{E}$-plane and principal $\overrightarrow{H}$-plane of the test antenna for both direct and cross polarizations. This is done by rotating the test antenna either along its principal $\overrightarrow{E}$-plane or along its principal $\overrightarrow{H}$-plane with the probe antenna polarization aligned either horizontally or vertically. The antenna under test is rotated along a constant radius circumference between 0 and 180 degrees[1]. S_{21} measurements

[1]Figure B.1 describes this procedure. The VNA used was Rohde & Schwarz ZVB20.

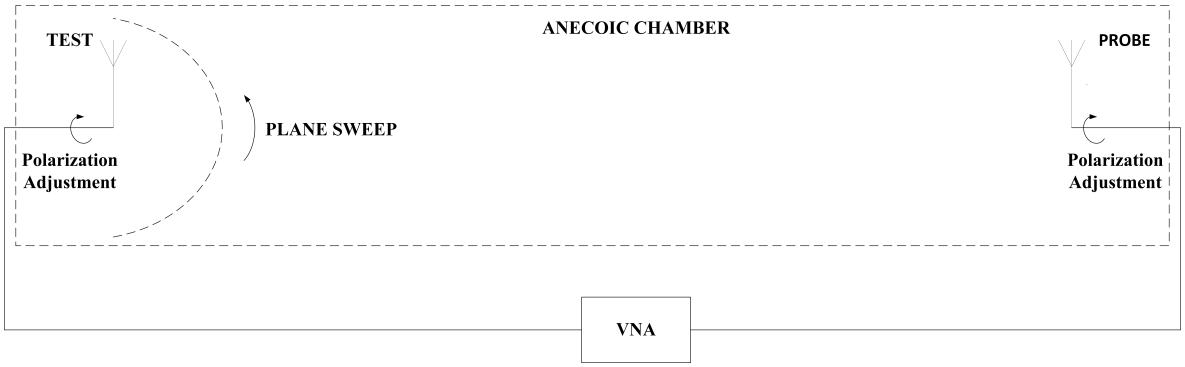

Figure B.1: Radiation pattern measurement apparatus.

are performed for each angle.

DETI's anechoic chamber was used to perform these measurements.

B.2.1 Gain

Array pattern measurements can be converted into realized gain metrics by using a gain transfer\comparison procedure. This consists on using a reference antenna of known gain to convert S_{21} measurements into gain, as expressed in (B.1)[2].

$$Gre_{test} = Gre_{ref} - (S21_{ref} - S21_{test}) \tag{B.1}$$

B.2.2 Nonlinear Antenna

The reciprocity principle doesn't apply to nonlinear antennas, therefore receiving and transmitting characteristics must be characterized separately. The developed design is a transmitter, so only the transmitting characteristics are of interest in this particular case.

To perform such characterization the anechoic chamber setup was adjusted so that the test antenna inside the chamber was the one transmitting and the probe antenna was the one receiving. DC power also had to be provided inside the chamber for proper polarization of the nonlinear antenna PAs. The power supply used for this purpose was Thurlby Thandar PL320QMT.

B.3 PA Characterization

As previously stated, proper PA characterization consists in an accurate representation of AM-AM conversion, AM-PM conversion and spectral regrowth properties of the PA in a real operation scenario. However, for the particular case of the nonlinear memoryless study developed only one-tone and two-tone AM-AM conversion characterization is required. The theory behind these characterization experiments was already presented in chapter 3. Procedures were adapted for the multiple PA board. In the performed measurements it was assumed that equipment nonlinearity is much smaller than Device Under Test (DUT) nonlinearity.

[2]This result is derivable from free-space Friis formula.

B.3.1 One-Tone Characterization

The one-tone characterization test was performed to measure the PA's gain compression characteristics.

The experimental setup is presented in figure B.2 and the measurement equipment used is listed in table B.1.

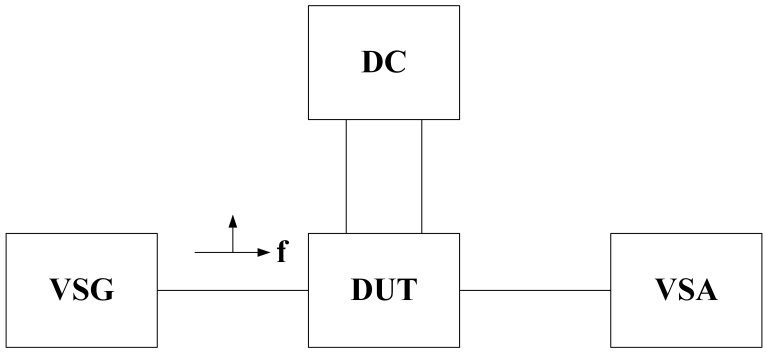

Figure B.2: One-tone measurement apparatus.

Equipment	Model
VSG	Rohde & Schwarz SMW 200A
VSA	Rohde & Schwarz FSQ8
DC	Thurly Thandar PL320 QMD

Table B.1: Nonlinear characterization measurement equipment.

The measurement procedure consists in generating an input tone with desired power in the Vector Signal Generator (VSG) and then measure the output power in the Vector Signal Analyser (VSA). The gain characteristics can then be indirectly extracted from expression (B.2).

$$G_p = \frac{P_{out}}{P_{in}} \tag{B.2}$$

The input power was swept from a low power value until at least $1dB$ gain compression observations.

The gain value is frequently normalized in the presented results because in this study the interest is in knowing for which input powers does gain compress instead of the gain absolute value.

B.3.2 Two-Tone Characterization

The two-tone characterization experiment was performed to prove that for the case under study the PA behaviour was memoryless.

The experimental procedure is equal to that of the one tone test, but the experimental setup is adapted to inject two symmetrically spaced tones about the carrier frequency at the PA input.

In this experiment, besides measuring the output power of the tones, the output power of the intermodulation distortion products is also measured.

Appendix C

Power Divider Design

The need to divide signal power by several transmit paths is often found in RF engineering. Such was the case when it was required to feed the 8−element linear antenna array from a single RF output of the VSG. To do this a 1 to 8 power splitter was designed based on a Wilkinson power divider module. This appendix explains the details of how such a power divider was designed.

C.1 Wilkinson Power Divider

C.1.1 Concept

The Wilkinson power divider is a circuit designed to provide equal power division and port isolation. This circuit is described by the schematic in figure C.1.

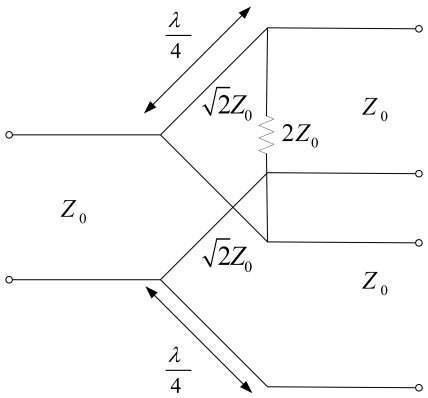

Figure C.1: Wilkinson power divider schematic.

This representation can be further simplified to the one seen in figure C.2[1].

From this representation it is now easy to understand the power divider operation. If all ports are matched the resistance of value $2Z_o$ is open circuited, thus providing port isolation.

[1]Impedances are normalized to Z_o in this representation.

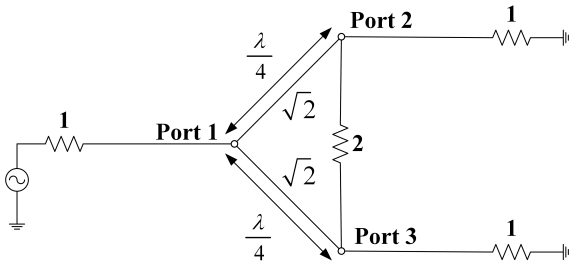

Figure C.2: Wilkinson schematic simplification.

In such conditions the S-Parameters are given by expression (C.1).

$$z\overrightarrow{S} = \begin{cases} S_{11} & = 0 \\ S_{22} = S_{33} & = 0 \\ S_{12} = S_{21} & = \frac{-j}{\sqrt{2}} \\ S_{13} = S_{31} & = \frac{-j}{\sqrt{2}} \\ S_{23} = S_{32} & = 0 \end{cases} \tag{C.1}$$

Therefore, this circuit achieves lossless equal power division with port isolation[2].

C.1.2 Design

Before starting the design procedure it was important to define the design frequency range. From the S-Parameters characterization of the antenna array presented in chapter 2 it was decided that the Wilkinson power divider operation should be guaranteed for the frequency range between $5.62GHz$ and $5.72GHz$, therefore covering the bandwidth where all antenna elements present maximum adaptation, being Z_o considered for the central frequency, $5.67GHz$.

Microstrip transmission lines were used to design the power splitter. The design consists in the optimization of the width and length of the $\frac{\lambda}{4}$ transformer to guarantee the conditions defined in C.1. This optimization follows the steps described in appendix A. Isola Astra 3 was the dielectric used, whose characteristics are also presented in appendix A.

The $\frac{\lambda}{4}$ transformer consists in a semicircle of radius $1.5mm$ followed by a line. This makes the splitting branch distance equal to $3mm$, which is the desired spacing for soldering the resistance of value $2Z_o$. The resulting layout is presented in figure C.3 and its dimensions are detailed in table C.1.

W_{50} [mm]	W_{trans} [mm]	L_{trans} [mm]
3.83	1.78	3.72

Table C.1: Wilkinson power divider layout dimensions.

The results presented in figure C.4 show that for the interest band the circuit behaves very close to an ideal balanced power divider, with transmission coefficients very near $-3dB$ and with all ports well adapted near $-20dB$ of reflection coefficient.

[2]The presented analysis of the Wilkinson Power divider is inspired on the explanation given in [65].

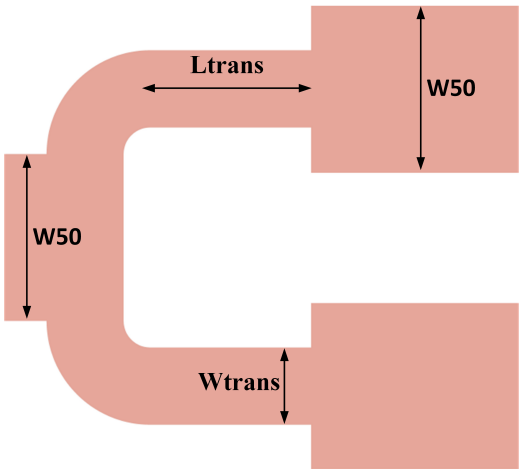

Figure C.3: Wilkinson power divider layout.

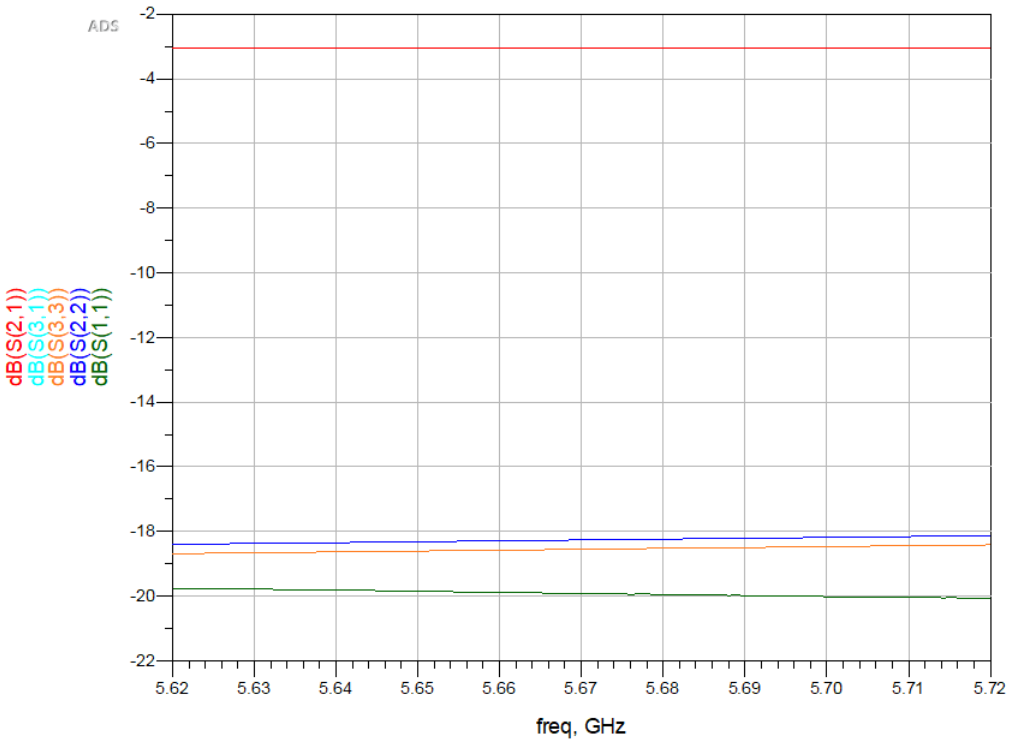

Figure C.4: Wilkinson power divider S-Parameters.

C.2 1 to 8 Power Divider

C.2.1 Concept

To properly feed the 8−element linear antenna array it is important to provide each element with equal power and phase. Therefore, transmit paths between input signal and each antenna element must be equal in length, and the separation between each output must equal the element spacing at the feed point.

To guarantee such conditions the antenna array was corporate fed with a three stage power splitter consisting on 7 Wilkinson power divider modules and branching lines. The branching lines are placed at the outputs of each stage to guarantee the desired output port spacing and to avoid overlapping\line crossing on each stage. These branching lines, however, introduce mismatch. So a open-line stub matching network is introduced at each end of the branching line to compensate this mismatch for the interest band. Both branching lines and stubs have 50Ω characteristic impedances at $5.67GHz$. The length of the branching lines is presented in table C.2 and the final design layout is presented in figure C.5.

L_1 [mm]	L_2 [mm]	L_3 [mm]
43.95	18.35	5.55

Table C.2: Branching line dimensions.

C.2.2 Design

To arrive at the final design presented in figure C.5 several iterative co-simulation procedures, base on appendix A, were performed. These steps are now described by order:

1. The optimization starts from the output stage toward the input stage because it is easier to guarantee that the output ports are presented with 50Ω loads.

2. EM simulation of the third stage branching lines is performed.

3. Third stage stubs are optimized with knowledge of the EM properties of the third stage branching lines and of the Wilkinson power divider module.

4. EM simulation of the third stage block is performed[3].

5. EM simulation of the second stage branching lines is performed.

6. Second stage stubs are optimized with knowledge of the EM properties of the second stage branching lines, of the Wilkinson power divider module and of the third stage block.

7. EM simulation of the second stage block is performed. This block contains all components from the second and third stages.

8. EM simulation of the first stage branching lines is performed.

[3]Each stage is constituted by Wilkinson power divider modules, branching lines and open-line stubs.

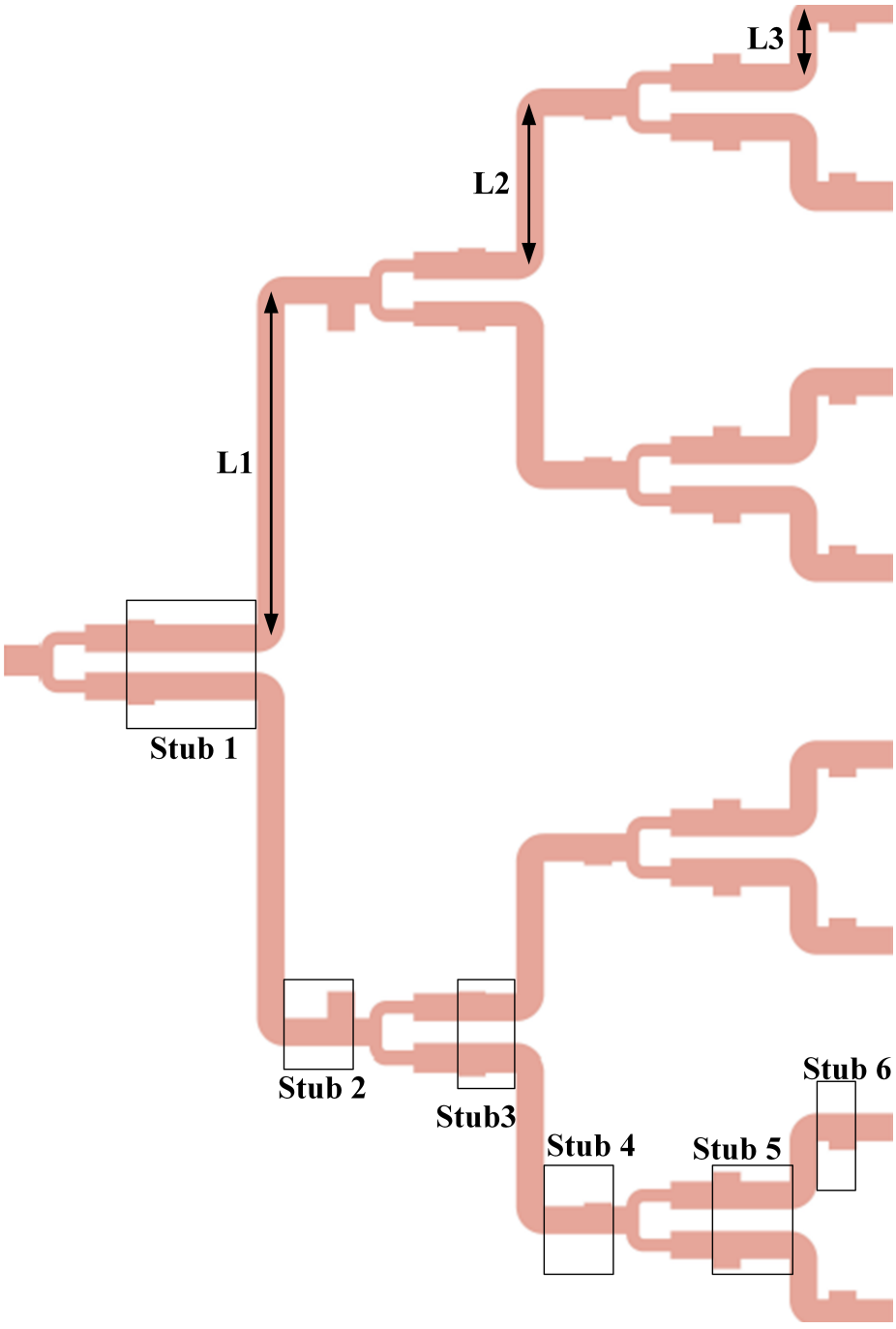

Figure C.5: 1:8 power splitter layout.

9. First stage stubs are optimized with knowledge of the EM properties of the first stage branching lines, of the Wilkinson power divider module and of the second stage block.

10. EM simulation of the complete 1 to 8 power divider is performed.

The optimized stub lengths are presented in table C.3 while the measured S-Parameters are presented in figures C.6 and C.7. The measurement of the 1 to 8 power divider followed the procedures described in appendix B.

stub	1	2	3	4	5	6
open length [mm]	00.66	3.91	0.50	0.50	1.34	1.20
line length [mm]	14.09	5.82	4.22	5.52	6.76	1.58

Table C.3: Stub dimensions.

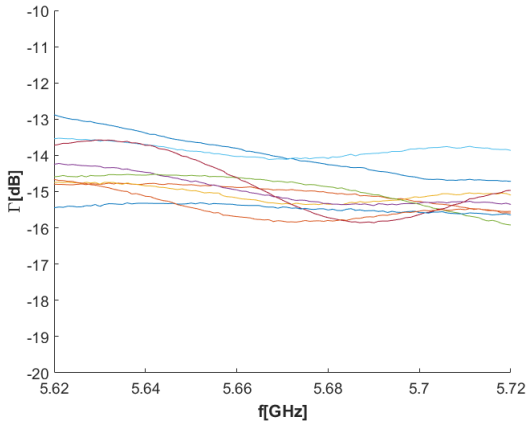

Figure C.6: Port Adaptation.

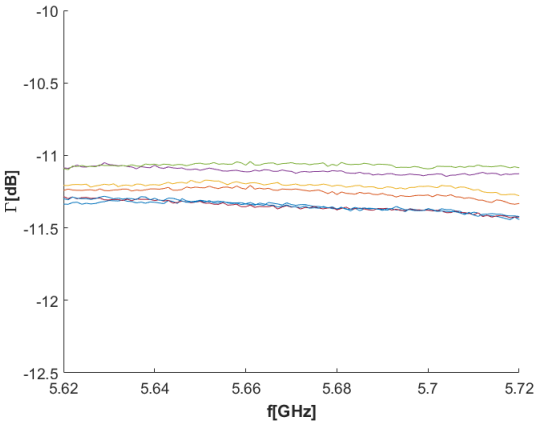

Figure C.7: Transmission Coefficients.

As can be seen, all ports are reasonably matched with reflection coefficients bellow $-10dB$ for the entire interest band. Within this band the power division between ports is well balanced, being the transmission form port 1 to any other port of about $-11.25dB$. These aren't perfect results, as it would be desirable to have better matching and more proximity to the ideal power splitter transmission of $-9dB$. However, such results agree well with simulation and constitute the best achieved design. Such was the case because ISOLA ASTRA 3 is a very thick substrate that enhances fringing fields and makes lines thicker, thus increasing radiation effects. This poor selection of substrate impeded a better power splitter performance, but it was followed through because expenses had already been made in SMA connectors for this substrate. Besides these shortcomings, results are satisfactory for the desired application scenarios.

Appendix D

Array Pattern Simulator

During this MSc dissertation a MATLAB simulator was developed to study array factor. This simulator was used to explore the impacts array factor has on array pattern, to understand how array factor can be used to implement important functions such as scanning, source synthesis and adaptive beamforming, and also to aid in the development of the proposed nonlinear model of array pattern distortion. Besides aiding in the understanding of the aforementioned phenomena, this simulator also guided circuit simulation, EM simulation and experimental procedures. This appendix now presents the developed scripts to implement the aforementioned algorithms and some visualization test programs.

D.1 AF Functions

D.1.1 Linear Array AF

```
function [theta,AF] = LinearAF(N,d,a,beta,lambda,resolution)
%Wave Number
k = 2*pi/lambda;
%Angle Sweep
theta = linspace(0,2*pi,360*resolution);
%AF vector
AF = zeros(1,length(theta));
%Implementation of Linear AF Formula
for n = 1:N
   AF = AF + a(n) * exp( j *( k * d(n) * (cos(theta)) + beta(n))
      );
end
%Normalization
AF = AF/max(abs(AF(:)));
```

D.1.2 Source Synthesis

D.1.2.1 Dolph-Tschebyscheff

```
function [a] = tschebyscheff(N,R)
%This Script Implements the algorithm presented in Balanis for
   computer
%implementations

m = N-1;
R0 = 10^(R/20);
z0 = cosh(1/m*acosh(R0));

if (rem(N,2) == 1)
    M = (N-1)/2;
    a = zeros(1,M+1);
    qsi = ones(1,M+1);
    for n = 1:M+1
        for q = n:M+1
            a(n) = a(n) + (-1)^(M+1-q)*(z0)^(2*(q-1))*((
               factorial(q+M-2)*(2*M))/(qsi(n)*factorial(q-n)*
               factorial(q+n-2)*factorial(M-q+1)));
        end
    end
    a = a/(a(1));
    a = [fliplr(a(2:end)) a];
else
    M = N/2;
    a = zeros(1,M);
    for n = 1:M
        for q = n:M
            a(n) = a(n) + (-1)^(M-q)*z0^(2*q-1)*((factorial(q+M
               -2)*(2*M-1))/(factorial(q-n)*factorial(q+n-1)*
               factorial(M-q)));
        end
    end
    a = a/(a(1));
    a = [fliplr(a) a];
end
end
```

D.1.2.2 Schelkunoff

```
function [an,bn,dn,N] = schelkunoff(lambda,d,z)
%an - amplitude exitation
%bn - phase excitation
%N  - number of elements
%d  - distance between elements
```

```
%z  - desired nulls

if (sum((z < 0) + (z > pi)) ~= 0)
display('ERROR! Angle range: 0 to pi')
end

%Wave Number
k = 2*pi/lambda;

%Determination of the nulls in complex plane
zn = exp(j*k*d*cos(z));
%Determination of polynomial with such nulls
a = poly(zn); a = fliplr(a);
N = length(a);
dn = (0:N-1)*d;
%Conversion of polynomial in amplitude and phase exitations
an = abs(a);
bn = phase(a);
bn = bn .* ( abs(bn) > 0.001);
```

D.1.3 3_{rd} Order Nonlinear Antenna Array

```
function [theta,AF] = LinearAF3rdO(N,d,a,ad,scan,f,resolution)
c = 3*10^8; lambda = c/f; k = 2*pi/lambda;
theta = linspace(0,2*pi,360*resolution);
AF = zeros(1,length(theta));
%ad represents the distortion contributions of the 3rd order
   model
for n = 1:N
   AF = AF + ( a(n) + a(n)^3 * 3/4 * ad(n) ) * exp( j * k * d(n)
      *(n-1) * (cos(theta) - cos(scan)) );
end
AF = AF/max(abs(AF(:)));
```

D.1.4 Visualization Functions

```
function AFdB = AF2dB(AF,dBnorm)
%This funtion centres the polar representation of AF to in the
   desired
%dBnorm
AFdB = 10*log(AF);
AFdB(AFdB < dBnorm) = dBnorm;
AFdB = AFdB+abs(dBnorm);

function AFdB = AF2dBnorm(AFdB,dBnorm)

AFdB(AFdB < dBnorm) = dBnorm;
AFdB = AFdB+abs(dBnorm);
```

D.2 Test Programs

D.2.1 Scanning

```
clear all; close all; clc;
%CST Result Files and Normalization
scan30 = load('scan30.txt');
scan30(:,3) = scan30(:,3) - abs(max(scan30(:,3)));
scan45 = load('scan45.txt');
scan45(:,3) = scan45(:,3) - abs(max(scan45(:,3)));
scan60 = load('scan60.txt');
scan60(:,3) = scan60(:,3) - abs(max(scan60(:,3)));
scan90 = load('scan90.txt');
scan90(:,3) = scan90(:,3) - abs(max(scan90(:,3)));
%Array Definitions
f = 5.67*10^9; c = 3*10^8; lambda = c/f; k = 2*pi/lambda;
N = 8; d = 0.0256*(1:N); a = ones(1,N); resolution = 1;
%Desored Scan Angles
b1 = -k*d*cos(pi/6);
b2 = -k*d*cos(pi/4);
b3 = -k*d*cos(pi/3);
b4 = -k*d*cos(pi/2);
%Array Factor Determination
[theta,AF1] = LinearAF(N,d,a,b1,lambda,resolution);
[theta,AF2] = LinearAF(N,d,a,b2,lambda,resolution);
[theta,AF3] = LinearAF(N,d,a,b3,lambda,resolution);
[theta,AF4] = LinearAF(N,d,a,b4,lambda,resolution);
%Polar Plot of the Dolph-Tschebyscheff Array
figure
graph = polaraxes;
hold on;
h = polarplot(graph,theta(1:180),AF2dB(abs(AF1(1:180)),-50));
h = polarplot(graph,scan30(:,1)/180*pi,AF2dBnorm(scan30(:,3)
   ,-50));
hold off;
graph.ThetaZeroLocation = 'top';
graph.ThetaDir = 'clockwise';
haxes = get(h,'Parent');
haxes.RTickLabel = {'-50','-40','-30','-20','-10','0'};
legend('MATLAB','CST')
figure
graph = polaraxes;
hold on
h = polarplot(graph,theta(1:180),AF2dB(abs(AF2(1:180)),-50));
h = polarplot(graph,scan45(:,1)/180*pi,AF2dBnorm(scan45(:,3)
   ,-50));
```

```
hold off
graph.ThetaZeroLocation = 'top';
graph.ThetaDir = 'clockwise';
haxes = get(h,'Parent');
haxes.RTickLabel = {'-50','-40','-30','-20','-10','0'};
legend('MATLAB','CST')
figure
graph = polaraxes;
hold on
h = polarplot(graph,theta(1:180),AF2dB(abs(AF3(1:180)),-50));
h = polarplot(graph,scan60(:,1)/180*pi,AF2dBnorm(scan60(:,3)
   ,-50));
hold off
graph.ThetaZeroLocation = 'top';
graph.ThetaDir = 'clockwise';
haxes = get(h,'Parent');
haxes.RTickLabel = {'-50','-40','-30','-20','-10','0'};
legend('MATLAB','CST')
figure
graph = polaraxes;
hold on
h = polarplot(graph,theta(1:180),AF2dB(abs(AF4(1:180)),-50));
h = polarplot(graph,scan90(:,1)/180*pi,AF2dBnorm(scan90(:,3)
   ,-50));
hold off
graph.ThetaZeroLocation = 'top';
graph.ThetaDir = 'clockwise';
haxes = get(h,'Parent');
haxes.RTickLabel = {'-50','-40','-30','-20','-10','0'};
legend('MATLAB','CST')
```

D.2.2 Dolph-Tschebyscheff

```
clear all; close all; clc;
%CST Result Files and Normalization
tsche = load('tschebyscheff.txt');
tsche(:,3) = tsche(:,3) - abs(max(tsche(:,3)));
%Array Definitions
f = 5.67*10^9; c = 3*10^8; lambda = c/f; k = 2*pi/lambda;
N = 8; d = 0.0256*(1:N); b = -k*d*cos(pi/2); resolution = 1;
R = 28; R = 10^(R/20);
%Determination of the Dolph-Tschebyscheff Array
a = tschebyscheff(N,R);
[theta,AF] = LinearAF(N,d,a,b,lambda,resolution);
%Polar Plot of the Dolph-Tschebyscheff Array
figure
graph = polaraxes;
```

```
hold on;
h = polarplot(graph,theta(1:180),AF2dB(abs(AF(1:180)),-50));
h = polarplot(graph,tsche(:,1)/180*pi,AF2dBnorm(tsche(:,3),-50))
   ;
hold off;
graph.ThetaZeroLocation = 'top';
graph.ThetaDir = 'clockwise';
haxes = get(h,'Parent');
haxes.RTickLabel = {'-50','-40','-30','-20','-10','0'};
legend('MATLAB','CST')
```

D.2.3 Schelkunoff

```
clear all; close all; clc;
%CST Result Files and Normalization
schel = load('schelkunoff.txt');
schel(:,3) = schel(:,3) - abs(max(schel(:,3)));
%Array Definitions
f = 5.67*10^9; c = 3*10^8; lambda = c/f; k = 2*pi/lambda; d =
   0.0256;
resolution = 1;
%Desired Nulls
z = [0 pi/6 pi/4 pi/3 2*pi/3 5*pi/6 pi];
%Determination of Schelkunoff Array
[an,bn,dn,N] = schelkunoff(lambda,d,z);
[theta,AF] = LinearAF(N,dn,an,bn,lambda,resolution);
%Polar Plot of Schelkunoff Source Synthesis
figure
graph = polaraxes;
hold on;
h = polarplot(graph,theta(1:180),AF2dB(abs(AF(1:180)),-100));
h = polarplot(graph,schel(:,1)/180*pi,AF2dBnorm(schel(:,3),-100)
   );
hold off;
graph.ThetaZeroLocation = 'top';
graph.ThetaDir = 'clockwise';
haxes = get(h,'Parent');
haxes.RTickLabel = {'-100','-80','-60','-40','-20','0'};
legend('MATLAB','CST')
```

D.2.4 3_{rd} Order Nonlinear Antenna Array

```
clear all; close all; clc;

%Array Definitions
f = 5.67*10^9; c = 3*10^8; lambda = c/f; k = 2*pi/lambda;  N =
   8;
d = 0.0256*ones(1,N); a = ones(1,N); resolution = 1; scan =  pi
   /2;
%Random generation of nonlinearities
distortion = rand(1,N)*0.05;
%Distorted AF Calculation
[theta,AF] = LinearAF3rdO(N,d,a,distortion,scan,f,resolution);
[theta,AF1] = LinearAF3rdO(N,d,a*100,distortion,scan,f,
   resolution);
%Plot of distorted AF for different input powers
figure
graph = polaraxes;
hold on
polarplot(graph,theta(1:180),AF2dB(abs(AF(1:180)),-40));
h = polarplot(graph,theta(1:180),AF2dB(abs(AF1(1:180)),-40));
hold off;
graph.ThetaZeroLocation = 'top';
graph.ThetaDir = 'clockwise';
haxes = get(h,'Parent');
haxes.RTickLabel = {'-40','-30','-20','-10','0'};
legend('Linear - a = 1','Distorted - a = 100')
```

References

[1] Jeffrey G Andrews, Stefano Buzzi, Wan Choi, Stephen V Hanly, Angel Lozano, Anthony CK Soong, and Jianzhong Charlie Zhang. "What will 5G be?" In: *IEEE Journal on selected areas in communications* 32.6 (2014), pp. 1065–1082. DOI: 10.1109/JSAC.2014.2328098.

[2] Federico Boccardi, Robert W Heath, Angel Lozano, Thomas L Marzetta, and Petar Popovski. "Five disruptive technology directions for 5G". In: *IEEE Communications Magazine* 52.2 (2014), pp. 74–80. DOI: 10.1109/MCOM.2014.6736746.

[3] Sanjay Raman, Robert Weigel, and Tim Lee. "The internet of space (IoS): A future backbone for the internet of things?" In: *Newsletter* 2014 (2014). URL: https://iot.ieee.org/newsletter/march-2016/the-internet-of-space-ios-a-future-backbone-for-the-internet-of-things.html.

[4] Thomas L Marzetta. "Massive MIMO: an introduction". In: *Bell Labs Technical Journal* 20 (2015), pp. 11–22. DOI: 10.15325/BLTJ.2015.2407793.

[5] Theodore S Rappaport, Shu Sun, Rimma Mayzus, Hang Zhao, Yaniv Azar, Kevin Wang, George N Wong, Jocelyn K Schulz, Mathew Samimi, and Felix Gutierrez. "Millimeter wave mobile communications for 5G cellular: It will work!" In: *IEEE access* 1 (2013), pp. 335–349. DOI: 10.1109/ACCESS.2013.2260813.

[6] Thomas Cameron. *RF TECHNOLOGY FOR THE 5G MILLIMETER WAVE RADIO*. Tech. rep. Analog Devices, 2016. URL: http://www.analog.com/media/en/technical-documentation/white-papers/RF-Technology-for-the-5G-Millimeter-Wave-Radio.pdf.

[7] Kate A Remley, Joshua A Gordon, David Novotny, Alexandra E Curtin, Christopher L Holloway, Matthew T Simons, Robert D Horansky, Michael S Allman, Damir Senic, Maria Becker, et al. "Measurement Challenges for 5G and Beyond: An Update from the National Institute of Standards and Technology". In: *IEEE Microwave Magazine* 18.5 (2017), pp. 41–56. DOI: 10.1109/MMM.2017.2690882.

[8] Erik G Larsson, Ove Edfors, Fredrik Tufvesson, and Thomas L Marzetta. "Massive MIMO for next generation wireless systems". In: *IEEE communications magazine* 52.2 (2014), pp. 186–195. DOI: 10.1109/MCOM.2014.6736761.

[9] Thomas L Marzetta. "Noncooperative cellular wireless with unlimited numbers of base station antennas". In: *IEEE Transactions on Wireless Communications* 9.11 (2010), pp. 3590–3600. DOI: 10.1109/TWC.2010.092810.091092.

[10] André Prata, Sérgio C Pires, Mustafa Acar, Arnaldo SR Oliveira, and Nuno Borges Carvalho. "Towards circulator-free multi antenna transmitters for 5G". In: *Microwave Symposium (IMS), 2017 IEEE MTT-S International*. IEEE. 2017, pp. 677–680. DOI: 10.1109/MWSYM.2017.8058661.

[11] Katharina Hausmair, Per N Landin, Ulf Gustavsson, Christian Fager, and Thomas Eriksson. "Digital Predistortion for Multi-Antenna Transmitters Affected by Antenna Crosstalk". In: *IEEE Transactions on Microwave Theory and Techniques* 66.3 (2018), pp. 1524–1535. DOI: 10.1109/TMTT.2017.2748948.

[12] Wonil Roh, Ji-Yun Seol, Jeongho Park, Byunghwan Lee, Jaekon Lee, Yungsoo Kim, Jaeweon Cho, Kyungwhoon Cheun, and Farshid Aryanfar. "Millimeter-wave beamforming as an enabling technology for 5G cellular communications: Theoretical feasibility and prototype results". In: *IEEE communications magazine* 52.2 (2014), pp. 106–113. DOI: 10.1109/MCOM.2014.6736750.

[13] M. Kottkamp and C. Rowell. *Antenna Array Testing - Conducted and Over the Air: The Way to 5G*. Tech. rep. Rohde & Schwarz, 2016. URL: https://cdn.rohde-schwarz.com/pws/dl_downloads/dl_application/application_notes/1ma286/1MA286_2e_AntArrTest_5G.pdf.

[14] M. Reil and G. Lloyd. *Millimeter-Wave Beamforming: Antenna Array Design Choices & Characterization*. Tech. rep. Rohde & Schwarz, 2016. URL: https://cdn.rohde-schwarz.com/pws/dl_downloads/dl_application/application_notes/1ma276/1MA276_2e_Beamform_mmW_AntArr.pdf.

[15] Rick L Sturdivant and Edwin KP Chong. "Systems engineering of a terabit elliptic orbit satellite and phased array ground station for IoT connectivity and consumer internet access". In: *IEEE Access* 4 (2016), pp. 9941–9957.

[16] 3GPP. *3GPP Webpage*. URL: http://www.3gpp.org/ (visited on 06/26/2018).

[17] ITU. *IMT-2020*. URL: https://www.itu.int/en/ITU-R/study-groups/rsg5/rwp5d/imt-2020/Pages/default.aspx (visited on 06/26/2018).

[18] ITU. *IMT-2020 and Beyond*. URL: https://www.itu.int/en/ITU-R/study-groups/rsg5/rwp5d/imt-2020/Pages/default.aspx (visited on 06/26/2018).

[19] J. L. Allen and B. L. Diamond. *Mutual Coupling in Array Antennas*. Tech. rep. M.I.T. Lincoln Laboratory, 1966. URL: http://www.dtic.mil/dtic/tr/fulltext/u2/648153.pdf.

[20] C.A. Balanis. *Antenna Theory: Analysis and Design*. Wiley, 2016. ISBN: 9781118642061. URL: https://books.google.pt/books?id=iFEBCgAAQBAJ.

[21] D Pozar and D Schaubert. "Scan blindness in infinite phased arrays of printed dipoles". In: *IEEE Transactions on Antennas and Propagation* 32.6 (1984), pp. 602–610. DOI: 10.1109/TAP.1984.1143375.

[22] Filipe M Barradas, Pedro M Tomé, José M Gomes, Telmo R Cunha, Pedro M Cabral, and José C Pedro. "Power, Linearity, and Efficiency Prediction for MIMO Arrays With Antenna Coupling". In: *IEEE Transactions on Microwave Theory and Techniques* 65.12 (2017), pp. 5284–5297. DOI: 10.1109/TMTT.2017.2766067.

[23] Christian Fager, Katharina Hausmair, Koen Buisman, Kristoffer Andersson, Esther Sienkiewicz, and David Gustafsson. "Analysis of nonlinear distortion in phased array transmitters". In: *Integrated Nonlinear Microwave and Millimetre-wave Circuits Workshop (INMMiC), 2017*. IEEE. 2017, pp. 1–4. DOI: 10.1109/INMMIC.2017.7927314.

[24] Katharina Hausmair, Sebastian Gustafsson, César Sánchez-Pérez, Per N Landin, Ulf Gustavsson, Thomas Eriksson, and Christian Fager. "Prediction of nonlinear distortion in wideband active antenna arrays". In: *IEEE Transactions on Microwave Theory and Techniques* 65.11 (2017), pp. 4550–4563. DOI: 10.1109/TMTT.2017.2699962.

[25] Analog Devices. *5G -The Microwave Perspective*. URL: http://www.analog.com/en/technical-articles/5g-the-microwave-perspective.html (visited on 07/01/2018).

[26] Analog Devices. *Measuring the Impact Of 5G*. URL: http://www.analog.com/en/technical-articles/measuring-the-impact-of-5g.html (visited on 07/01/2018).

[27] Analog Devices. *Instrumenting a 5G future*. URL: http://www.analog.com/en/landing-pages/001/national-instruments.html (visited on 07/01/2018).

[28] Huawei. *Huawei's 5G mini site*. URL: https://www.huawei.com/minisite/5g/en/ (visited on 07/01/2018).

[29] Keysight. *Examining the Challenges in Implementing and Testing Massive MIMO for 5G*. Tech. rep. Keysight Technologies, 2017. URL: http://literature.cdn.keysight.com/litweb/pdf/5992-1448EN.pdf.

[30] Keysight. *5G Over-the-Air Performance Measurement and Evaluation Using FieldFox Handheld Analyzers*. Tech. rep. Keysight Technologies, 2017. URL: http://literature.cdn.keysight.com/litweb/pdf/5992-2429EN.pdf.

[31] National Instruments. *NI Trend Watch*. Tech. rep. National Instruments, 2018. URL: http://nationalinstruments.lookbookhq.com/trend-watch-2018-en/trendwatch-2018.

[32] National Instruments. *The Road to 5G FAQs*. URL: http://www.ni.com/tutorial/51960/en/ (visited on 07/01/2018).

[33] National Instruments. *5 Things to Know About 5G New Radio*. URL: http://www.ni.com/pt-pt/innovations/5g/new-radio.html (visited on 07/01/2018).

[34] National Instruments. *5G Standardization 3GPP Status Update and Overview*. URL: http://images.demand.ni.com/Web/NationalInstruments/%7B945b23ec-b871-4d25-9fd4-cdb447045359%7D_3GPP_Resource_Guide_2017_final.pdf?espuid=CNATL000021712124%5C&cid=Direct_Marketing---em115737 (visited on 07/01/2018).

[35] National Instruments. *Prototyping Massive MIMO*. URL: http://www.ni.com/tutorial/51985/en/ (visited on 07/01/2018).

[36] National Instruments. *Introduction to the NI MIMO Prototyping System Hardware*. URL: http://www.ni.com/white-paper/53197/en/ (visited on 07/01/2018).

[37] National Instruments. *NI partnership with Bristol and Lund Universities*. URL: http://sine.ni.com/cs/app/doc/p/id/cs-17101# (visited on 07/01/2018).

[38] National Instruments. *Introduction to the NI mmWave Transceiver System Hardware*. URL: http://www.ni.com/white-paper/53095/en/ (visited on 07/01/2018).

[39] National Instruments. *Wireless Research Handbook Build 5G Wireless with Software Defined Radio*. URL: ftp://ftp.ni.com/evaluation/rf/NI_Wireless_Research_Handbook_May_2016_FINAL.pdf (visited on 07/01/2018).

[40] Qorvo. *5G: The Future of RF*. URL: https://www.qorvo.com/innovation/5g (visited on 07/01/2018).

[41] Qorvo. *5G RF For Dummies E-Book*. URL: https://www.qorvo.com/design-hub/ebooks/5g-rf-for-dummies (visited on 07/01/2018).

[42] Qualcomm. *Everything You Need to Know About 5G*. URL: https://www.qualcomm.com/invention/5g/what-is-5g (visited on 07/01/2018).

[43] Qualcomm. *Making 5G NR a Commercial Reality*. URL: https://www.qualcomm.com/media/documents/files/making-5g-nr-a-commercial-reality.pdf (visited on 07/01/2018).

[44] Qualcomm. *Our 5G vision is closer to reality than ever*. URL: https://www.qualcomm.com/news/onq/2018/02/14/our-5g-vision-closer-reality-ever (visited on 07/01/2018).

[45] Qualcomm. *Leading the LTE IoT evolution to connect the massive Internet of Things*. URL: https://www.qualcomm.com/media/documents/files/leading-the-lte-iot-evolution-to-connect-the-massive-internet-of-things.pdf (visited on 07/01/2018).

[46] Qualcomm. *What can we do with 5G NR Spectrum Sharing that isn't possible today?* URL: https://www.qualcomm.com/media/documents/files/new-3gpp-effort-on-nr-in-unlicensed-spectrum-expands-5g-to-new-areas.pdf (visited on 07/01/2018).

[47] Qualcomm. *Mobilizing 5G NR Millimeter Wave: Network Coverage Simulation Studies for Global Cities*. URL: https://www.qualcomm.com/media/documents/files/white-paper-5g-nr-millimeter-wave-network-coverage-simulation.pdf (visited on 07/01/2018).

[48] Said M Mikki and Yahia MM Antar. "A theory of antenna electromagnetic near field—Part I". In: *IEEE Transactions on Antennas and Propagation* 59.12 (2011), pp. 4691–4705.

[49] Said M Mikki and Yahia MM Antar. "A theory of antenna electromagnetic near field—Part II". In: *IEEE Transactions on Antennas and Propagation* 59.12 (2011), p. 4706.

[50] R. Garg, P. Bhartia, I.J. Bahl, and A. Ittipiboon. *Microstrip Antenna Design Handbook*. Antennas and Propagation Library. Artech House, 2001. ISBN: 9780890065136. URL: https://books.google.pt/books?id=%5C_er1LO5pEnUC.

[51] Cinch Connectivity Solutions. *Datasheet of SMA connectors*. URL: https://pt.mouser.com/datasheet/2/643/pi-CCS-JOHN-142-0701-801-1290116.pdf (visited on 09/07/2018).

[52] J.C. Pedro and N.B. Carvalho. *Intermodulation Distortion in Microwave and Wireless Circuits*. Artech House microwave library. Artech House, 2003. ISBN: 9781580536912. URL: https://books.google.pt/books?id=eGUtCZq8iwAC.

[53] Sergey L Loyka and Juan R Mosig. "Nonlinear modeling and simulation of active array antennas". In: *the 8th COST* 259 (1999).

[54] Cheng-Nan Hu and Dau-Chyrh Chang. "Nonlinear Effects of Power Amplifiers on Adaptive Antenna Systems". In: *IEEE Transactions on Antennas and Propagation* 64.4 (2016), pp. 1444–1453. DOI: 10.1109/TAP.2016.2515126.

[55] Takana Kaho, Tadao Nakagawa, Katsuhiko Araki, and Kohji Horikawa. "Carrier power to intermodulation-distortion power-ratio-increasing technique in active phased-array antenna systems". In: *IEEE transactions on microwave theory and techniques* 50.12 (2002), pp. 2987–2994. DOI: 10.1109/TMTT.2002.805136.

[56] Lorena Cabria, José Angel García, Antonio Tazón, and Angel Mediavilla. "Nonlinear distortion reduction in active arrays taking advantage of their spatial power-combining properties". In: *International Journal of RF and Microwave Computer-Aided Engineering: Co-sponsored by the Center for Advanced Manufacturing and Packaging of Microwave, Optical, and Digital Electronics (CAMPmode) at the University of Colorado at Boulder* 16.1 (2006), pp. 24–33.

[57] Khalil J Maalouf and Erik Lier. "Theoretical and experimental study of interference in multibeam active phased array transmit antenna for satellite communications". In: *IEEE Transactions on Antennas and Propagation* 52.2 (2004), pp. 587–592. DOI: 10.1109/TAP.2004.823900.

[58] C. Mollén, U. Gustavsson, T. Eriksson, and E. G. Larsson. "Spatial Characteristics of Distortion Radiated from Antenna Arrays with Transceiver Nonlinearities". In: *IEEE Transactions on Wireless Communications* (2018), pp. 1–1. ISSN: 1536-1276. DOI: 10.1109/TWC.2018.2861872.

[59] Antonius Johannes van den Biggelaar, Ulf Johannsen, Paul Mattheijssen, and Adrianus Bart Smolders. "Improved statistical model on the effect of random errors in the phase and amplitude of element excitations on the array radiation pattern". In: *IEEE Transactions on Antennas and Propagation* 66.5 (2018), pp. 2309–2317.

[60] Minicircuits. *Datasheet of era 2 power amplifier*. URL: https://ww2.minicircuits.com/pdfs/ERA-2+.pdf (visited on 09/07/2018).

[61] Minicircuits. *Datasheet of tcch 80 RFC*. URL: https://ww2.minicircuits.com/pdfs/TCCH-80+.pdf (visited on 09/07/2018).

[62] Murata. *Datasheet of GJM1555 high-Q RF capacitor*. URL: https://psearch.en.murata.com/capacitor/product/GJM1555C1H2R4BB01%23.html (visited on 09/07/2018).

[63] VISHAY. *Datasheet of TSM4 multi-turn trimmer*. URL: https://docs-emea.rs-online.com/webdocs/0442/0900766b80442f5a.pdf (visited on 09/07/2018).

[64] K. Technologies. *ADS Example Book: Focused on RF and Microwave Design*. CreateSpace Independent Publishing Platform, 2016. ISBN: 9781539542216. URL: https://books.google.pt/books?id=PFgDMQAACAAJ.

[65] D.M. Pozar. *Microwave Engineering*. Wiley, 2012. ISBN: 9780470631553. URL: https://books.google.pt/books?id=%5C_YEbGAXCcAMC.

Acronyms

1D	One Dimensional
2D	Two Dimensional
3D	Three Dimensional
3GPP	3rd Generation Partnership Project
4G	Fourth Generation
5G	Fifth Generation
5G-NR	5G New Radio
ADS	Avanced Design System
AF	Array Factor
AI	Artificial Intelligence
AM	Amplitude Modulation
BER	Bit Error Rate
BS	Base Station
C-RAN	Centralized Radio Access Network
CMOS	Complementary Metal-Oxide Semiconductor
CSI	Channel State Information
CST	Computer Simulation Technology
D2D	Device to Device
DAC	Digital to Analog Converter
DC	Direct Current
DETI	Departamento de Eletrónica, Telecomunicações e Informática
DoA	Direction of Arrival
DPD	Digital Pre-Distortion
DUT	Device Under Test
EM	Electromagnetic
EVM	Error Vector Magnitude
FAQs	Frequently Asked Questions
FDD	Frequency Division Duplex
FIR	Finite Impulse Response
FNBW	First-Null Beamwidth
HPBW	Half-Power Beamwidth
IC	Integrated Circuit
IEEE	Institute of Electrical and Electronics Engineers

IM	Intermodulation
IMD	Intermodulation Distortion
IMR	Intermodulation Ratio
IMT-2020	International Mobile Telecommunication 2020
IoS	Internet of Space
IoT	Internet of Things
IP3	Third Order Intercept Point
ITU	International Telecommunication Union
LEO	Low Earth Orbit
LMS	Least Mean Square
LTE	Long Term Evolution
M2M	Machine to Machine
MAC	Media Access Control
MATLAB	Matrix Laboratory
MIMO	Multiple Input Multiple Output
MISO	Multiple Input Single Output
MMIC	Monolitic Microwave Integrated Circuit
MMS	Multimedia Message Service
MSc	Master of Science
NI	National Instruments
NIST	National Institute of Standard and Technology
NLoS	Non-Line-of-Sight
OFDM	Orthogonal Frequency-Division Multiplexing
OTA	Over the Air
PA	Power Amplifier
PAPR	Peak-to-Average Power Ratio
PCB	Printed Circuit Board
PEC	Perfect Electric Conductor
PM	Phase Modulation
PMW	Perfect Magnectic Wall
RF	Radio Frequency
S-Parameters	Scattering Parameters
SDN	Software Defined Network
SDR	Software Defined Radio
SIR	Signal-to-Interference Ratio
SLL	Side Lobe Level
SNoI	Signal Not of Interest
SNR	Signal-to-Noise Ratio
SoC	System on Chip
SoI	Signal of Interest
TDD	Time Division Duplex
VNA	Vector Network Analyzer

VNF Virtual Network Function
VSA Vector Signal Analyser
VSG Vector Signal Generator
WPT Wireless Power Transfer